

CARBONATED MANTLE LITHOSPHERE IN THE
WESTERN CANADIAN CORDILLERA

by

Nils Daniel Peterson

B.Sc. (Honors), The University of Alberta, 2005

A THESIS SUBMITTED IN PARTIAL FULFILLMENT
OF THE REQUIREMENTS FOR THE DEGREE OF

MASTER OF SCIENCE

in

The Faculty of Graduate Studies

(Geological Sciences)

THE UNIVERSITY OF BRITISH COLUMBIA

(Vancouver)

August 2010

© Nils Daniel Peterson, 2010

ABSTRACT

Accessory minerals such as carbonates and sulfides are important indicators of metasomatic enrichment events in the mantle lithosphere and ultimately control mantle melting. However, these phases are rarely expressed modally in mantle-derived peridotitic xenoliths. Here we report on a unique occurrence of primary mantle-derived carbonate preserved in spinel peridotite xenoliths within a 19 Ma basanite dike. The dike, defined as part of the Cheslatta Lake suite, intrudes Jurassic volcanoclastic rocks near the Intermontane - Coast Belt boundary in western British Columbia, and contains primary magmatic calcite. The peridotite xenoliths are concentrated in a 4 metre interval where the dike is narrowest and are dominated by lherzolite, with less abundant harzburgite, dunite, and websterite. Thermometry (Taylor, 1998) produces paleoequilibration temperatures of 792 to 1044 °C, corresponding to approximately 32 to 49 km depth on an average geotherm for warm, thin Cordilleran-style lithosphere. Magnesian calcite occurs in all of the 51 xenoliths examined. The Mg-calcite appears as intergranular grains that appear to have been in textural equilibrium with neighbouring minerals, as inclusions, and as fracture-filling veins, commonly in association with pentlandite and chalcopyrite. Carbon-oxygen isotopic compositions of carbonates from the dike, wall rock, and xenoliths indicates that each have distinct compositions. Oxygen isotopic compositions of the xenoliths' carbonate indicates that, consistent with textural observations, the carbonates have equilibrated with the host mantle, having $\delta^{18}\text{O}$ compositions less than 3 ‰ greater than compositions interpreted for primary mantle-derived carbonatites. In addition, carbonates from the mantle xenoliths fall into two separate groups identified by different $\delta^{13}\text{C}$ and $^{87}\text{Sr}/^{86}\text{Sr}$ isotopic compositions, indicating different sources for carbonate in the two xenolith groups, and thus multiple enrichment events. Strontium isotopic ratios also show that the dike scavenged carbonate from disaggregated mantle xenoliths, becoming enriched in CO_2 . Timing of enrichment is unconstrained, and no

relationships between the host magma and mantle-derived xenoliths is required, contrasting with other studies. A plausible metasomatic agent is a carbonate melt with associated monosulfide solution, derived from the subduction of oceanic crust beneath North America during Coast Plutonic Belt magmatism, when Mt. Preston was in an arc to back arc position.

PREFACE

Chapters 1 and 2 contain a regional and site-specific description originally published as “Mantle-Derived Peridotite Xenoliths from the Western Intermontane Belt, Whitesail Lake map area (NTS 093E), Western British Columbia” in the British Columbia (BC) Ministry of Energy, Mines and Petroleum Resources publication “Geological Fieldwork 2005” (Peterson et al., 2006). The paper was researched and written by myself, and co-authored by J.K. Russell and J.B. Mahoney, who made multiple stages of editorial contributions to the manuscript.

TABLE OF CONTENTS

ABSTRACT	ii
PREFACE	iv
TABLE OF CONTENTS	v
LIST OF TABLES.....	viii
LIST OF FIGURES.....	ix
ACKNOWLEDGEMENTS	xi
DEDICATION.....	xiii
1. INTRODUCTION	1
2. MT. PRESTON.....	4
2.1 Tectonic Setting	8
2.2 Regional Geology.....	10
2.3 Geological and Stratigraphic Relationships.....	11
2.3.1 Dike	14
2.3.2 Mantle xenoliths	18
2.3.3 Crustal xenoliths and xenocrysts	20
2.4 Discussion.....	20
3. HOST BASANITE DIKE	23
3.1 Petrography	23
3.2 Carbonate.....	25
3.3 Chemistry	26
3.4 Ar-Ar Dating.....	32
3.5 Radiogenic Isotopes	34
3.6 Oxygen Isotopes – Silicates	40
3.7 Discussion	42
4. MANTLE XENOLITHS.....	44
4.1 Petrography	44
4.2 Mineral Modes	50
4.3 Geothermometry	50
4.3.1 Mineral compositions	50
4.3.2 Geothermometry results	51
4.4 Geotherm.....	59

4.5 Chemistry	62
4.6 Re-Os Isotopes	73
5. MANTLE CARBONATE	76
5.1 Occurrence	76
5.2 Sulfides	85
5.3 Stable Isotopes	88
5.4 Strontium Isotopes	96
6. DISCUSSION.....	101
6.1 Cordilleran Mantle Lithosphere as Host.....	101
6.1.1 Thermal properties and depth	101
6.1.2 Modal mineralogy.....	102
6.1.3 Textures	103
6.1.4 Major element compositions.....	103
6.1.5 Trace and rare earth element compositions.....	104
6.1.6 Summary	104
6.2 Mantle-Sourced Carbonate	105
6.2.1 Occurrence and source in the mantle lithosphere	105
6.2.2 Stability of calcite and sulfides in the mantle lithosphere.....	108
6.2.3 Equilibration within the mantle	109
6.2.4 Comments on preservation	111
6.3 Carbonate Enrichment Events.....	112
6.3.1 Timing of enrichment.....	113
6.3.2 Metasomatic agent.....	113
6.3.3 Metasomatic source	115
CONCLUSION.....	119
REFERENCES	121
APPENDIX A – SAMPLE SUITE	135
APPENDIX B – GEOCHEMISTRY	136
APPENDIX C – AR-AR DATING.....	139
APPENDIX D – RADIOGENIC ISOTOPES	142
D.1 Sr-Nd-Pb Isotopes.....	142
D.2 Re-Os Isotopes	142
APPENDIX E – STABLE ISOTOPES	144
E.1 Oxygen Isotopes (Silicates).....	144
E.2 Oxygen and Carbon Isotopes (Carbonate).....	144

APPENDIX F – RIETVELD METHOD	146
APPENDIX G – ELECTRON MICROPROBE ANALYSES.....	150
APPENDIX H – GEOTHERMOMETRY	154
APPENDIX I – HELIUM PYCNOMETRY	159

LIST OF TABLES

Table 3.1 – Major element compositions and normative mineralogy of dike whole rock	27
Table 3.2 – Trace and rare earth element compositions of dike whole rock.....	28
Table 3.3 – Strontium isotopic composition of dike whole rock.....	36
Table 3.4 – Lead isotopic composition of dike whole rock.....	37
Table 3.5 – Neodymium isotopic composition of dike whole rock	38
Table 3.6 – Oxygen isotopic composition of dike silicates.....	41
Table 4.1 – Modal mineralogy of mantle xenoliths by Rietveld analysis.....	47
Table 4.2 – Physical and thermal properties of mantle xenoliths	53
Table 4.3 – Major element compositions of mantle xenoliths.....	65
Table 4.4 – Trace and rare earth element compositions of mantle xenoliths.....	68
Table 4.5 – Rhenium-osmium isotopic results for mantle xenoliths	74
Table 5.1 – Carbon and oxygen isotopic compositions of dike carbonate	90
Table 5.2 – Carbon and oxygen isotopic compositions of wall rock carbonate	91
Table 5.3 – Carbon and oxygen isotopic compositions of mantle xenolith carbonate.....	92
Table 5.4 – Strontium isotopic compositions of wall rock and dike carbonate.....	98
Table 5.5 – Strontium isotopic compositions of mantle xenolith carbonate.....	99
Table B.1 – Major element compositions of wall rock and crustal xenolith	137
Table B.2 – Trace and rare earth element compositions of wall rock and crustal xenolith	138
Table C.1 – Statistics for $^{40}\text{Ar}/^{39}\text{Ar}$ dating.....	141
Table G.1 – Standards used in electron microprobe analyses.....	151
Table G.2 – Mineral compositions for major phases in mantle xenoliths	152
Table H.1 – Geothermometry results for mantle xenoliths	157

LIST OF FIGURES

Figure 2.1 – Tectonomorphologic belts of the Canadian Cordillera.....	5
Figure 2.2 – Regional schematic geology	6
Figure 2.3 – Geology of the Mt. Preston area	7
Figure 2.4 – Volcanic centres of the Canadian Cordillera.....	12
Figure 2.5 – Large scale morphology of the Mt. Preston dike.....	13
Figure 2.6 – Geologic map of the Mt. Preston dike	15
Figure 2.7 – Volcanological features of the dike	17
Figure 2.8 – Mantle xenolith occurrence within the dike	19
Figure 3.1 – Dike rock textures	24
Figure 3.2 – Major, trace and rare earth element diagrams for the dike.....	30
Figure 3.3 – $^{40}\text{Ar}/^{39}\text{Ar}$ release spectra graphs	33
Figure 3.4 – Isotopic compositions of the Mt. Preston dike	35
Figure 4.1 – Petrographic images of mantle xenoliths	45
Figure 4.2 – Modal classification of mantle xenoliths	46
Figure 4.3 – Mantle xenolith geothermometry	52
Figure 4.4 – Mineral compositions in mantle xenoliths	58
Figure 4.5 – Model geotherm for lithosphere.....	61
Figure 4.6 – Major element depletion diagrams for mantle xenoliths.....	63
Figure 4.7 – Ca-Al depletion diagram for mantle xenoliths	64
Figure 4.8 – Rare earth element diagrams for mantle xenoliths.....	67
Figure 4.9 – Tb/Yb depletion diagram for mantle xenoliths	72
Figure 5.1 – Carbonate occurrences and habits in mantle xenoliths	77
Figure 5.2 – Granular calcite in mantle xenoliths	78
Figure 5.3 – Carbonate inclusions in mantle xenolith phases.....	79
Figure 5.4 – Fe-Ni sulfides in mantle xenoliths.....	80

Figure 5.5 – Carbonate veins and inclusion trails in mantle xenoliths	81
Figure 5.6 – BSE single element maps of coexisting sulfides	86
Figure 5.7 – Compositions of coexisting sulfides	87
Figure 5.8 – Carbon and oxygen isotopic compositions for carbonate occurrences.....	89
Figure 5.9 – Strontium isotopic compositions for carbonate occurrences	97
Figure F.1 – Comparison of modal mineralogy estimates	148
Figure F.2 – Relative deviations of modal mineralogy estimates	149
Figure H.1 – Comparison of geothermometers.....	156
Figure I.1 – Sample volume to sample cell volume pycnometry test	161
Figure I.2 – Mantle xenolith densities by pycnometry	162
Figure I.3 – Modal abundance of xenolith phases versus density	163

ACKNOWLEDGEMENTS

This project was funded by the Natural Sciences and Engineering Research Council (NSERC) Discovery Grant held by J.K. Russell and the NSERC Collaborative Research Opportunities (CRO) grant (BATHOLITHS: Generation and Evolution of Crust in Continental Magmatic Arcs) held by Ron Clowes and others. I was also partially funded by a University Graduate Fellowship (UGF) from the University of British Columbia (UBC), the Egil H. Lorntzen Scholarship from the Department of Earth and Ocean Sciences, UBC, and an NSERC Undergraduate Student Research Award. I would also like to acknowledge the research grants awarded by the Geological Society of America and the Mineralogical Association of Canada.

I would like to thank my advisory committee past and present, Greg Dipple, Derek Thorkelson, and Lori Kennedy, for taking the time and effort to help guide this research, and thanks to Lee Groat for being my external examiner. This research benefited from the capable assistance of Adam Kjos in the field. Thanks to J. Brian Mahoney, who reported the locality and accompanied and assisted me in the field. Discussions with James Scoates, Terry Gordon, Jim Mortensen, Dominique Weis, and Maya Kopylova were illuminating. I am indebted to Mati Raudsepp, Tom Ullrich, and Janet Gabites for their superb technical knowledge and willingness to help. Sasha Wilson gets her own acknowledgement sentence because she probably thinks she doesn't deserve it. Geneviève Robert gets her own sentence and she should know she deserves it; she is a great friend and a constant source of support. Thank you to Shelley Oliver for her much needed and appreciated assistance during the latter days of this project. The VPL past and present are too many to list here, but R-E Farrell, Stephen Moss, Curtis Brett, Jacqueline Dohaney and Krista Michol must be included for making this experience enjoyable. Many thanks to Bruce Kienlen and Graham Gill of Diamonds North for their understanding, support and patience during their busy summer season.

Thank you Kelly, not for using all our stove fuel in the field for ‘melting experiments’ and then leaving, but for your constant availability and your willingness to let this project evolve.

Your enthusiasm is infectious.

DEDICATION

Thank you Amy.

1. INTRODUCTION

Mantle-derived xenoliths are commonly sampled and transported to the surface in mafic magmas, and represent direct samples of the Earth's lithospheric mantle. Beneath mobile belts such as the Canadian Cordillera, the mantle lithosphere is relatively thin and warm, and comprises olivine, clinopyroxene, orthopyroxene, and spinel in varying proportions. In addition to these major phases, accessory minerals such as carbonates, sulfides, amphiboles or micas may occur. These accessories serve to elucidate differences in the lithospheric mantle that underlies the Earth's crust. These accessory phases can also be important indicators of past metasomatic (i.e. fluid or melt) enrichment events that ultimately control mantle melting events (Falloon and Green, 1990). Primary (i.e. derived from the mantle and unrelated to the sampling magma) carbonate has been reported in some xenolith suites (Perkins et al. (2006) and references therein) deriving from a variety of tectonic settings such as current or paleosubduction zones (e.g. Laurora et al., 2001; Demeny et al., 2004; Ducea et al., 2005), intraplate settings (e.g. Delpech et al., 2004; Moine et al., 2004) or rifts (e.g. Lee et al., 2000). These occurrences are in conflict with earlier ideas that rapid decarbonation should occur during entrainment and transport of carbonated peridotite (Canil, 1990). However, rarely (Ionov et al., 1996) have primary carbonates been interpreted as preserved in the xenoliths and equilibrated in the mantle; most are considered the result of enrichment shortly before eruption, due to textural/chemical (e.g. Lee et al., 2000; Delpech et al., 2004; Demeny et al., 2004; Moine et al., 2004; Ducea et al., 2005; Ionov et al., 2006) or isotopic (e.g. Perkins et al., 2006) disequilibrium.

Mafic volcanic centres are ubiquitous in the Canadian Cordillera, and they commonly sample the mantle and/or crust beneath their eruptive localities (Edwards and Russell (2000) and references therein). This has led to numerous studies of the Cordillera's mantle lithosphere (Littlejohn and Greenwood, 1974; Nicholls et al., 1982; Ross, 1983; Canil et al., 1987; Francis,

1987; Mitchell (1987) and references therein; Peslier et al., 2000a, 2000b; Peslier et al., 2002; Harder, 2004; Harder and Russell, 2006). Despite the complex tectonic history of the Cordillera, these studies have found the mantle lithosphere underlying the Cordillera to be relatively uniform in composition, thermal regime, and age (Harder, 2004; Peslier et al., 2000b). The evidence for metasomatic events within the Cordilleran mantle lithosphere is relatively rare. Most evidence is based on geochemical compositions of peridotite xenoliths, indicating only cryptic metasomatism (Carignan et al., 1996; Peslier et al., 2002). Rare direct evidence (e.g. modal mineralogy) for mantle metasomatic events within the Cordilleran mantle derives from sparse phlogopite (Canil and Scarfe, 1989) or amphibole (Brearley and Scarfe, 1984; Peslier et al., 2002; B. Edwards, pers. comm., 2010) within peridotite.

This study reports on a new and geographically unique suite of lithospheric mantle-derived xenoliths from Mt. Preston in western British Columbia (BC), Canada. The xenoliths are hosted by a basanitic dike that intrudes Intermontane Belt rocks exposed near its boundary with the Coast Belt. The mantle-derived peridotitic xenoliths are used here to map the chemical and thermal properties of the mantle lithosphere beneath this region of the British Columbia Cordillera. The peridotitic suite of xenoliths is mineralogically unique in that every xenolith contains modal carbonate and some contain sulfides. The textural and isotopic properties of the carbonate here suggest that not only was it fully equilibrated at mantle conditions prior to being sampled by the basanite magma, but also that it was preserved pristinely during and after emplacement.

These represent the first carbonate-bearing xenoliths described in North America north of central California (Ducea et al., 2005). Furthermore, to the author's knowledge, these are the first carbonates to show isotopic and textural evidence for being fully equilibrated at mantle conditions and the preservation of these properties. The physical, thermal and chemical properties of the host mantle xenoliths and the occurrence of these carbonates and sulfides, and

the metasomatic enrichment they represent, has implications for the tectonic history of this part of British Columbia. The morphology of these mantle-equilibrated carbonates may be of importance to future models of the Earth's mantle and how it is enriched and melted.

2. MT. PRESTON

The Whitesail Lake map area (NTS 93E), immediately north and east of Bella Coola, BC was the focus of regional mapping programs during 2004 and 2005. The mapping programs were supported by the BC Government's Rocks to Riches program (Mahoney et al., 2005), and by Geoscience BC (Mahoney et al., 2006). Mapping in support of these programs identified a new occurrence of mantle-derived peridotitic xenoliths in the BC Cordillera near Mt. Preston (Fig. 2.1), hosted by a mafic dike intruding Hazelton Group rocks of the Intermontane Belt. The dike contains abundant fresh, unaltered crustal and mantle-derived peridotite xenoliths.

This occurrence of mantle-derived xenoliths is unique because of its geographical and geological position. It is on the western margin of the Intermontane Belt and within 40 km of Coast Belt rocks (Figs. 2.2, 2.3). Most other occurrences of mantle xenoliths in British Columbia are situated well within or east of the Intermontane Belt (e.g. Edwards and Russell, 2000). The mantle xenoliths at this locality provide direct evidence for the thermal and compositional state of the mantle lithosphere underlying the western margin of the Intermontane Belt. Information derived from this study complements the BATHOLITHS geophysical project, which is designed to explore the structure of the Coast Belt lithosphere (Andronicos and Ducea, 2004). The BATHOLITHS operational area encompasses Mt. Preston (Fig. 2.2).

The purpose of this chapter is to (a) summarize the setting of the Mt. Preston locality, (b) report on the field occurrence of this xenolith-bearing dike, (c) describe the nature and distribution of mantle and crustal xenoliths within the dike, and (d) explore some of the implications of these observations for the transport and emplacement of this mantle-derived magma.

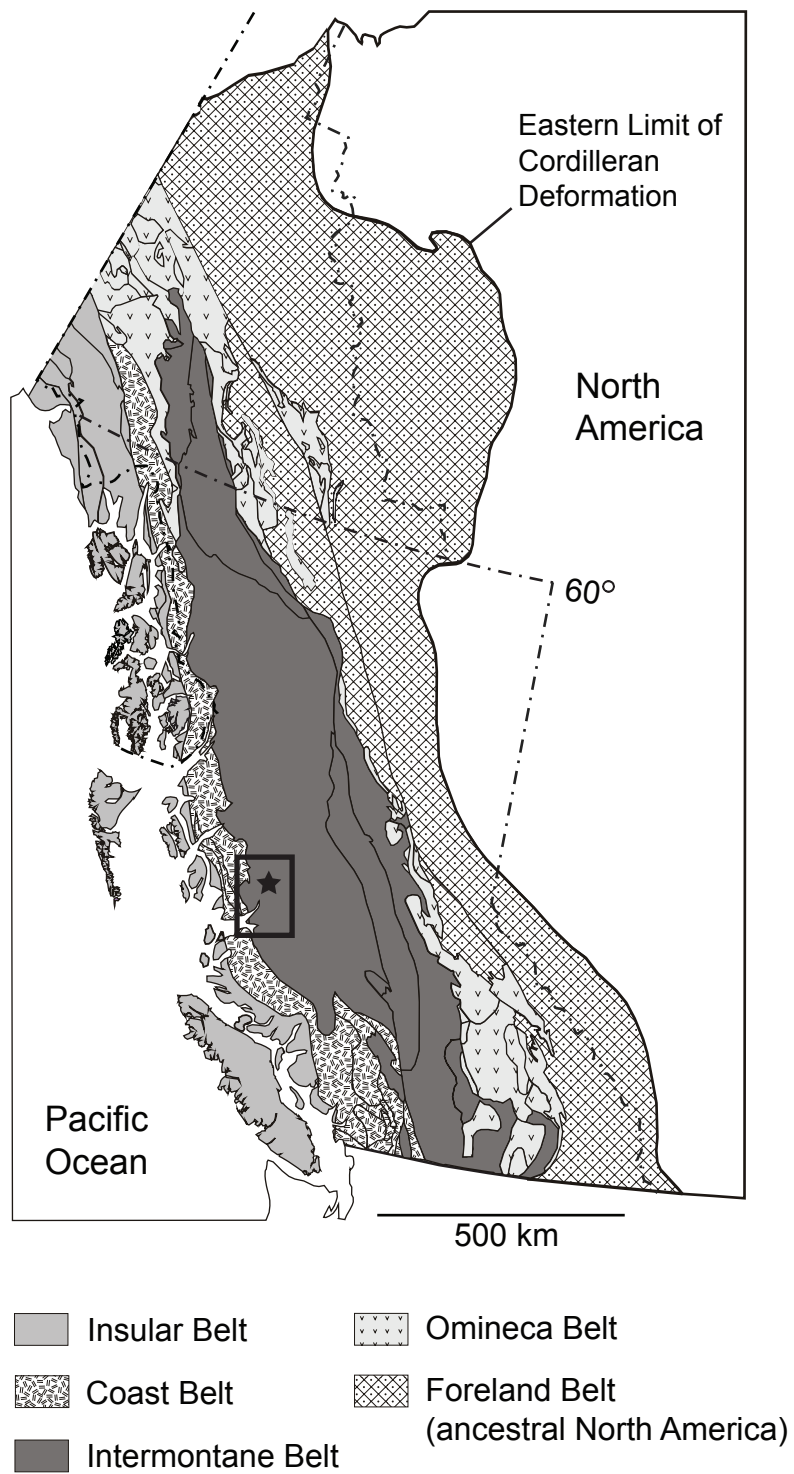


Figure 2.1 Location of study area near Mt. Preston (star) shown against the major tectono-morphologic belts of the Canadian Cordillera (modified from Wheeler and McFeely, 1991). The eastern extent of Cordilleran deformation of ancestral North American rocks is also shown. Outline indicates the area shown in Figure 2.2.

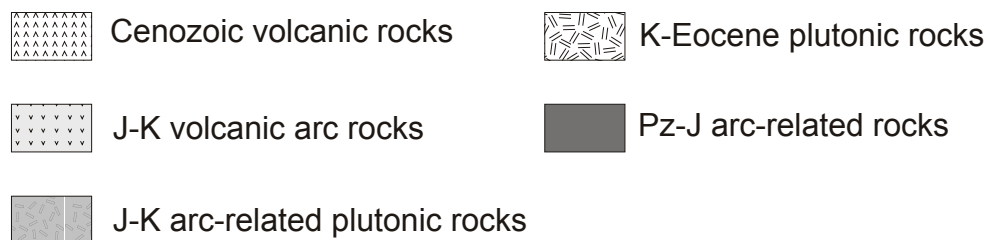
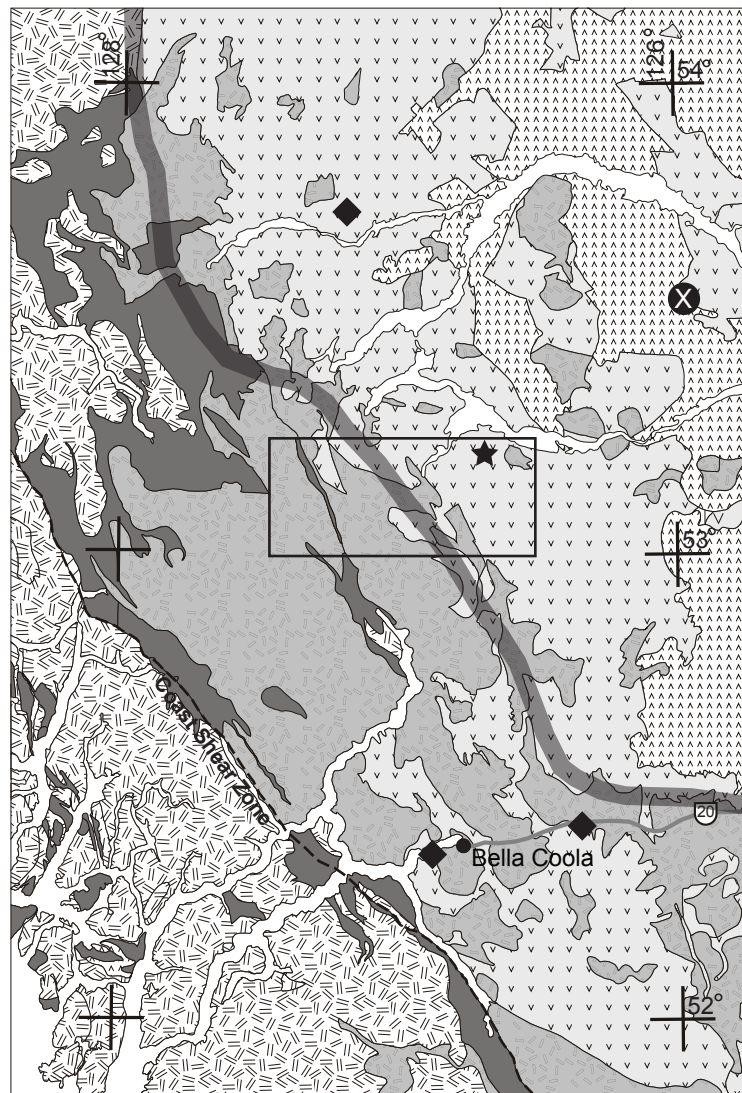


Figure 2.2 Schematic geology of the region surrounding Mt. Preston. The study area (star) is situated immediately south of Eutsuk Lake, approximately 40 km east of the Coast Belt. 'X' indicates the nearest mantle xenolith occurrence to Mt. Preston, one of the Nechako River localities of Resnick et al. (1999). Broad shaded line indicates Intermontane Belt - Coast Belt boundary (Wheeler et al., 1991). Diamonds indicate planned shot locations for BATHOLITHS project geophysics. Box indicates area shown in Figure 2.3. Figure modified from Diakow et al. (2003).

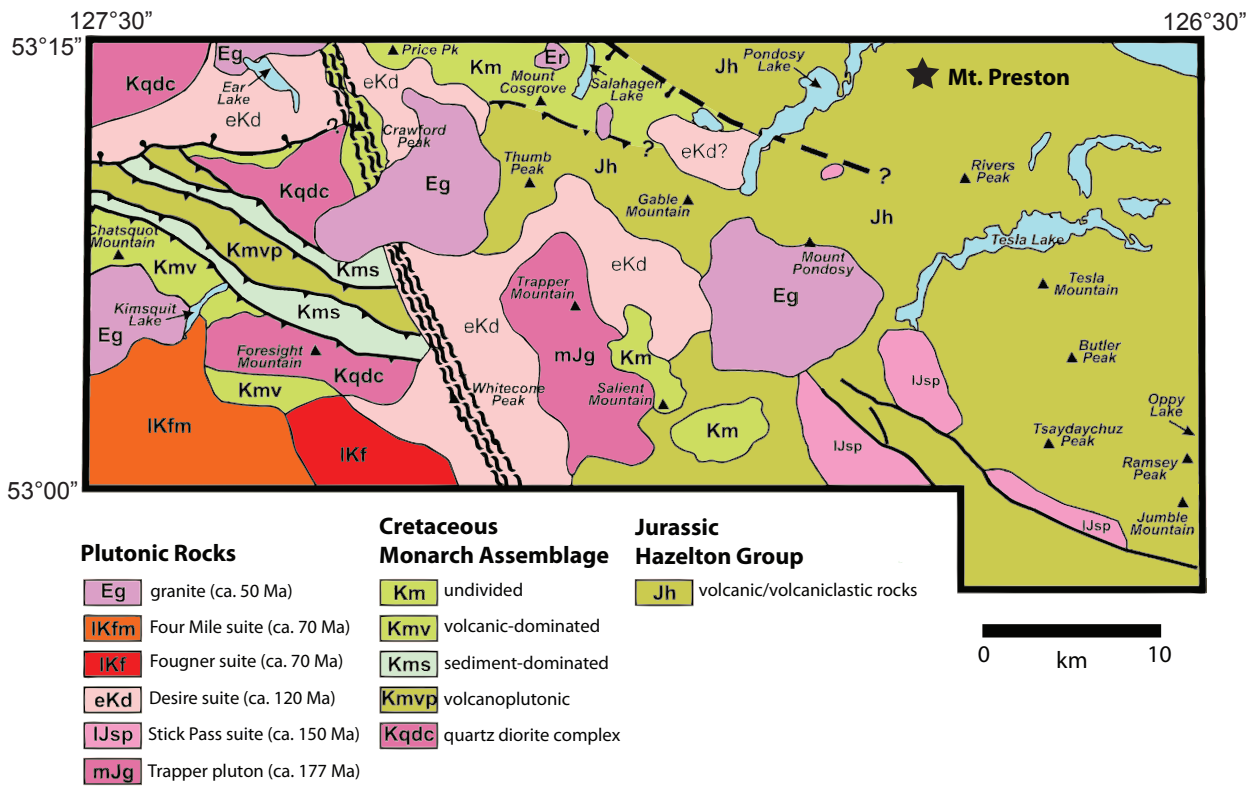


Figure 2.3 Generalized geology of the Mt. Preston area, showing major lithological units, structures, and physiographic features. Figure modified from Mahoney et al. (2005).

2.1 Tectonic Setting

The Canadian Cordillera is an amalgamation of rocks related to ancestral North America and allochthonous terranes which accreted onto the North American margin from the Middle Jurassic (185 Ma, Intermontane Belt rocks) to the Late Cretaceous (90 to 85 Ma, Insular Belt rocks) (Monger and Price, 2002; Gehrels et al., 2009). The Cordillera has been divided into five geomorphological belts based on their geological properties and structural styles (Monger et al., 1982; Gabrielse et al., 1991); the area of Mt. Preston lies within the Intermontane Belt near its boundary with the Coast Belt. The Intermontane Belt comprises several terranes which accreted onto the North American margin, ending in the Middle Jurassic (van der Heyden (1992) and references therein). The terranes comprising the Intermontane Belt have been interpreted as related fragments of a late Paleozoic to early Mesozoic island arc (Stikine and Quesnel terranes), and its associated accretionary complex (Cache Creek terrane) (Monger and Price, 2002). The Intermontane Belt is separated from the Insular Belt to the west by the Coast Belt, comprising the Coast Mountains Batholith (or Coast Plutonic Complex), the roots of a Middle Jurassic to Eocene magmatic arc (van der Heyden, 1992; Monger et al., 1994; Gehrels et al., 2009), and related rocks. Coast Mountains Batholith magmatism began as a continuous continental arc (~170 Ma), which was then split into northern and southern portions, translated, and juxtaposed into outboard and inboard portions respectively (ending ~100 Ma); magmatism from 100 Ma to the end of the arc's life (~50 Ma) overprinted these earlier intrusives and the boundary between the Insular Belt and the Intermontane Belt (Monger et al., 1994; Gehrels et al., 2009).

The Cordillera appears to comprise Phanerozoic and Mesoproterozoic crust (overlying Paleoproterozoic 'basement' in the east), all underlain by mantle lithosphere approximately 1.1 Ga in age (Peslier et al. (2000b) and references therein); however, the origin of the Cordilleran lithospheric mantle is not certain. Two hypotheses are (1) that the Cordillera is underlain by

exotic mantle lithosphere that was coupled to individual terranes before their accretion (e.g. Abraham et al., 2001), or (2) that North American crust and mantle lithosphere extends beneath the Cordillera, implying a decoupling of accreting terranes' crust and lithospheric mantle (e.g. Clowes et al., 1998; Peslier et al., 2000b; Monger and Price, 2002; Cook et al., 2004). Proponents of the latter hypothesis (Monger and Price, 2002; Cook et al., 2005; Evenchick et al., 2005) vary in their estimation of the amount of crust superposed on the colder, older North American 'basement' (e.g. ≤ 10 km thick tectonic 'flakes' of Monger and Price, 2002). Some authors have interpreted seismic survey data as showing lower crust (>20 km depth) extending beneath British Columbia from the craton margin (e.g. Clowes et al., 1998). However, others suggest that the geophysical data are consistent with both (1) the emplacement of terrane crust over older mantle lithosphere prior to accretion (though this mantle lithosphere may have been rifted from ancient North America) or (2) mantle sourced from a continuous wedge of North American lithosphere (Cook and Erdmer, 2005).

Rhenium-osmium dating of lithospheric mantle-derived xenoliths (Peslier et al., 2000b) has recovered Proterozoic model ages across the Cordillera, consistent with a single source for the Cordilleran lithospheric mantle, whether autochthonous or allochthonous, or at least indicating a common melting history. This result also precludes the suggestion of a simple extension of cratonic crust coupled to its own lithospheric mantle residing beneath the eastern Cordillera, as the mantle lithosphere in that region appears to be much younger than the wedge of cratonic crustal basement that overlies it.

The Mt. Preston area was in an arc to back-arc position during the Middle Jurassic to Eocene (~ 170 -50 Ma) subduction regime that supported the prolific magmatism responsible for the Coast Mountains Batholith until that arc's extinction at ~ 50 Ma (Haeussler et al., 2003; Gehrels et al., 2009). In middle Eocene time the subducted Resurrection plate supported the magmatism producing the trench-parallel (ie. NW-SE) oriented Challis-Kamloops volcanic belt

in the BC interior (Breitsprecher et al 2003, Haeussler et al 2003) including the Ootsa Lake and Endako Groups to the east of Mt. Preston (emplaced 53-45 Ma; Grainger et al., 2001). The Mt. Preston area would have been in the forearc region of this arc.

The plate boundary between the North American plate and the oceanic plates became a transform fault ca. 40 Ma, ending subduction of the broadly trench-parallel ridge system separating the Resurrection and Pacific (Kula/Eshamy) oceanic plates (Madsen et al., 2006). This resulted in the foundering of the subducted Resurrection plate remnant, and the northward translation and enlargement of the Pacific-Farallon slab window (created by the subduction of the broadly trench-perpendicular ridge separating the Resurrection plate to the north from the Farallon plate to the south). The Mt. Preston area has remained within or on the margin of this projected slab window since ~35 Ma (Madsen et al., 2006).

2.2 Regional Geology

The Mt. Preston area is underlain by Early to Middle Jurassic volcanoclastic rocks of the Hazelton Group. This large volcanic and sedimentary succession has been interpreted as the remnants of two coeval volcanic arcs created by facing subduction zones, with a marine back-arc basin between (Marsden and Thorkelson, 1992). The Hazelton features metamorphosed volcanic to volcanoclastic and mudstone-dominated sedimentary rocks in the region of Mt. Preston (Figs. 2.2, 2.3; Gordee et al., 2005; Mahoney et al., 2005). Here, the Hazelton Group rocks are intruded by post-Hazelton, post-ca. 136 Ma metamorphosed mafic to intermediate dikes (Gordee et al., 2005); one of these dikes, a small (<1 m width) one located within 10 m of the xenolith-bearing dike of interest, was sampled and dated using ^{40}Ar - ^{39}Ar methods. The youngest magmatic intrusion in the area is a rhyolite porphyry dike dated at 52 Ma. There are no carbonate-rich lithologies within several kilometres of Mt. Preston.

Since the time of transition to a transform plate boundary between the Pacific and North American plates, crustal extension has resulted in the production of numerous small alkaline volcanic centres (Fig. 2.4), especially in the Northern Cordilleran Volcanic Province (beginning 20 Ma; Edwards and Russell, 1999). Other volcanic suites in the region of Mt. Preston include the Chilcotin Flood Basalts (beginning 31 Ma; Mathews, 1989), a discrete alkaline, mantle xenolith-bearing portion of the Chilcotin known as the Cheslatta Lake Volcanic Suite (beginning 21 Ma; Anderson et al., 2001), and the east-trending Anahim Volcanic Belt (beginning 14 Ma; Bevier, 1989). The nearest occurrence of mantle-derived peridotitic xenoliths to this new locale is the Chelaslie River locality within the Cheslatta Lake volcanics, ~50 km northeast of Mt. Preston (Fig. 2.2; Resnick et al., 1999).

2.3 Geological and Stratigraphic Relationships

This research is based on a single dike that strikes 145° across a saddle on a ridge 3 km southeast of the peak of Mt. Preston (Fig. 2.5a). The dike is exposed on the ridge crest and in the south-facing slope that forms the east-trending ridge. The ridge crest exposes the top of the dike and is situated 2063 m above mean sea level (amsl) at $53^\circ 13' 2.64''$ N, $126^\circ 41' 51.86''$ W (NAD83 datum). Exposure begins at the top of the ridge, continuing intermittently down the southern face for about 110 m (60 m vertical; Fig. 2.5b). Much of the dike is covered by talus, but the contact between dike and country rock is locally well exposed. Where exposed, the contact dips steeply to the west (between 50 and 64°). The dike is not exposed on the north side of the ridge.

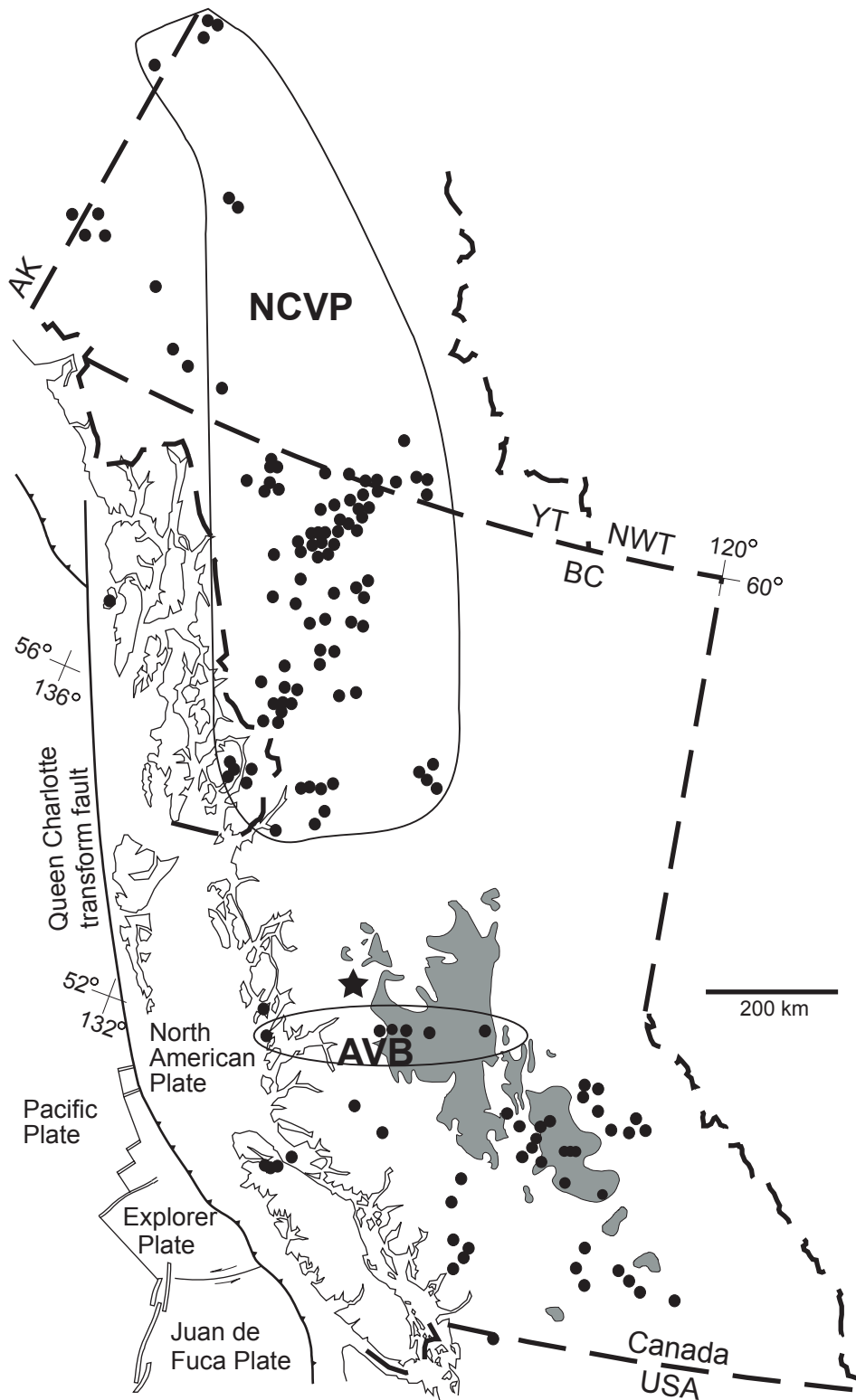


Figure 2.4 Location of Mt. Preston (star) against Neogene to recent volcanic centres in British Columbia. Relevant volcanic provinces and belts are highlighted: Anahim Volcanic Belt (AVB), Northern Cordilleran Volcanic Province (NCVP), and Chilcotin Basalts / Cheslatta Lake Volcanic Suite (shaded). Modified from Edwards and Russell (2000).

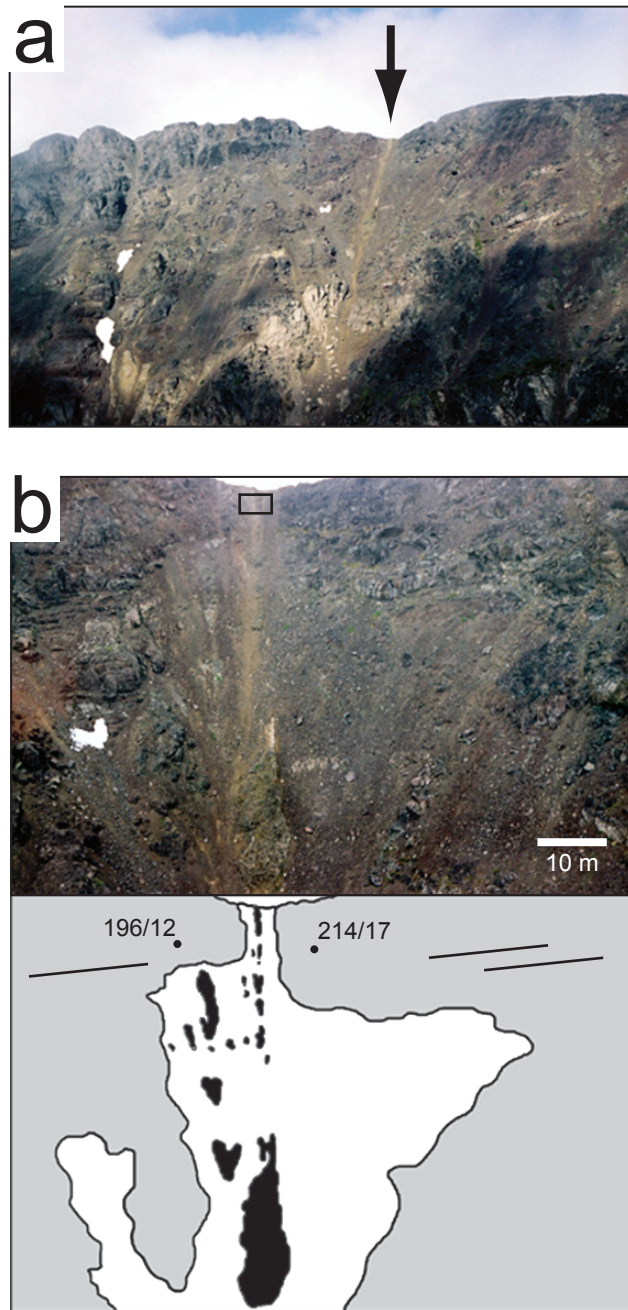


Figure 2.5 Field photographs and sketch showing the large-scale features of the dike. (a) Dike (beneath arrow) exposed in a 300 m steep cliff face, its trace downslope marked by light green-grey talus. (b) Photograph and sketch map of cliff face; dike and associated outcrop (black) intrudes Hazelton Group units (shaded) that dip gently to the south (two bedding measurements shown). Outcrop is often obscured by talus (white). Dike is 1 m wide at the top of the cliff but widens downslope to >7 m. Solid box denotes portion of dike that is enriched in mantle-derived xenoliths (see Figure 2.8).

The dike crosscuts all stratigraphic units; the dike and the associated xenoliths generally appear fresh and show no alteration or recrystallization, though some oxidation was observed in the dike rock at lower elevations. A small normal fault with an orientation of $192^{\circ}/76^{\circ}$ (dip direction/dip) and having an offset of ~ 1 m, crosscuts Hazelton stratigraphy in the nearby outcrop but does not crosscut the dike.

The following observations are based on a five-day field mapping program designed to delineate the extent of the dike, its stratigraphic relationships and the physical nature of its contacts against country rocks, and to collect a comprehensive sample suite of the xenoliths from the lithospheric mantle. The extent of the exposed dike was mapped to constrain the contacts and to understand the dike morphology (Fig. 2.6).

2.3.1 Dike

The dike varies in thickness, from ~ 1 m where both contacts are visible to ≥ 7 m; at its widest point, only a single contact is exposed (Fig. 2.6). The outcrop is intermittent due to talus coverage, but visible outcrop extends 107 m downslope, or more than 60 vertical metres. At the lowest elevation of the exposure, the dike is defined by a large 7 m wide outcrop. At higher elevations, it bifurcates to form two lithologically identical, connected dikes separated by 2–3 m of talus. Specifically, the body splits at 2025 m elevation into a 1–4 m thick arm that strikes directly upslope (325°) to the ridge top and another wider, shorter arm that strikes 310° uphill but terminates at 2049 m absolute elevation (Figs. 2.5, 2.6).

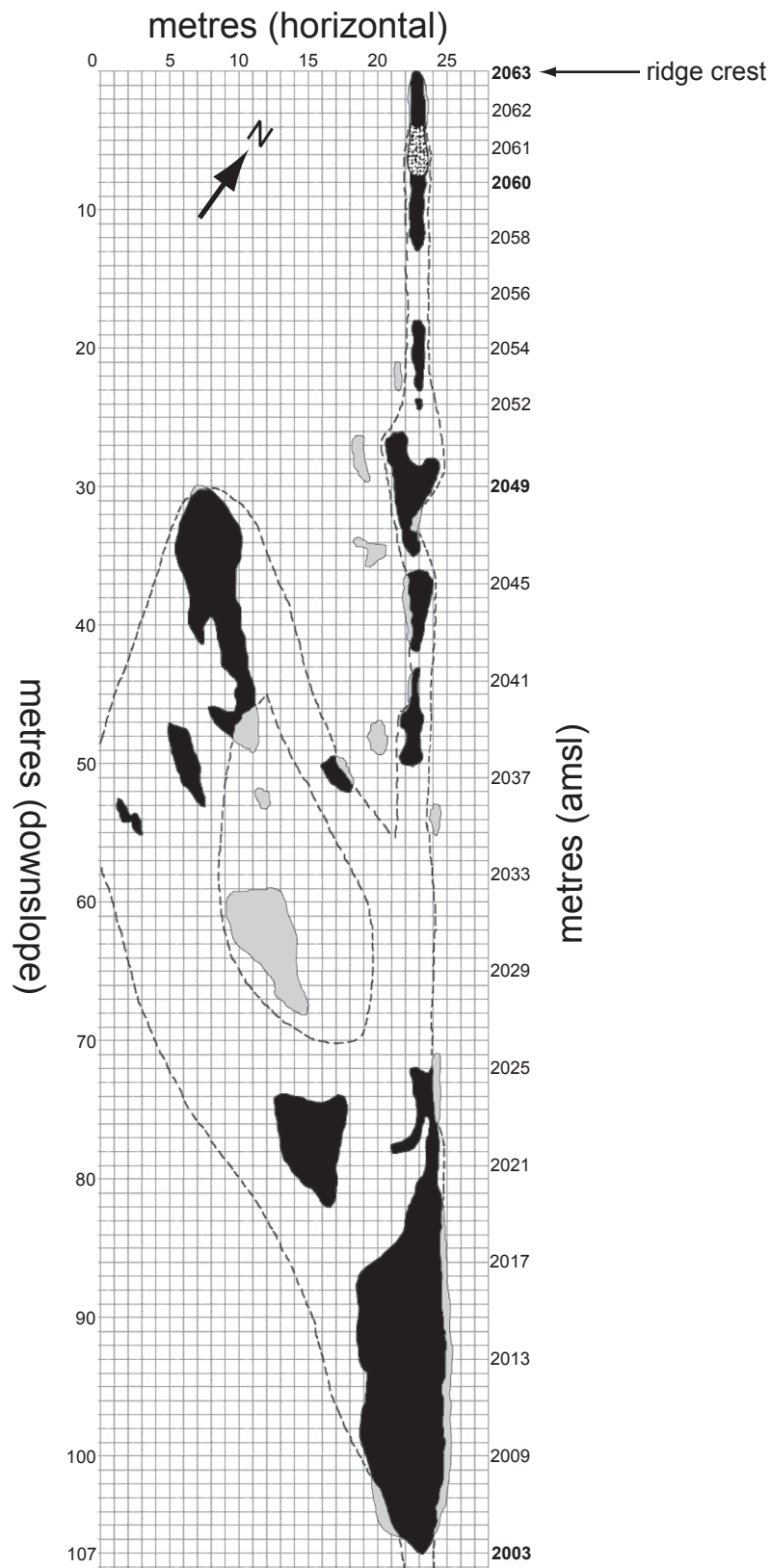


Figure 2.6 Map of dike (black) and country rock (shaded) outcrop, with xenolith-rich interval shown as textured. Dike exposures are limited by talus cover, but inferred contacts against Hazelton Group wall rocks are shown (dashed). Absolute elevations marked in bold denote a change in slope (and thus scale of elevation markers).

The dike is aphanitic and grey- to tan-coloured on fresh surfaces. Weathered surfaces are light grey to dark brown, or sometimes oxidized to a reddish brown colour. The dike is vesicular in many places, locally up to 30 % (Fig. 2.7a), with the vesicles varying from 0.5 to 10 mm in diameter. Banding on the scale of 5–10 cm is common, and is commonly defined or accentuated by changes in vesicularity (Fig. 2.7b). The larger vesicles are sometimes stretched. Vesicles are commonly filled or coated with fine grained material.

Locally, the dike has a fragmental character or appearance, with some ‘clasts’ of mafic rock visible within the dike. The clasts are commonly identified by changes in colour and vesicle characteristics (Fig. 2.7a). Clasts are only weakly vesicular but are surrounded by highly vesicular material. Clasts up to 10 cm in size were observed. The contact between clast and host magma is sharp and there are no indications of melting. However, the clast boundaries are locally accentuated by oxidation rinds up to 1 cm in width. These clasts constitute <1 % of the dike.

Contacts with country rock are abundant and sharply defined. The dike commonly displays one or more internal bands near the wall rock margin (Fig. 2.7c), which may represent chilled margin(s), or internal banding formed during emplacement. Marginal bands aside, physical properties such as xenolith content or vesicularity do not appear to change near the contact. Wherever contacts are visible, the country rock near the contact is partially melted. Melt is segregated into patches and lenses, which are sometimes vesicular. Commonly the lenses impart a foliation parallel to the contact. This contact zone varies in width from 10–30 cm. Wall rock samples collected at the maximum exposed distance away from a contact with the dike (approximately 1.4 m, limited by talus cover) appeared affected by the nearby intrusion.

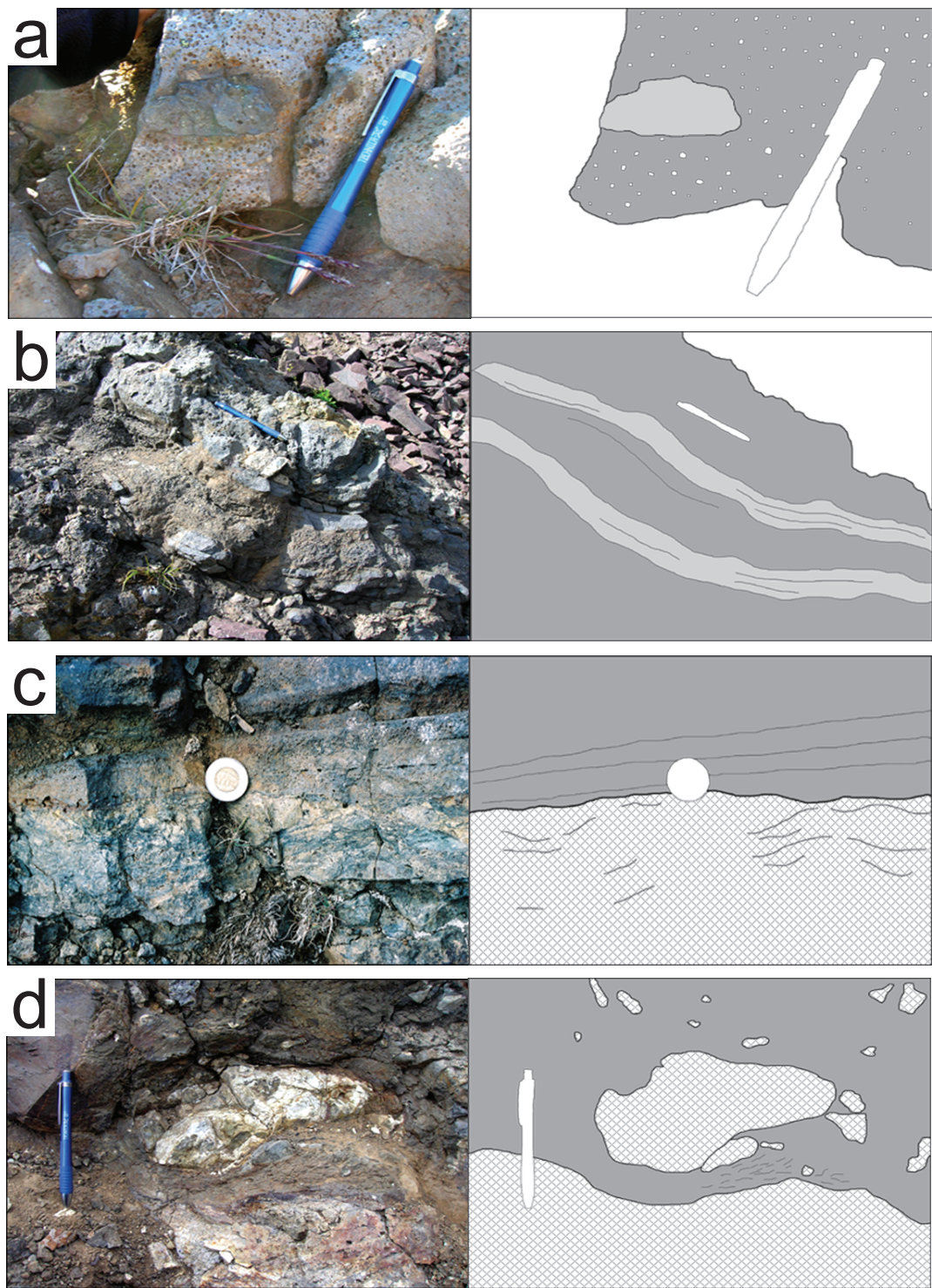


Figure 2.7 Field photographs and matching sketch maps showing specific volcanological aspects of the dike. (a) Vesicularity of the dike; photo includes a subrounded clast of melt within the vesicular dike, the clast showing several amygdules (pencil is 14 cm long). (b) Banding, defined by high (dark shade) versus low (light shade) vesicularity. (c) Nature of contact between the dike and the country rock, showing bands within dike, and melted wall rock. (d) Crustal xenolith within the dike derived from local country rock; contact between dike and wall rock is sharp.

2.3.2 Mantle xenoliths

Mantle-derived xenoliths are especially abundant in the interval 4–8 m from the top of the outcrop, where the dike narrows to 1 m in width (Fig. 2.8). Volumetrically they constitute 50–80 % of the dike over this interval (Fig. 2.8b) and are present over the entire width of the dike. This concentration of xenoliths commonly appears clast-supported within the dike rock. The mean diameter of xenoliths at this locality is ~15 cm; the largest xenolith measured was approximately 40 cm in diameter. There is no discernible sorting of the xenoliths within the dike either vertically or horizontally. In other areas of the dike, peridotite xenoliths constitute <1 % of the dike and none are more than 5 cm in diameter. There is no gradient in xenolith concentration; the upper contact between xenolith-rich and xenolith-poor dike rock is sharp and horizontal, and the lower contact is unclear, though xenolith abundance drops suddenly (Fig. 2.8a). The peridotite xenoliths are very well preserved and show no signs of reacting with the host magma, although many peridotite blocks are crosscut by one to several thin (1–5 mm) planar veins of melt. Xenolith angularity correlates inversely with size.

Individual xenoliths exhibit granular textures and rarely contain porphyroblasts, although there are substantial median grain size variations (~0.5–2 mm) between xenoliths. Coarse grained xenoliths are more friable than fine grained ones. About a third of the xenoliths show weak to moderate planar fabrics at the hand-sample scale. These fabrics are most easily seen in the finer grained samples and are less apparent in coarser grained samples. Planar fabrics include mineralogical banding and mineral foliation. Banding is observed as 1–3 mm wide bands of spinel, repeating on a 1 cm scale, or 2–3 mm wide indistinct bands of clinopyroxene, repeating on an approximately 1–2 cm scale. Larger scale segregations or possibly bands of olivine and clinopyroxene (1 cm width or greater) also occur. Foliation tends to be stronger (or more easily observed) in fine-grained samples, weakening with increasing grain size. Most commonly, the

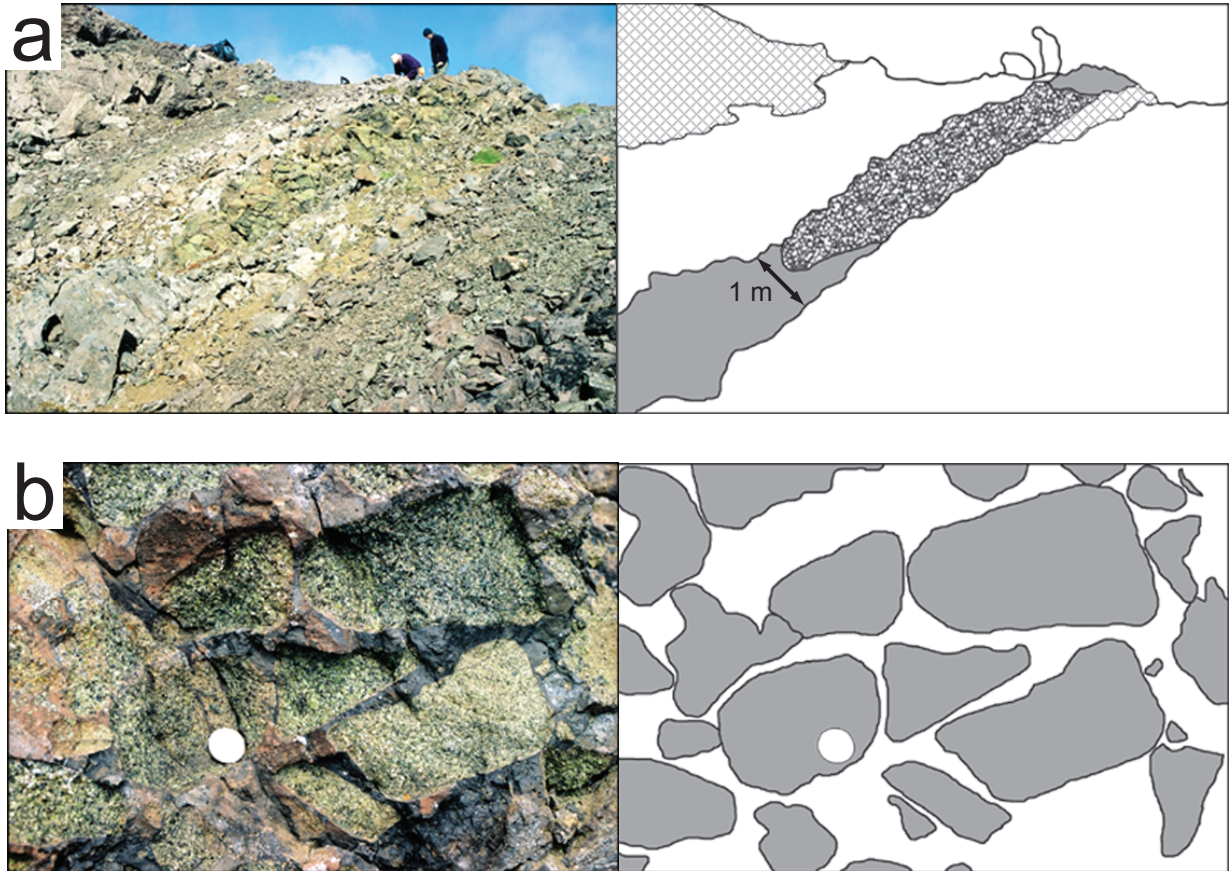


Figure 2.8 Field photographs and matching sketch maps showing detailed aspects of the peridotite-bearing facies of the dike. (a) Distribution of xenoliths (textured) in the dike (shaded) and contacts with wall rocks (crosshatched), showing the width of the dike where it intersects the ridge top. (b) Local relationships between the melt phase and the mantle-derived xenoliths (shaded). Xenoliths appear to be clast supported; they comprise ~60 % of the view. Coin is 2.8 cm in diameter.

foliation is defined by spinel grains, though clinopyroxene foliation was generally noted in the same samples.

2.3.3 Crustal xenoliths and xenocrysts

The dike also contains xenocrysts and crustal xenoliths. Xenocrysts of olivine (1–2 mm), presumably derived from the mechanical breakdown of peridotite, and large (2–5 cm) xenocrysts of orthopyroxene (possibly from xenoliths), are ubiquitous, although both types make up <1 % of the dike. Crustal xenoliths are more abundant and constitute more than 10 % of the dike in some areas (Fig. 2.7d). Crustal xenoliths are generally <5 cm in diameter, although two were observed that were ~30 cm in diameter. Angularity ranges from angular to rounded, and appears inversely related to size (i.e. largest xenoliths are most rounded). Some crustal xenoliths resemble nearby country rock, and do not show textures indicating heating. In contrast, others show textures indicating partial melting of the clasts and internal vesiculation, and cannot be correlated with observable wall rocks. One sample is a 20 cm diameter gabbro xenolith; it is relatively fresh and does not resemble any observable country rock. At the upper contact of the short arm of the dike, the contact with country rock is well exposed; the country rock appears melted, and angular clasts of the same are entrained within the dike. Crustal xenoliths are more abundant in the lower, more massive parts of the dike; in the upper 25 m of outcrop, the dike is more vesicular to massive, with much fewer crustal xenoliths. Where crustal xenoliths are most abundant, the dike surface commonly appears ‘knobby’ in texture.

2.4 Discussion

The highly vesicular nature of the dike suggests a shallow depth, near surface emplacement, and the partially fused wall rocks and metre-scale width suggests the passage of a

substantial volume of magma. This implies that the dike would have fed surface volcanic rocks, though none are extant; no young volcanic rocks have been reported in the immediate area (Gordee et al., 2005; Mahoney et al., 2005). There were also no unmetamorphosed volcanic rocks observed comprising the talus on the top or north side of the ridge. Parrish (1983) calculated uplift in the area of approximately 1 km in the last 10 Ma based on fission track data. The uplift and this location's already high altitude would result in more intense erosion than the surrounding lowlands; any fragile volcanic edifice such as a cinder cone would erode quickly, followed by any lava.

The fact that the upper boundary of mantle xenolith concentration is horizontal suggests that, if the concentration of xenoliths was the result of a gravitationally controlled process, no tectonic tilting has occurred since dike emplacement.

The dike is considerable in size, and even at the dike's narrowest part alteration is visible in the wall rock at least 1.4 m from the dike margin. This implies long term heat transfer from the dike—particularly if melting or plucking of wall rock eroded the original wall margin—and thus sustained magma flow or multiple magma pulses to supply a continual or renewable source of heat (Petcovic and Dufek (2005) and references therein). Discrete energetic pulses of magma within the dike may explain the abundance of crustal xenoliths and appearance of mafic, possibly juvenile clasts: if flow waned and the dike relaxed, brittle failure of the wall rock margins and the chilled dike margin may have occurred. This process may also be represented by the appearance of multiple internal margins seen at high levels of dike exposure, and the apparently active sampling of wall rock at the time of emplacement seen at lower levels of dike exposure. Another possibility is that there was sufficient vesiculation to promote fragmentation of the magma by primary vesiculation (Dingwell, 1996; Cashman et al., 2000). The existence of banding defined by varying degrees of vesicularity may represent magma fragmentation in the dike. Magma fragmentation within the dike, charged with volatiles (especially CO₂), followed

by coalescence and continued flow may have produced the bands and heterogeneous vesicle distributions. Dike vesicularity suggests that the exposed portion of this dike was at shallow crustal levels (<2 km?), or was rich in volatile-bearing (e.g. CO₂) fluids.

The concentration of peridotite xenoliths in a 4 m long interval in the dike is very unusual and has not been reported previously in the Cordillera. Through this interval, the width of the dike is at its narrowest observed. It is possible that this narrow passage resulted in a blockage of xenoliths, probably as they descended through the column of magma when flow became insufficient to buoy the rocks, considering that less dense crustal xenoliths are not included in the accumulation. Considering the grain-supported nature of the xenoliths in this interval, it may represent relaxation of the inflated dike, and the consequent trapping of xenoliths as the dike closed.

This site is well suited for mantle studies. There are several large xenoliths in the suite, the largest transported being approximately 40 cm in diameter, indicating that at least some xenoliths were rapidly transported to the surface (Spera, 1984). Because the dike is aphyric and mafic in composition, the magma would have had a high temperature and a low Newtonian viscosity (i.e. no yield strength) during flow. This implies rapid transport of xenoliths, if large, dense xenoliths are to be transported from the lithospheric mantle. Conventional ascent velocities for such magmas (Fujii and Scarfe, 1982; Spera, 1984) vary between 0.1 and 10 m/s, thus suggesting total transit times of between 1.4 hours and 5.8 days (assuming a source depth within the mantle lithosphere of 50 km). Given these estimated residence times, the xenoliths would have had limited time to react with the magma, ensuring preservation of pristine mantle mineral compositions (Edwards and Russell, 1998; Canil and Fedortchouk, 1999).

3. HOST BASANITE DIKE

The following chapter presents analyses and observations on the xenolith-bearing basanite dike at Mt. Preston. Analyses and measurements were conducted on two bulk samples: NP-MP05-1, which was sampled 1-10 m from the top of outcrop, and NP-MP05-3, which was sampled from the lowest 10-20 m of the dike outcrop (see Fig. 2.6 for dike map).

3.1 Petrography

The mineralogy of the dike rock (sample NP-MP05-1) comprises ~40 vol.% plagioclase, ~25 % olivine (≤ 0.5 mm), ~35 % clinopyroxene (≤ 0.2 mm), and ~3 % of ≤ 0.1 mm subhedral to anhedral crystals of ulvöspinel. Calcite occurs in ≤ 0.5 mm patches in the groundmass, and as larger subhedral grains (≤ 1 mm) filling or lining vesicles (Fig. 3.1). Minor phases include potassium feldspar, nepheline, and apatite. X-ray diffraction (XRD) conducted on samples from lined and filled vesicles from the dike reveal dominant calcite and minor vermiculite, the only hydrous mineral found in the rock. No glass was found in the dike rock.

Mineral compositions were determined by electron microprobe and methods are found in Appendix G. Plagioclase compositions are An_{21-71} ($An = 100 \cdot Ca / (Ca + Na)$). Olivine composition ranges from Fo_{38-83} ($Fo = 100 \cdot Mg / (Mg + Fe)$). Calcite in the groundmass and lining or filling vesicles has an X_{Ca} ($100 \cdot Ca / (Ca + Mg + Fe)$) of 97-99. Clinopyroxenes have an $Mg\#$ ($100 \cdot Mg / (Mg + Fe)$) of 70-73.

The dike rock (sample NP-MP05-1) is aphanitic and vesicular (Fig. 3.1), with an average of ~5 % vesicles. The plagioclase shows Carlsbad and polysynthetic twinning. In some areas, especially at the dike margins, the rock displays sub-trachytic texture with plagioclase. Some olivine crystals, especially large ones, feature corroded crystal boundaries.

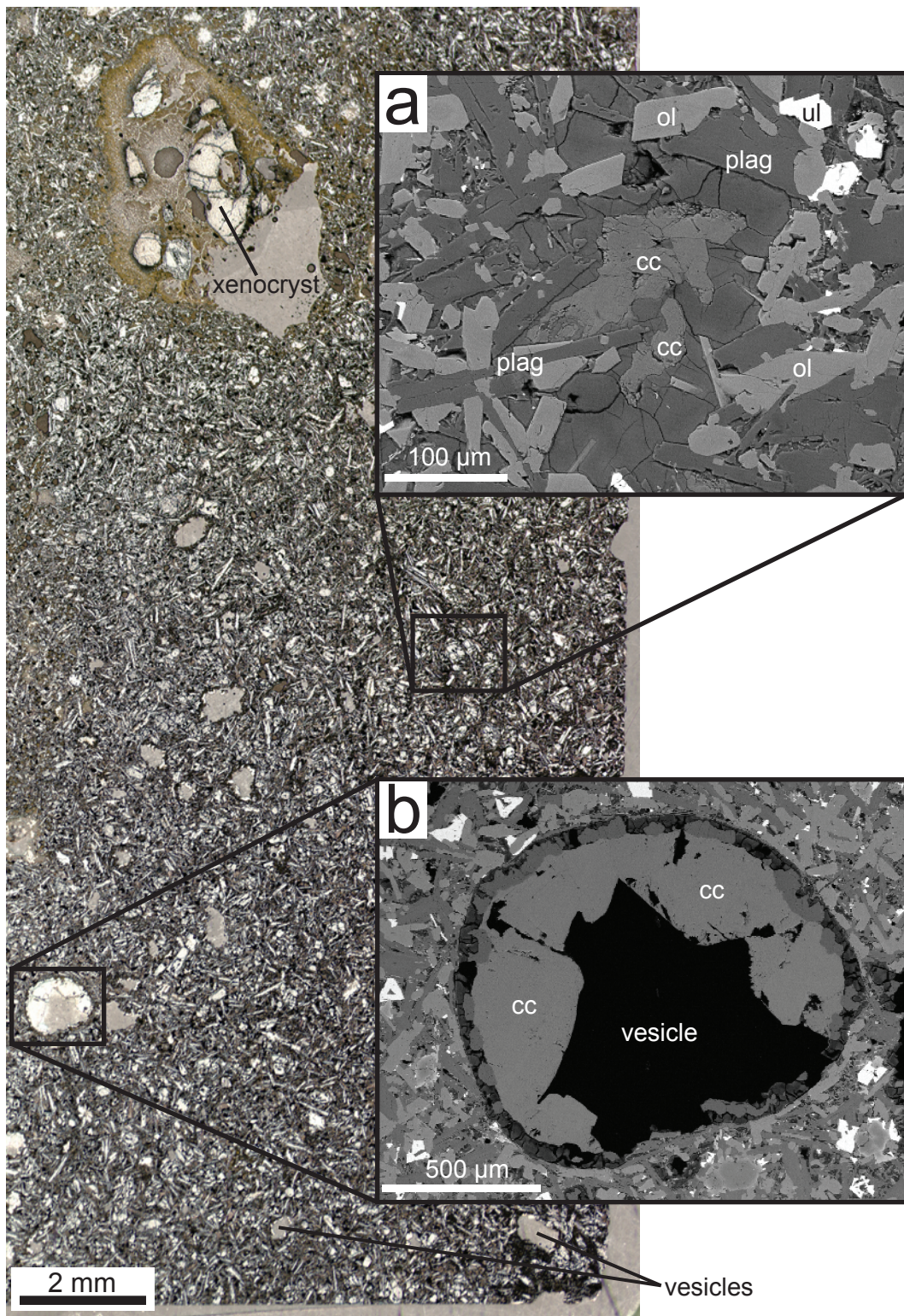


Figure 3.1 Photomicrograph and SEM (inset) images illustrating the fresh appearance of the dike, and the presence of vesicles and a mantle-derived xenocryst (labeled). Carbonate morphologies in the groundmass (a) and vesicles (b) are also shown. Minerals indicated are calcite (cc), olivine (ol), plagioclase (plag), ulvöspinel (ul).

Very large clinopyroxene or orthopyroxene crystals (>2 mm) are rare (Fig. 3.1) and are interpreted to be xenocrysts from mechanical breakdown of mantle xenoliths; their Mg-rich compositions (Mg# 90-91) are consistent with this interpretation.

Brown “feathery” alteration appears to weakly affect mafic minerals of the rock in faint but discrete waves. A similar weak alteration affecting the mafic minerals is commonly observed immediately surrounding (<50 μm) vesicles. This alteration overprints calcite at the vesicle margin.

The primary phases in the dike rock are similar in type and composition to other silica undersaturated basalts (e.g. Anderson et al., 2001). The very minor amount of hydrous minerals and the abundance of calcite in the groundmass and vesicles may indicate that the volatile components of the dike were H₂O-poor and CO₂-rich. The dike rock is fresh and shows no indication of post-emplacement alteration; the weak mafic alteration visible at vesicle margins and in the groundmass is attributed to interaction with trapped magmatic fluids during dike cooling. The presence of vesicles is indicative of vapour saturation in the magma during emplacement, and is consistent with shallow levels of intrusion.

3.2 Carbonate

Within the dike, calcite ($X_{\text{Ca}} = 97-99$) occurs in ≤ 0.5 mm patches in the groundmass (Fig. 3.1a), and as larger subhedral grains (≤ 1 mm) filling or lining vesicles (Fig. 3.1b). See Chapter 5 for isotopic data and discussion.

The carbonate lining and filling of vesicles suggests that CO₂ was a major component of a late-stage fluid phase that exsolved as the dike cooled. Lavas from the Llangorse Mtn. volcanic

suite (Harder and Russell, 2007) and the Cheslatta Lake volcanic suite (Resnick et al., 1999; Anderson et al., 2001) were examined for carbonate; both contained very little carbonate compared to the Mt. Preston dike, indicating that the lavas were able to efficiently degas.

Despite the problems inherent in comparing degassed lavas to a volatile-rich dike, it should be noted that in at least three other xenolith suites that contained mantle-derived carbonate (Ionov et al., 1993; Lee et al., 2000; Laurora et al., 2001), the lavas xenoliths were collected from also contained carbonate. This may indicate that these magmas originate enriched in CO₂ from carbonate or that as the magmas transit carbonated mantle lithosphere they scavenge enough carbonate to become significantly more CO₂ enriched (Ionov et al., 1993). Given these examples, primary carbonate in a mantle xenolith-bearing dike or lava should be considered a possible indicator of carbonate-bearing xenoliths.

3.3 Chemistry

Major element chemistry compositions are tabulated in Table 3.1; trace and rare earth elements are tabulated in Table 3.2. Representative samples from other volcanic groups (Cheslatta Lake suite, Chilcotin basalts, NCVP) are also tabulated. The sample from the lowest 10 m of the dike (NP-MP05-3A/B) is oxidized (indicated by low Fe²⁺/Fe³⁺, Table 3.1), and shows slightly higher SiO₂, lower TiO₂ and lower P₂O₅, which have been used to indicate the assimilation of some crustal material (e.g. Dostal et al., 1996). This is consistent with the much greater abundance of crustal xenoliths in the lower exposed sections of the dike. NP-MP05-1 (taken from the highest 10 m of the dike) is taken as the ‘fresh’ representative sample for comparison and discussion of parameters using major elements. Analytical methods are described in Appendix B.

Table 3.1 Whole rock major element contents (wt.%) and normative mineralogy of mafic dike samples from Mt. Preston, and lava samples from other regional volcanic suites for comparison.

Sample Suite	MP05-1	MP05-3	MP05-3 ²	ATR98-3308 ³	AT98-3305A ³	HF-18a ⁴
	Mt. Preston	Mt. Preston	Mt. Preston	Cheslatta Lk	Chilcotin	NCVP (Atlin)
Rock Type ¹	BAS	BAS	BAS	BAS	SAB	BAS
SiO ₂	43.11	45.47	45.46	43.90	48.50	44.24
TiO ₂	2.70	2.27	2.27	2.04	2.34	2.37
Al ₂ O ₃	12.99	13.55	13.61	12.6	13.5	13.06
Fe ₂ O ₃	2.76	10.15	10.26	3.9	4.6	2.90
FeO	9.35	2.56	2.69	8.2	7.8	9.80
MnO	0.182	0.177	0.179	0.19	0.17	0.19
MgO	10.91	10.13	10.25	11.46	7.36	10.69
CaO	10.59	9.82	9.75	8.91	7.95	9.45
Na ₂ O	2.33	2.85	2.88	3.2	3.3	3.51
K ₂ O	1.40	1.02	1.03	1.17	1.14	1.39
P ₂ O ₅	0.48	0.35	0.35	0.88	0.56	0.59
H ₂ O ⁺	0.74	0.41	0.40			-
H ₂ O ⁻	0.67	0.32	0.24	3.6	3.1	-
CO ₂	0.7	<d/l	<d/l	0.1	0.1	-
Total	98.24	98.75	99.14	100.15	100.42	98.19
FeO _{Total}	11.83	11.69	11.92	11.71	11.94	12.41
LOI	1.98	1.19	0.93	-	-	0.46
Calculated CIPW normative mineralogy (wt.%) based on whole rock composition ⁵						
Albite	10.51	16.87	16.41	15.11	28.77	10.10
Anorthite	21.15	21.55	21.43	16.86	19.04	15.86
Orthoclase	8.89	6.44	6.50	7.73	7.20	8.77
Nepheline	5.26	4.24	4.59	6.99	0	10.90
Diopside	20.33	21.29	20.95	18.35	14.21	22.94
Hypersthene	0	0	0	0	9.21	0
Olivine	23.73	22.31	22.81	26.45	13.32	23.29
Ilmenite	5.24	4.41	4.41	4.01	4.58	4.58
Magnetite	1.96	1.93	1.96	1.96	1.99	2.03
Apatite	1.16	0.83	0.83	2.11	1.34	1.39
Zircon	0.03	0.03	0.03	0.04	0.03	0.04
Chromite	0.06	0.07	0.07	0.10	0.04	0.07
Calcite	1.64	0	0	0.23	0.23	0

¹ BAS, basanite; SAB, subalkaline basalt; classified following Le Bas et al. (1986) and Le Bas (1989).

² Replicate sample, split before powdering.

³ Anderson et al. (2001).

⁴ Francis and Ludden (1995).

⁵ Normalized to 100%; Fe³⁺/Fe^{tot} ratio set at 0.1; Sr, Ba, Ni, Cr, Zr, and CO₂ included if available.

Table 3.2 Whole rock trace and rare earth element concentrations (ppm) of basaltic samples from Mt. Preston and other Cordilleran volcanic suites.

Sample Suite	MP05-1 Mt. Preston	MP05-3 Mt. Preston	MP05-3 ² Mt. Preston	ATR98-3308 ³ Cheslatta Lk	AT98-3305A ³ Chilcotin	HF-46 ⁴ NCVP (Atlin)
Rock Type ¹	BAS	AOB	AOB	BAS	BAS	BAS
Rb	28.3	16.6	16.8	43	20	25
Sr	690.9	520.3	513.9	980	480	840
Ba ⁵	521	332	342	690	380	532
V ⁵	256	235	241	167	202	234
Cr ⁵	281	335	348	460	226	382
Co ⁵	64	56	62	54	37	60
Ni ⁵	256	214	218	327	132	297
Zn ⁵	83	78	80	90	134	
Cu ⁵	93	84	83	45	49	
Ga	18.7	18.2	17.1	19	23	
Y	21.7	21.6	21.2	25	31.0	18
Zr	173.5	118.3	116.7	250	170	209
Nb	32.2	18.7	18.2	73	26	52
Th	3.7	2.5	1.9	4.8	1.7	4.2
U	3.9	2.5	2.7	1.4	0.64	1.0
Pb	<d/l	<d/l	<d/l	4	2	
La	24.94	16.96	19.04	52	18	38.2
Ce	49.60	35.61	39.88	100	41	74
Pr	6.37	4.94	5.46	12	5.8	
Nd	26.91	21.68	24.37	52	26	36
Sm	5.77	5.16	5.67	9.2	7.4	7.79
Eu	2.034	1.756	1.993	2.7	2.5	
Gd	4.38	3.97	4.47	7.2	7.6	
Tb	0.813	0.764	0.861	1	1	0.85
Dy	4.38	4.38	4.97	5	5.9	
Ho	0.741	0.823	0.924	0.78	1	2.45
Er	2.029	2.266	2.546	2.1	2.7	
Tm	0.259	0.318	0.369	0.26	0.36	
Yb	1.65	1.98	2.21	1.4	2.5	1.3
Lu	0.225	0.260	0.286	0.22	0.34	0.14

¹ BAS, basanite; AOB, alkali olivine basalt; BAS AND, basaltic andesite; classified following Le Bas et al. (1986).

² Replicate sample, split before powdering.

³ Anderson et al. (2001).

⁴ Francis and Ludden (1995).

⁵ By X-ray fluorescence.

The dike can be broadly characterized as an alkaline basalt, like many low volume isolated volcanic centres in British Columbia (e.g. Edwards and Russell, 2000). By the classification of Francis and Ludden (1990), which uses normative nepheline (ne) to classify lavas (Table 3.1), the dike is a basanite (>5 wt.% ne). It is also classified as a basanite by the Total Alkali-Silica (TAS) diagram (Fig. 3.2a) after Le Bas et al. (1986) and the supplemental classification for nephelinites and basanites by Le Bas (1989). The dike sample shows a sodic alkaline composition (Na:K of 2.5:1).

In terms of major elements the Mt. Preston dike sample is very similar to basaltic rocks from other locales (Table 3.1, Fig. 3.2a). The Mt. Preston dike sample has an SiO₂ content of 43.1 wt.%, an Mg# of 62 and contains 5 wt.% normative nepheline (Table 3.1); this is consistent with Cheslatta Lake Suite volcanic rocks (Anderson et al., 2001). Anderson et al. (2001) used Mg# and normative nepheline to contrast Cheslatta Lake and Chilcotin lavas, implying the Chilcotin lavas are unrelated to the dike as well. The normative nepheline and Mg# also distinguishes the dike from the Endako Group basaltic andesites to the east by its silica-poor composition and more alkaline character (Anderson et al., 1998). The dike sample has a lower H₂O/CO₂ than similar lavas from the Chilcotin and the Cheslatta Lake volcanics (Table 3.1). This is consistent with the ubiquity of carbonate in the Mt. Preston dike and the scarcity of carbonate in the Cheslatta volcanics (several lava samples from the sample suite of Resnick et al. (1999) were examined).

The dike sample Mg# is lower than that of volcanic rocks considered “primary” mantle melts (Mg# ~66-75; Wilkinson and Le Maitre (1987) and references therein), though its composition is primitive. If the dike did fractionally crystallize a phase (as the dike rock appears aphanitic), likely olivine, the dike composition nonetheless indicates a liquidus of >1250 °C (by MELTS modeling; 15 kbar, quartz-fayalite-magnetite oxygen buffer, variable H₂O content; Ghiorso et al., 1995; Asimow and Ghiorso, 1998). This temperature is above the range of

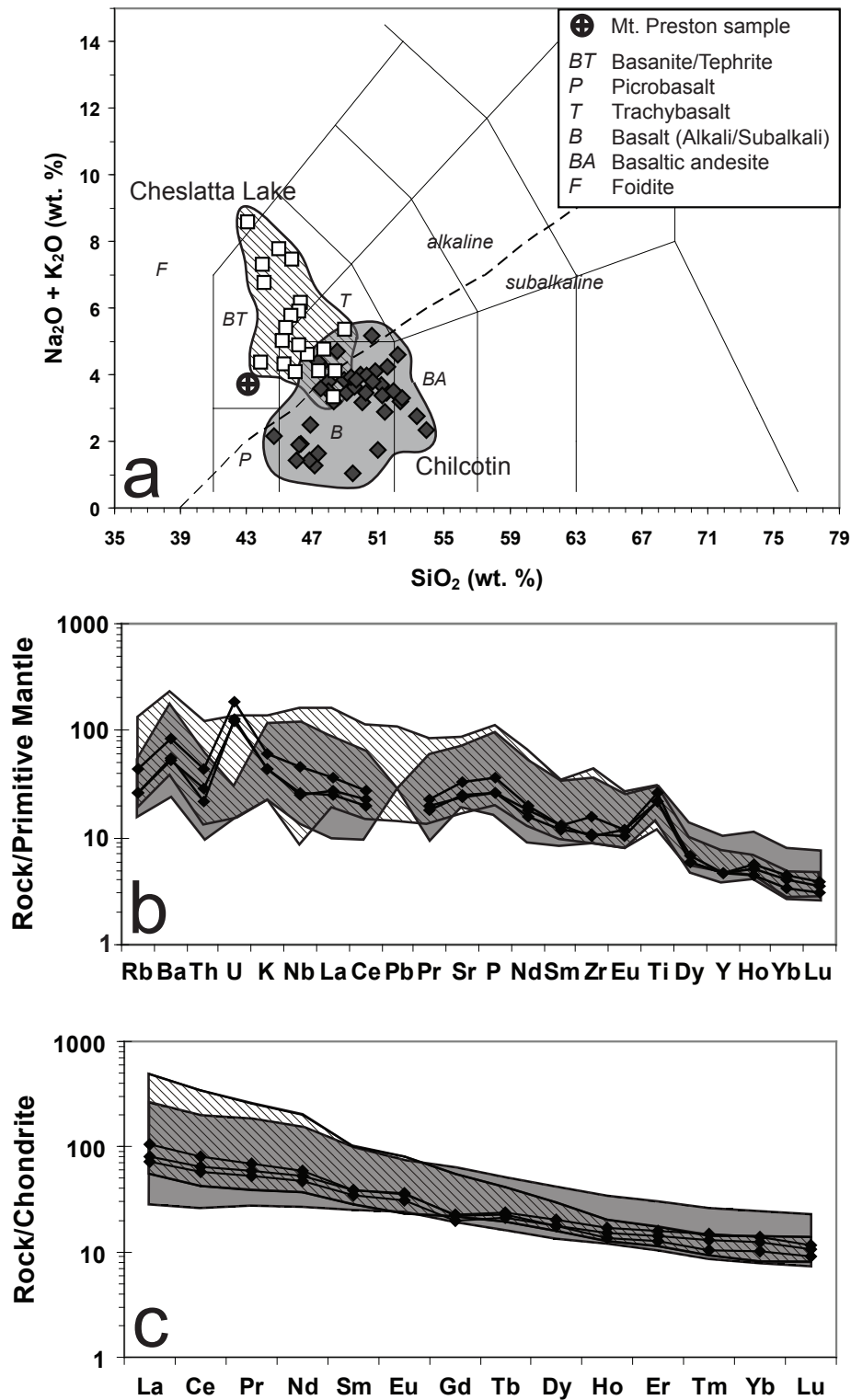


Figure 3.2 Major, trace, and rare earth element plots for the Mt. Preston dike and regional volcanic suites. (a) Total alkali vs. silica (TAS) diagram; alkaline-subalkaline division from Irvine and Baragar (1971). (b) and (c) Trace element and rare earth element abundance diagrams normalized to primitive mantle (Sun and McDonough, 1989) and chondrite (McDonough and Sun, 1995) respectively, for Mt. Preston and regional basaltic ($\text{SiO}_2 < 52$ wt.%) samples. Data from Anderson et al. (2001) and Dostal et al. (1996).

temperatures recorded by the mantle xenoliths sampled (see section 4.3.2) and those recorded in other xenolith suites (Harder, 2004 and references therein).

The dike samples are indistinguishable from the range of reported Chilcotin and Cheslatta Lake lavas in all trace elements but uranium (Table 3.2, Fig. 3.2b). The uranium content is at least 3 times higher than the most uranium-enriched Chilcotin basalt, but is approximately the same as the most uranium-enriched of the Cheslatta Lake suite. The uranium enrichment in the dike samples are likely a primary feature, as the uranium content of the wall rocks is lower than the dike rock (Table 3.2, B.2). Lead was below detection (1.0 ppm) in the dike samples, which is consistent with some samples from the Chilcotin and the Cheslatta Lake lavas. The trace elements are distinguished from the Endako Group basaltic andesites to the east by the Endako samples' positive Ba and negative Nb and Ti anomalies, though generally element concentrations are similar (Anderson et al., 1998). Dostal et al. (1996) found several quartz normative tholeiites with negative Nb and Ta anomalies in the Chilcotin suite, though generally Chilcotin and Cheslatta Lake (Anderson et al., 2001) lavas lack this feature; no negative anomaly is seen in the Mt. Preston samples (Fig. 3.2b). Negative Nb, Ta, and Ti anomalies are typical of subduction related calc-alkaline rocks (Pearce and Peate, 1995), as these high field strength elements (HFSEs) are usually not as easily transferred to the upper mantle from the subducting slab as large ion lithophile elements (LILEs) are.

Rare earth elements (REEs) for the Mt. Preston dike samples (Table 3.2, Fig. 3.2c) show highly fractionated REE profiles relative to chondrite, with enriched light rare earth elements (LREEs) relative to the heavy rare earth elements (HREEs). The samples have $La_N / Yb_N = 5.8-10.3$ and $Gd_N / Yb_N = 1.6-2.1$. It is similar in REE contents and patterns to the Cheslatta Lake and Chilcotin lavas, but dissimilar from basaltic andesites of the Endako Group, which show distinct Eu anomalies (Anderson et al., 1998). The relatively undepleted HREE contents have

been interpreted in other basalts from BC as representing a parental mantle melt originating in the spinel peridotite stability field (Dostal et al., 2008).

3.4 Ar-Ar Dating

Results of $^{40}\text{Ar}/^{39}\text{Ar}$ dating are presented in Figure 3.3 and Table C.1. The basanite dike sample has a plateau age of 18.72 ± 0.26 Ma, and the sample from the nearby small altered dike has a plateau age of 87.74 ± 0.71 Ma. The plateau and correlation ages were calculated using Isoplot 3.09 (Ludwig, 2003). Errors are quoted at the 2-sigma (95% confidence) level and are propagated from all sources except mass spectrometer sensitivity and age of the flux monitor. See Appendix C for details.

For these samples the plateau age is taken as the sample's crystallization age, as the dike of interest is relatively fresh, and the Hazelton dike shows only low grade alteration minerals such as serpentine and calcite.

The basanite dike has an early Neogene, early Miocene crystallization age. This indicates that the section of the dike studied was at shallow depth during emplacement, as there has only been 19 Ma since emplacement to unload overlying rock, in an area with an estimated 1 km of uplift in the last 10 Ma (Parrish, 1983). The age of the dike at Mt. Preston precludes a relation to the Anahim Volcanic Belt; within the framework of Anahim volcanism progressing eastward over time (Bevier et al., 1979), the nearest Anahim volcanic centre to Mt. Preston (the Rainbow Range) post-dates the Mt. Preston intrusion by at least 11 Ma (Bevier, 1978). Even when disregarding the Anahim age progression, the Mt. Preston dike pre-dates the oldest parts of the Anahim belt, the Bella Bella dikes, by 5 Ma (Baer, 1973; Souther, 1986). The basanite dike post-dates the Eocene volcanics and correlative intrusives to the east (the Ootsa Lake Group and the

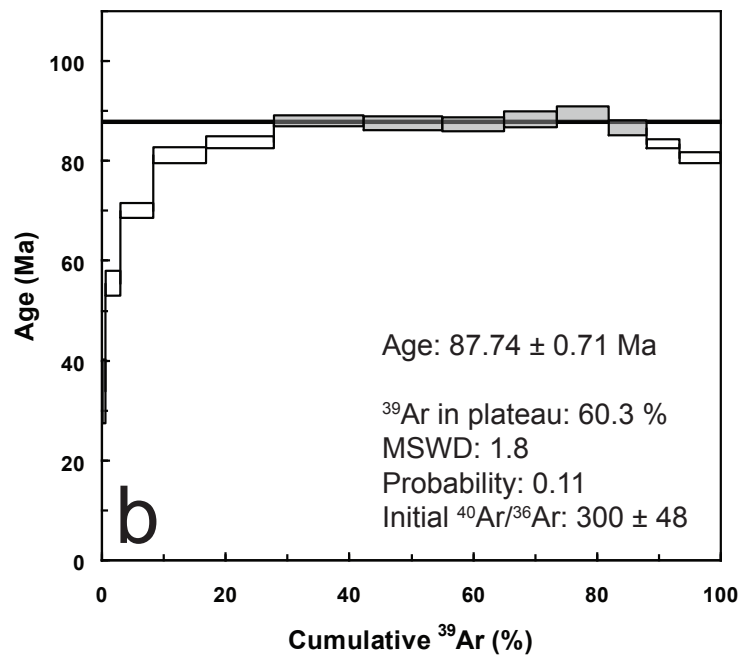
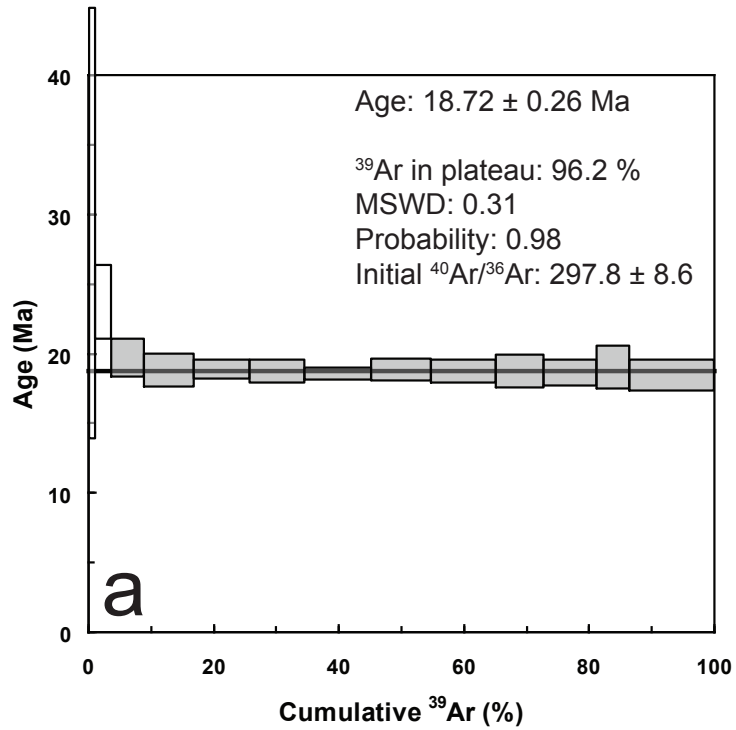


Figure 3.3 Release spectra graphs for $^{40}\text{Ar}/^{39}\text{Ar}$ dating of (a) the basanite dike (NP-MP05-3) and (b) the nearby metamorphosed dike (NP-MP05-2). Plateau steps are filled, rejected steps are open. Box heights and quoted errors are 2σ .

Endako Group), which were emplaced from 53-45 Ma (Grainger et al., 2001). However, the dike's age is consistent with other volcanic centres from the Cheslatta Lake suite, including the Quanchus Range (~20 Ma, K-Ar), which is closest to Mt. Preston; the date is broadly consistent with the eruptive history of the Chilcotin basalts (Anderson et al. (2001) and references therein).

The small altered dike near the basanite dike displays a late Cretaceous crystallization age. Gordee et al. (2005) described numerous similar basalt to andesite dikes that occur throughout the Mt. Preston area, intruding Hazelton group rocks. Based on cross-cutting relationships, Gordee et al. interpreted post-ca. 136 Ma ages for some of the dikes. Those inferences are consistent with the new Ar-Ar age.

3.5 Radiogenic Isotopes

Isotopic geochemical results are tabulated in Table 3.3, 3.4, and 3.5; methods are fully described in Appendix D and by Weis et al. (2006). Age corrections were not performed due to the young ages of the dike and other volcanic centres. In $^{207}\text{Pb}/^{204}\text{Pb}$ and $^{208}\text{Pb}/^{204}\text{Pb}$ isotope ratios (Fig. 3.4a, b) the Mt. Preston basanite dike is similar to other young volcanic centres within the Intermontane Belt, as well as centres from the Coast Belt and the Chilcotin basalts. However, in $^{206}\text{Pb}/^{204}\text{Pb}$ the basanite is far less radiogenic than all other centres reported in the Canadian Cordillera. On an epsilon Nd- $^{87}\text{Sr}/^{86}\text{Sr}$ diagram (Fig. 3.4c) all of the NCVP samples and the basanite dike plot in the depleted quadrant relative to bulk earth. The dike's composition is similar to other young volcanics from within the Intermontane Belt.

The Pb isotopic composition of the Mt. Preston dike source is depleted in ^{206}Pb relative to other Cordilleran volcanic centres, and departs from the Northern Hemisphere Reference Line (NHRL) of Hart (1984), a mixing line between Depleted Mantle (DM) and HIMU (High μ

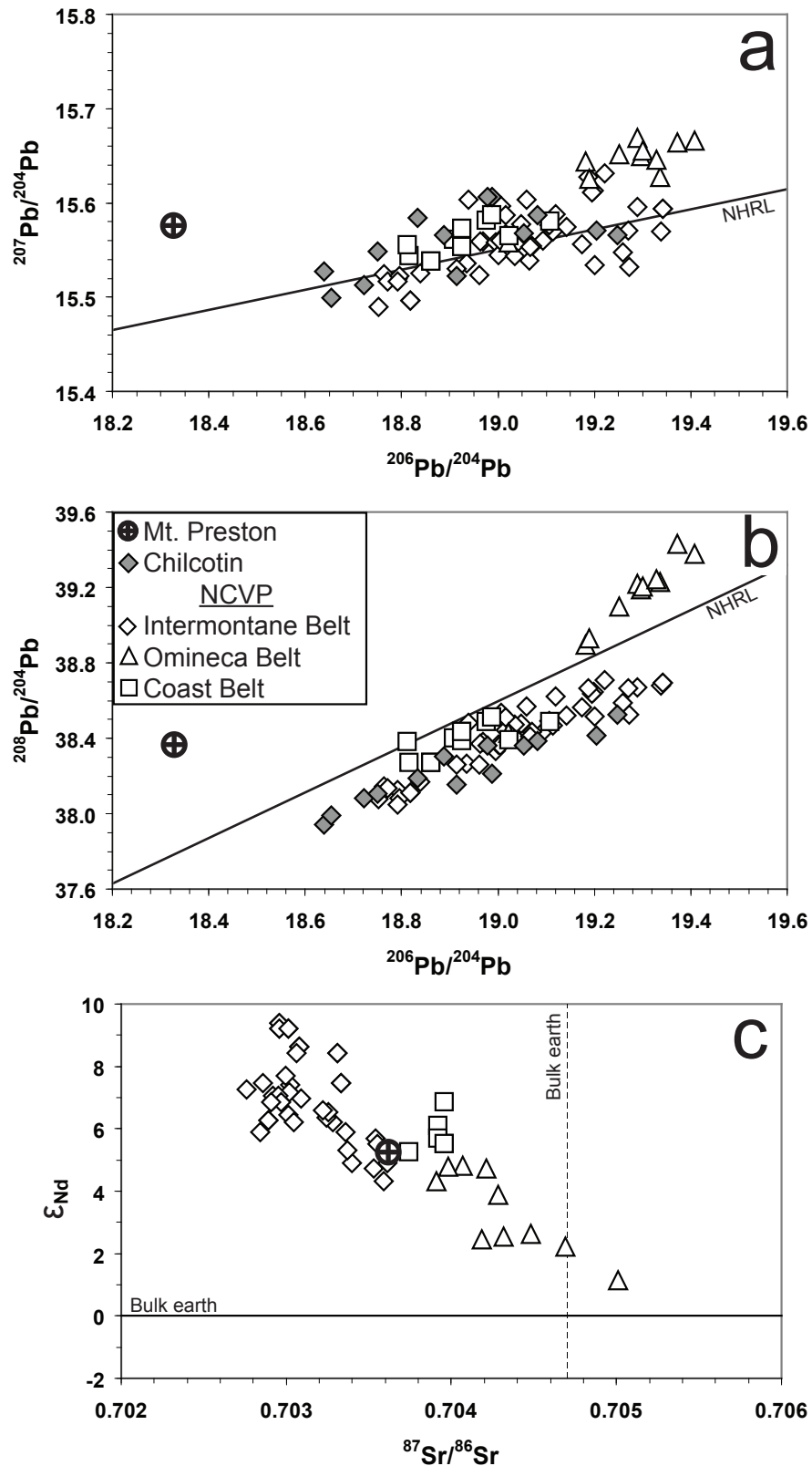


Figure 3.4 Isotopic composition of the Mt. Preston dike compared to basaltic samples from the NCVP (subdivided by tectonic belt) and the Chilcotin. NCVP data from Abraham et al. (2001) and references therein, and Abraham et al. (2005). Chilcotin data from Bevier (1983b). NHRL is Northern Hemisphere Reference Line (Hart, 1984). Epsilon Nd calculated using modern $^{143}\text{Nd}/^{144}\text{Nd}$ of 0.512638 for chondrite uniform reservoir (CHUR).

Table 3.3 Strontium isotopic composition of basanite dike whole rock, and standards used in analysis. Errors are 2σ .

Sample	$^{87}\text{Sr}/^{86}\text{Sr}$	Cycles	$^{86}\text{Sr}/^{88}\text{Sr}$
NP-MP05-3B	0.703615 ± 0.000010	108	0.1199
Standard			
SRM987 (600 ng)	0.710220 ± 0.000008	130	0.1195
SRM987 (300 ng)	0.710233 ± 0.000008	148	0.1200
SRM987 (600 ng)	0.710232 ± 0.000007	142	0.1192

Table 3.4 Lead isotopic composition of basanite dike whole rock, and standard used in analysis. Errors are 2σ .

Sample	$^{206}\text{Pb}/^{204}\text{Pb}$	$^{207}\text{Pb}/^{204}\text{Pb}$	$^{208}\text{Pb}/^{204}\text{Pb}$
NP-MP05-3B	18.3277 ± 0.0008	15.5757 ± 0.0007	38.3663 ± 0.0020
Standard			
NBS 981	16.9416 ± 0.0012	15.4995 ± 0.0011	36.7205 ± 0.0028

Table 3.5 Neodymium isotopic composition of basanite dike whole rock, and standards used in analyses. Errors are 2σ . Epsilon Nd calculated using modern $^{143}\text{Nd}/^{144}\text{Nd}$ for chondrite uniform reservoir (CHUR) of 0.512638.

Sample	$^{143}\text{Nd}/^{144}\text{Nd}$	Cycles	$^{145}\text{Nd}/^{144}\text{Nd}$	$^{146}\text{Nd}/^{144}\text{Nd}$	ϵ_{Nd}
NP-MP05-3B	0.512908 ± 0.000008	115	0.348403 ± 0.000005	0.7202	5.3
Standard					
La Jolla (150 ng)	0.511856 ± 0.000006	118	0.348411 ± 0.000005	0.7200	
La Jolla (150 ng)	0.511855 ± 0.000007	115	0.348407 ± 0.000004	0.7208	

($^{238}\text{U}/^{204}\text{Pb}$) mantle reservoirs which most northern hemisphere MORBs and OIBs follow, relative to other Cordilleran centres. Because U, Pb, and Th are concentrated into silicic reservoirs like continental crust, old continental crust is highly enriched in radiogenic Pb isotopes. In addition, the dominance of ^{238}U in natural uranium, which decays to ^{206}Pb , makes ^{206}Pb a very sensitive measure of crustal contamination. The low $^{206}\text{Pb}/^{204}\text{Pb}$ relative to other Cordilleran centres suggests that old continental crust was not assimilated this magma. In addition, the $^{206}\text{Pb}/^{204}\text{Pb}$ is less than that of Cordilleran spinel lherzolites from the Yukon (~ 19.07 ; Carignan et al., 1996). However, the fact that ^{206}Pb is the only Pb isotope which shows significant departure from other volcanic centres, and Sr and Nd are also similar to other locales, indicates that a duplicate analysis should be conducted.

Relative to bulk earth the Mt. Preston dike is depleted in ^{87}Sr and enriched in ^{143}Nd , indicating a depleted mantle source region. The isotopic composition lies on the mantle array between depleted mantle and bulk silicate Earth reservoirs, similar to other Cordilleran basaltic volcanic centres. It is also consistent with the isotopic compositions of Nd and Sr, and MgO content, from volcanics erupted in the Intermontane Belt in the NCVP (Abraham et al., 2001).

Crustal contamination has been used to explain isotopic heterogeneities between eruptive centres in British Columbia (Cousens and Bevier, 1995). Abraham et al. (2001) interpreted isotopic heterogeneities in NCVP volcanic centres as largely representative of the composition of the mantle lithosphere beneath the sampled volcanic centre, due to correlations between isotopic variations and tectonic features and processes. The Nd, Sr, ^{208}Pb , and ^{207}Pb compositions closely follow those of other young volcanic centres in the Cordillera, suggesting the isotopic composition of the Mt. Preston dike is representative of its source region. If a duplicate ^{206}Pb analysis verifies the current value, the isotopic heterogeneity likely represents compositional differences in the mantle source region, and thus a mantle source significantly different from other young BC volcanics.

3.6 Oxygen Isotopes – Silicates

When compared to other primitive mantle melts, the ^{18}O composition of the dike's silicates is a tool for evaluating the degree of contamination the dike magma experienced in the source region or during emplacement (e.g. Garcia et al., 1998; Harmon and Hoefs, 1995); post-emplacement events would also alter the isotopic composition, e.g. metamorphism in the presence of ^{18}O -depleted meteoric fluids. Bulk silicate oxygen isotope compositions are presented in Table 3.6. Details of sample preparation and analysis are summarized in Appendix E. The dike's silicates (i.e. carbonate absent) have a $\delta^{18}\text{O}$ composition of approximately 5.8 to 6.5 ‰.

The dike was emplaced at or near liquidus temperatures (based on its aphanitic texture); chemical components from xenoliths or the wall margin that were fused by the high temperature dike would have been able to mix with the magma. Despite the prevalence of crustal xenoliths in parts of the dike, the appearance of fused and vesiculated crustal xenoliths, and the melted dike margin, there is no evidence for contamination based on the dike's oxygen isotope composition. The oxygen isotope composition of the bulk silicates is near mantle values (see Fig. 5.8), and of a typical value for alkaline continental intraplate basalts (Harmon and Hoefs, 1995). Matthey et al. (1994) found that the $\delta^{18}\text{O}$ of basaltic melts could not be in equilibrium with the mantle with compositions above 6 to 6.5 ‰, depending on the peridotite solidus. Thus the ^{18}O composition of the Mt. Preston dike does not imply significant enrichment from crustal sources, or post-emplacement alteration.

Table 3.6 Oxygen isotope composition of silicate minerals (acid leached whole rock powder) from the basanite dike.

Sample	Yield ($\mu\text{moles CO}_2/\text{mg}$)	$\delta^{18}\text{O}$ (‰ vs. VSMOW)
NP-MP05-1	10.3 ± 0.2	6.5 ± 0.2
NP-MP05-1 ¹	10.2 ± 0.2	5.8 ± 0.2

¹ Duplicate analysis.

3.7 Discussion

The dike rock samples do not show chemical indications of high degrees of contamination, though the major elements in a sample taken from the crustal xenolith-rich lower area of the dike may have been affected. The samples are chemically similar to lavas from the Cheslatta Lake volcanic suite (Anderson et al., 2001), even those that lack crustal and mantle xenoliths. This implies very little contamination of the magma occurred. This interpretation is corroborated by the ^{18}O isotope value of the dike silicates, which shows a typical composition of continental intraplate basalts, the high $^{143}\text{Nd}/^{144}\text{Nd}$ and low $^{87}\text{Sr}/^{86}\text{Sr}$ and $^{206}\text{Pb}/^{204}\text{Pb}$ isotope values, which reflect a depleted mantle source region uncontaminated by radiogenically enriched crust. When taken together, the chemical attributes, along with physical observations such as the presence of large dense xenoliths, suggests the dike was a primitive swiftly emplacing mantle melt that did not interact significantly with evolved crustal sources.

The Mt. Preston dike shows many similarities to the Cheslatta Lake suite defined by Anderson et al. (2001). The dike's composition is mafic and sodic alkaline (compositionally a basanite), carries mantle-derived xenoliths, and is consistent geographically and temporally with the Cheslatta Lake suite. The Mt. Preston dike is thus grouped with the Cheslatta Lake suite, and defines the suite's southwestern margin.

Bevier (1983a, 1983b) interpreted the Paleogene-Neogene magmatism of the Chilcotin basalts in south-central British Columbia as the result of asthenospheric melting in the back-arc of the Pemberton volcanic belt and Masset Formation. Dostal et al. (1996) found that the composition of most Chilcotin basalts could be obtained by fractional crystallization of a partial melt of a heterogeneous garnet-bearing mantle source, which was interpreted as asthenospheric. They noted that most Chilcotin basalts resemble ocean island basalts (OIBs), and that an asthenospheric source is consistent with their Pb and Sr isotopic compositions. A subduction-

altered subcontinental lithospheric mantle (SCLM) was interpreted as the source rock of the minority of Chilcotin basalts that do not resemble OIB (quartz-normative LILE-enriched tholeiites). Anderson et al. (2001) adhered to the interpretation of asthenospheric back-arc melting when defining the Cheslatta Lake suite; one site studied by Dostal et al. (1996) (Poplar Buttes) was defined as part of the Cheslatta Lake suite.

The Mt. Preston dike samples appear unrelated to the Eocene-aged volcanics and correlative intrusives (called the Challis-Kamloops belt by Souther (1991)) that form an inland belt in the Canadian Cordillera, extending from central British Columbia to the northwest United States. Different parts of the belt have been interpreted as the result of arc volcanism, rifting in an arc, arc to intraplate magmatism related to a slab window, and decompression melting; arc processes are the dominant hypothesis in British Columbia (Ickert et al. (2009) and references therein). The volcanic belt is typically characterized as calc-alkaline with moderate to high-K content (Dostal et al., 2008), though compositions vary from mafic to felsic (e.g. Dostal et al., 2008; Grainger and Anderson, 1999; Dostal et al., 1998; Haskin et al., 1998). To the northeast of Mt. Preston are the Eocene volcanics of the Buck Creek basin, near the northernmost extension of the Challis-Kamloops volcanic belt, and to the east are the Ootsa Lake and Endako Groups. The Buck Creek basin rocks show chemical indications of being derived from lithospheric mantle enriched by subduction processes, related to Resurrection/Eshamy/Kula plate subduction in the Eocene (Dostal et al., 1998, 2001). The Ootsa Lake and Endako Group rocks range from basaltic andesite to rhyolite in composition (Grainger and Anderson, 1999; Haskin et al., 1998), and are also interpreted as the products of Eocene arc volcanism. Mt. Preston would have been in the forearc region of this Eocene arc.

4. MANTLE XENOLITHS

More than 150 xenoliths were collected from Mt. Preston (see Appendix A). A representative group of 51 xenoliths from the suite collected from Mt. Preston was studied in detail, and is the subject of this chapter. They are all spinel-bearing mafic rocks, generally comprising olivine, orthopyroxene, clinopyroxene, and spinel. All 51 samples studied contain carbonate as an accessory phase.

4.1 Petrography

All mantle xenoliths in the Mt. Preston suite are spinel-bearing. None contain garnet and there is no evidence of garnet replacement. The only plagioclase-bearing xenolith also contains spinel.

Individual xenoliths exhibit granular textures and rarely contain megacrysts, although there are substantial median grain size variations ($\sim 0.5\text{--}2$ mm) between xenoliths (Fig. 4.1). The xenolith suite is dominantly lherzolitic in composition, although it also contains minor websterite, harzburgite, and dunite (Fig. 4.2; Tables 4.1, G.2).

Of the 51 xenolith samples studied in detail, 48 have olivine (ol), clinopyroxene (cpx), orthopyroxene (opx), spinel (sp), and accessory carbonate (Fig. 4.1a). Three xenoliths differ from this mineral assemblage: two websterites that lack olivine, of which one (NP-MP05-69) contains plagioclase (Fig. 4.1b), and a dunite that does not contain orthopyroxene.

Coarse (>3 mm) pyroxene grains commonly show exsolution lamellae (Fig. 4.1c). Spinel occurs as anhedral grains and is brown in colour; spinel is green in the websterite with plagioclase. Olivine grains are commonly the largest phase (≤ 5 mm), although, rarely, samples feature orthopyroxene megacrysts which are up to 10 mm in diameter. No hydrous minerals or

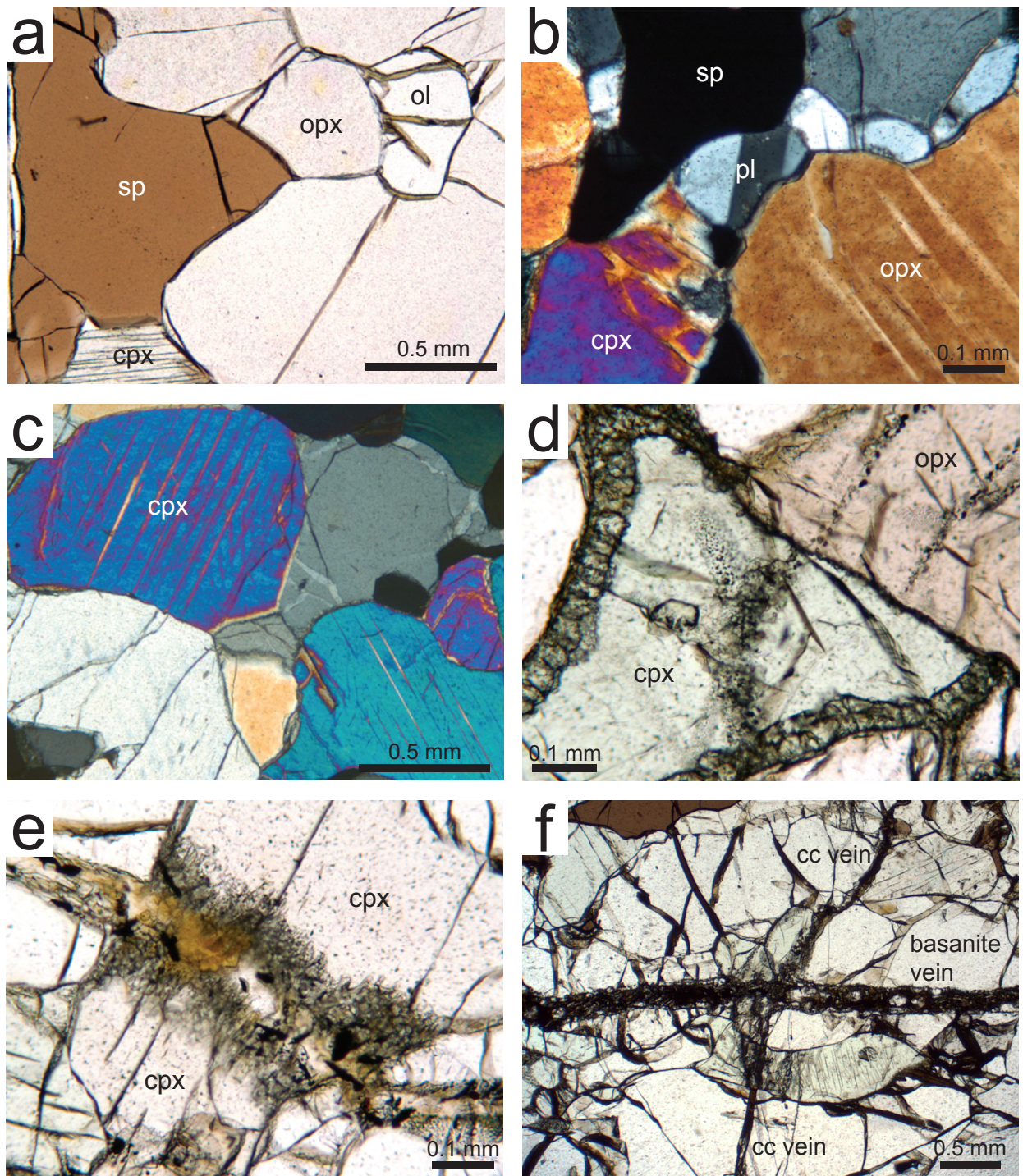


Figure 4.1 Photographs under plane (a, d, e) and crossed (b, c) polarized light for mantle xenoliths from Mt. Preston, showing: (a) equilibrium texture between phases; (b) plagioclase (pl) in a spinel (sp)-plagioclase websterite; (c) exsolution lamellae in clinopyroxene (cpx); (d) disequilibrium texture indicated by reaction coronae on clinopyroxene; (e) disequilibrium texture in clinopyroxene, associated with a veinlet of basanite; and (f) a basanite vein cross-cutting a calcite (cc) vein. Orthopyroxene (opx) and olivine (ol) are also labeled (a, b, d).

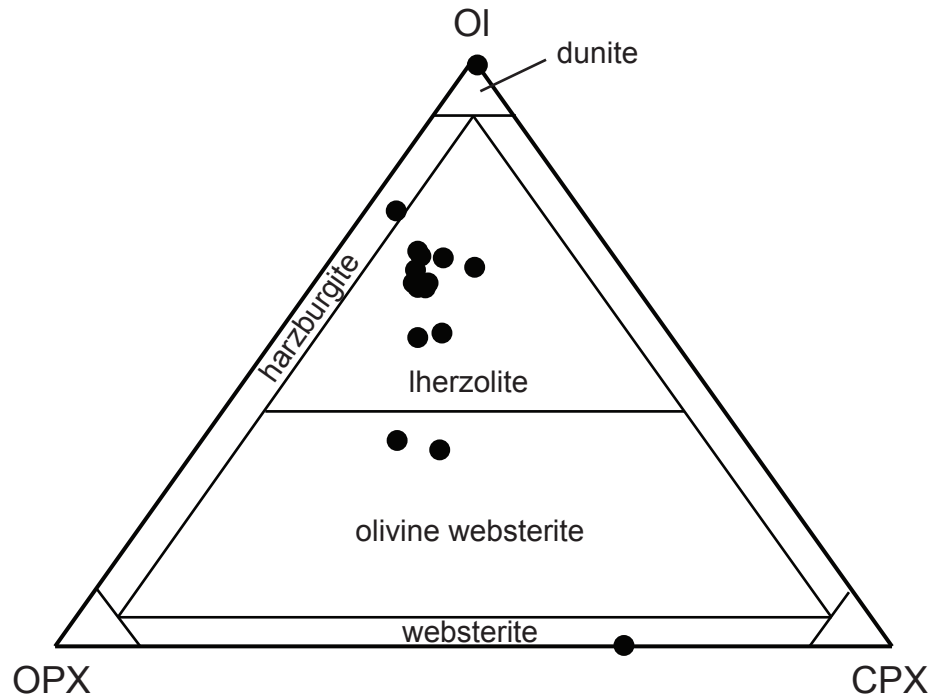


Figure 4.2 Modal compositions of 15 representative xenoliths from Mt. Preston. Modal abundances (wt.%) determined by Rietveld X-ray diffraction analysis, with sums of OPX, CPX, and olivine normalized to 100 % to obtain proportions.

Table 4.1 Modal mineralogy (wt.%) and statistics of analysis for selected mantle xenolith samples, by the Rietveld method.

Sample	Olivine	Orthopyroxene	Clinopyroxene	Spinel	Calcite	R _{wp}	d	χ^2
NP-MP05-31	59.2	24.5	13.8	1.9	0.7	6.03	1.24	1.52
NP-MP05-35	65.4	22.7	10.8	1.0	0.2	5.56	1.32	1.40
NP-MP05-35 ¹	65.8	22.5	9.9	1.4	0.5	5.60	1.28	1.42
NP-MP05-44	62.5	24.3	11.2	1.8	0.2	5.63	1.36	1.42
NP-MP05-50	60.5	25.7	12.1	1.5	0.2	5.70	1.34	1.44
NP-MP05-69 ²	<d/1	26.8	62.9	5.3	<d/1	7.23	1.16	1.44
NP-MP05-70A	59.4	25.4	12.9	1.9	0.4	5.80	1.43	1.45
NP-MP05-78	62.5	17.0	17.8	2.1	0.6	5.60	1.25	1.43
NP-MP05-79A	31.8	35.6	28.4	3.6	0.6	5.79	1.30	1.38
NP-MP05-139	50.8	25.8	19.1	3.7	0.6	5.64	1.34	1.42
NP-MP05-159A	60.2	23.8	13.7	1.9	0.3	5.41	1.36	1.38
NP-MP05-160A	50.7	29.3	16.9	2.7	0.4	5.13	1.38	1.30
NP-MP05-160B	98.4	<d/1	1.4	0.2	<d/1	4.86	1.45	1.38
NP-MP05-161D	73.0	21.8	4.1	1.1	<d/1	6.00	1.23	1.54
NP-MP05-162A	33.4	39.8	22.8	3.8	0.3	5.86	1.28	1.42
NP-MP05-164A	64.2	19.9	13.4	2.1	0.5	5.50	1.45	1.38

R_{wp} = Weighted profile residual (residual, weighted to be insensitive to point density). Reported as a percentage.

d = Durbin-Watson statistic (measure of serial correlation of residual). Range of 0 to 4, ideal value of 2.

χ^2 = Reduced chi-square (measure of goodness of fit to data).

¹ Replicate sample based on splitting of sample before powdering.

² Sample contains 5.1 % plagioclase.

glass was observed. One olivine-absent websterite contains 5 % plagioclase (An_{61-70}) by volume (Table 4.1). Some plagioclase grains feature polysynthetic twinning and all appear texturally equilibrated (granoblastic texture) with neighbouring phases.

Calcite grains and/or veins are found in all xenoliths, and are commonly associated with sulfides (pentlandite and chalcopyrite). A small rutile grain was found included in one calcite grain. See Chapter 5 for full descriptions. Calcite veins (≤ 0.1 mm wide) appear as intergranular and crosscutting features; when in contact with clinopyroxene, ≤ 0.2 mm wide reaction zones are occasionally seen. Some xenoliths also contain some brown fine-grained veins which appear as intergranular or cross cutting features. The veins do not appear to be composed of glass, and they do not appear to be the result of the degeneration of any particular phase.

Equilibrium (i.e. granoblastic) textures are common (Fig. 4.1a). However, in some samples there are grains showing reaction zones at the margins, indicative of disequilibrium (Fig. 4.1d). These are commonly related to contact with basalt veins or at the xenolith margin; less commonly they are related to carbonate grain or vein contact. In this context reaction margins are < 0.3 mm wide. In one sample (NP-MP05-160B) spinel and clinopyroxene feature reaction coronae (< 0.5 mm wide) around entire grains, commonly without observable vein contacts.

Linear inclusion trails (≤ 2 mm wide; Figs. 4.1d, 5.3c, 5.5b) are observed in all 51 xenoliths examined in thin section; these appear as “dusty” fine trails, and some include discrete (≤ 0.1 mm diameter) calcite and/or sulfide inclusions. These inclusion trails affect pyroxenes preferentially, and some can be traced over 2 cm across thin sections, crossing multiple phases.

Sparse veinlets of basanite crosscut all features (Fig. 4.1e), including carbonate veins. Grains in contact with basalt veins commonly show a reaction zone (≤ 0.3 mm wide) at the vein margin, preferentially affecting pyroxenes.

Carbonatite metasomatism of mantle peridotite classically shows orthopyroxene dissolution, a trend towards wehrlite (i.e. replacement of orthopyroxene by clinopyroxene), and the presence of apatite (Yaxley et al., 1991; Rudnick et al., 1993). None of these features were observed in the Mt. Preston xenoliths, though these phases and textures are not always seen in carbonatite-metasomatised mantle rocks (Lee et al., 2000). The Mt. Preston xenolith suite lacks hydrous minerals like phlogopite or amphibole that indicate hydrous metasomatism. There is also no metasomatic (secondary) mineral crystallization (e.g. clinopyroxene, phlogopite, rutile) with compositions differing from the peridotite host that would suggest silicate metasomatism (Lee et al., 2000).

It has been argued that the reaction rims on clinopyroxene and spinel are the result of reacting peridotite with silica-undersaturated high temperature magma (Francis, 1987; Shaw et al., 2006). While this is a definite cause for the reaction zones next to melt veins, the textures next to carbonate grains or veins are more ambiguous, and may be related to high temperature carbonate enrichment. Another carbonated xenolith suite (Laurora et al., 2001) included samples that had been more heavily metasomatized, resulting in reaction rims on clinopyroxenes. This is similar in appearance to the pervasive reaction rims on pyroxenes in one Mt. Preston xenolith (NP-MP05-160B).

Inclusion trails within the Mt. Preston peridotites almost exclusively affect pyroxenes. Preferential metasomatism of pyroxenes has been noted by others (e.g. Matthey et al., 1994); intruding metasomatic agents likely exploit the pyroxenes' crystallographic pathways such as exsolution lamellae and cleavage planes (Perkins et al., 2006). Other metasomatised xenolith suites (e.g. Iherzolites and websterites from New Mexico; Perkins et al., 2006) commonly display inclusion trails similar to those from the Mt. Preston suite. These features, and the fact that basanite veins crosscut carbonate veins, is strong evidence for a carbonate source within the mantle lithosphere.

4.2 Mineral Modes

Mineral modes for 15 xenoliths are presented in Table 4.1, and plotted on a classification diagram in Figure 4.2. Modes are determined by the Rietveld method (see Appendix F) and normalized to 100 wt.%. Modal percent olivine varies from below detection to 98, clinopyroxene from 1 to 65, orthopyroxene from below detection to 40, and spinel from below detection to 5. Calcite is below detection in several xenoliths; it is always <1 wt.%. Several xenoliths' diffraction patterns included a small unidentifiable peak corresponding to clay minerals.

The xenolith suite is unimodal (i.e. lherzolite-dominated) by the definition of Shi et al. (1998), indicating that this suite is part of relatively fertile mantle lithosphere. Most xenolith suites in the Canadian Cordillera are unimodal; bimodal suites which contain more harzburgites have been found in northwestern BC and southern Yukon (Shi et al., 1998).

4.3 Geothermometry

4.3.1 Mineral compositions

Mineral chemical compositions of all major phases (clinopyroxene (cpx), orthopyroxene (opx), olivine (ol), and spinel (sp)) in 51 xenoliths were measured by electron microprobe (EMP) at the University of British Columbia. The methodology is described in Appendix G. In each xenolith, at least 8 coexisting clinopyroxene and orthopyroxene grains were analyzed for geothermometry calculations. These analyses were made for each phase adjacent to shared grain boundaries (~20 μm from grain edges); cores of grains for at least two mineral pairs in each xenolith were also analyzed, to evaluate the extent of chemical zoning. Each xenolith had at least 5 analyses on olivine, including at least one rim-core pair, and at least 3 analyses on spinel,

including at least one rim-core pair. Two websterites (NP-MP05-69, -96) lacked olivine. One dunite (NP-MP05-150) lacked orthopyroxene, which precluded geothermometry for that xenolith.

All compositions (Table G.2) are consistent with mantle-derived rocks. Clinopyroxene Mg# ranges from 84 to 93. This phase shows the most variation within individual xenoliths, with a typical variation of ~1. Orthopyroxene Mg# within the suite ranges from 86 to 93, and olivine Mg# ranges from 86 to 91. Within individual xenoliths olivine Mg# variation is less than 0.5 except in one sample (160B). Spinel Cr# ($100 \cdot \text{Cr}/(\text{Cr}+\text{Al})$) range in the suite is 2.5 (websterite) to 34.1 (dunite); there is very little variation (<2.0) within xenoliths except in NP-MP05-160B which has some Cr-enriched spinel rims, and in 150 (a dunite).

4.3.2 Geothermometry results

Results for the 50 xenoliths analyzed are presented in Table 4.2, Fig. 4.3, and Table H.1. Temperatures are calculated with the geothermometer of Taylor (1998), assuming a pressure of 12 kbar (see Appendix H). Temperatures calculated using the geothermometer of Brey and Köhler (1990) (T_{BK90}) are also included due to the thermometer's use in other Cordilleran mantle studies (see Appendix H). The highest and lowest temperatures obtained for each xenolith were removed to eliminate outliers; thus each xenolith's paleo-equilibration temperature is based on 4 to 6 pyroxene pairs. The lowest equilibration temperature obtained is 792 °C with 1σ error of 18 °C (826 ± 7 °C by T_{BK90} , the thermometer of Brey and Köhler (1990)). The highest temperature xenolith equilibrated at 1044 ± 7 °C (1119 ± 7 °C, T_{BK90}). This is the minimum temperature of the lithosphere/asthenosphere boundary; the asthenosphere deforms viscously and will not be sampled via brittle fracturing by the dike (Kohlstedt and Holtzman (2009) and references therein). Hotter asthenospheric mantle beneath the depth of the highest temperature sample should be able to sustain convection (Harder and Russell, 2006). Thus, the minimum temperature

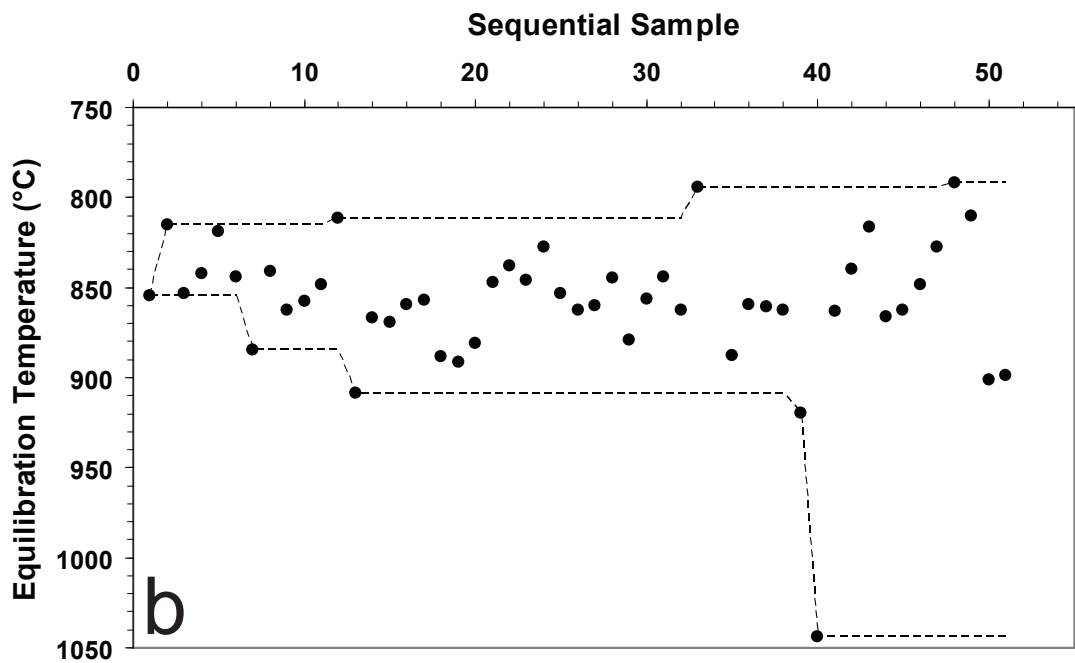
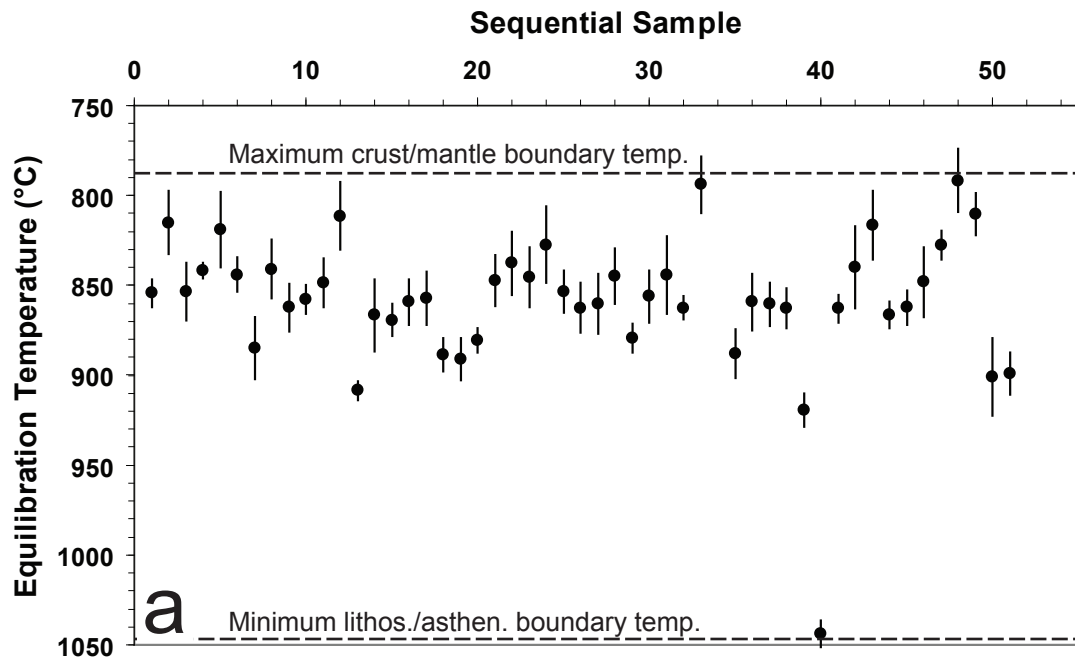


Figure 4.3 Results of geothermometry on 50 mantle xenoliths, using the geothermometer of Taylor (1998). (a) Xenoliths' mean equilibration temperatures (ie. ambient mantle), with 1σ error calculated by variation of temperatures between separate mineral pairs. Minimum and maximum equilibration temperatures define minimum lithospheric mantle temperature range. (b) Mean temperatures used to show the maximum range of xenolith temperatures as samples were progressively analyzed. The minimum temperature was attained on the 39th sample, the maximum on the 47th sample.

Table 4.2 Physical and thermal properties of mantle xenoliths. Error is 1σ .

Sample	Density (g/cm ³)	Equilibration Temperature (TA97, °C)				Carbonate Habit (Grains/Veins)
		Mean	1σ	Min	Max	
A1	3.314 ± 0.015	854	8	846	865	V
A2	3.306 ± 0.007	815	18	785	833	V
A4	3.311 ± 0.010	854	16	839	879	V
31	3.300 ± 0.012	842	4	835	847	G/V
32	3.285 ± 0.009	819	21	785	842	G/V
33	3.307 ± 0.003	844	10	834	854	V
34A	3.320 ± 0.024	885	17	868	903	V
34B	3.309 ± 0.013	841	16	822	861	V
35	3.289 ± 0.007	862	13	848	879	G/V
44	3.296 ± 0.038	858	8	851	870	V
45	3.309 ± 0.014	849	13	833	864	G
50	3.292 ± 0.013	811	19	785	842	G/V
56A	3.313 ± 0.011	909	5	904	917	G/V
69	3.281 ± 0.004	867	20	838	888	G
70A	3.300 ± 0.009	869	9	854	880	G/V
72	3.302 ± 0.006	859	13	845	872	G/V
74	3.279 ± 0.019	857	15	834	872	G/V
78	3.302 ± 0.018	888	9	875	897	G/V
79A	3.282 ± 0.004	891	12	878	908	G/V
81A	3.293 ± 0.008	881	7	876	892	G/V
85	3.283 ± 0.017	847	14	828	863	G/V
89	3.274 ± 0.006	838	17	812	855	G/V
90	3.312 ± 0.012	846	17	823	870	G/V
95	3.298 ± 0.010	827	21	801	855	G/V
96	3.299 ± 0.011	853	12	833	865	G
101	-	862	14	841	879	G/V
110	3.316 ± 0.014	860	16	843	884	G/V
113	3.314 ± 0.014	845	15	822	862	G/V
118	-	879	8	867	890	G/V
121A	3.303 ± 0.004	856	15	835	868	G/V
121B	3.296 ± 0.008	844	22	819	872	G/V
139	3.300 ± 0.011	862	6	856	872	G/V
149	3.332 ± 0.012	794	16	775	811	G/V
150	-	-	-	-	-	V

All sample numbers prefixed by "NP-MP05-"

Table 4.2 (cont'd)

Sample	Density (g/cm ³)	Equilibration Temperature (TA97, °C)				Carbonate Habit (Grains/Veins)
		Mean	1 σ	Min	Max	
156A	3.302 ± 0.007	888	13	866	905	G/V
157A	-	859	16	842	880	G/V
157B	3.293 ± 0.007	860	12	845	873	G/V
159A	3.304 ± 0.012	863	11	849	881	V
160A	3.310 ± 0.041	919	9	902	929	G/V
160B	3.350 ± 0.005	1044	7	1035	1055	G/V
161A	3.297 ± 0.012	863	8	850	870	G/V
161B	3.365 ± 0.006	840	23	806	859	G
161D	3.290 ± 0.008	816	19	789	846	G/V
162A	3.309 ± 0.034	866	7	858	874	G/V
163A	3.280 ± 0.013	862	9	847	876	G/V
163C	3.284 ± 0.011	848	20	826	874	G/V
164A	3.302 ± 0.020	828	8	820	835	G/V
164B	3.297 ± 0.003	792	18	776	823	V
164C	3.266 ± 0.020	810	12	796	827	G/V
165A	3.312 ± 0.004	901	22	871	927	G/V
166	3.308 ± 0.005	899	12	884	914	G/V

All sample numbers prefixed by "NP-MP05-"

range of the lithospheric mantle is $>250\text{ }^{\circ}\text{C}$ ($>290\text{ }^{\circ}\text{C}$, T_{BK90}) beneath Mt. Preston at $\sim 19\text{ Ma}$, with a Moho temperature of no more than $792\text{ }^{\circ}\text{C}$ ($826\text{ }^{\circ}\text{C}$, T_{BK90}), and a lithosphere/asthenosphere boundary temperature of no less than $1044\text{ }^{\circ}\text{C}$ ($1119\text{ }^{\circ}\text{C}$, T_{BK90}).

The highest paleo-equilibration temperature recorded from a xenolith in the suite (sample NP-MP05-160B) is over $120\text{ }^{\circ}\text{C}$ ($140\text{ }^{\circ}\text{C}$, T_{BK90}) higher than the next hottest; on a model geotherm for Mt. Preston this represents over 8 km vertical difference (see section 4.3.3). Many of the clinopyroxenes and spinels in this xenolith have reaction rims, which has been interpreted by Shaw and Dingwell (2008) as consistent with xenolith-melt interaction, although it has also been seen in a carbonate-bearing xenolith suite (Laurora et al., 2001). No basanite veins were observed in this sample. Thermometry results for this sample are relatively uniform; Harder (2004) found that magma-heated samples (inferred by textures and tested by EMP analysis) produced low ambient mantle temperatures as well as high disturbed temperatures. The equilibration temperature ($1044\text{ }^{\circ}\text{C}$; $1119\text{ }^{\circ}\text{C}$ by T_{BK90}) is not near a practical limit for application of the two pyroxene thermometer, and it falls far short of magmatic temperatures ($>1250\text{ }^{\circ}\text{C}$; section 3.3). Glass indicative of melting during transport was not observed in the sieve textured grain margins or interstitially. The presence of carbonate and sulfides in the sample argues against magma-induced heating, as the carbonates and sulfides should readily volatilize. Due to these factors, it is concluded that the high temperature xenolith records ambient mantle temperatures, and features textures resulting from earlier melt or fluid interactions.

The appearance of plagioclase in two xenoliths (Fig. 4.1b) along with spinel is interesting, as plagioclase and spinel are stable together over a very restrictive range of P-T conditions in most mantle assemblages. Plagioclase is replaced by spinel with increasing pressure and temperature. Using the bulk chemistry of sample NP-MP05-69, phase diagrams were created with the `Perple_X` thermodynamic software set (Connolly (1990); includes chromium solution

model update of 2006). The equilibration temperature of the xenolith is $867\text{ }^{\circ}\text{C} \pm 20 (1\sigma)$; in this rock plagioclase and spinel are both stable over this $40\text{ }^{\circ}\text{C}$ temperature range up to a pressure of 9.3 kbar. Assuming a crustal density of 2700 kg/m^3 and a Moho depth of 32 km (Calkins et al., 2010), Moho pressure is 8.5 kbar. Thus, plagioclase and spinel can be stable in a rock of this composition in the mantle lithosphere beneath Mt. Preston. One other Cordilleran suite (Rayfield River; Canil et al., 1987) reported plagioclase-spinel websterite, though it was considered the result of a retrograde process.

The 50 xenoliths examined record paleoequilibration temperatures between 792 and 1044 $^{\circ}\text{C}$ (826 and 1119 $^{\circ}\text{C}$ by T_{BK90}), though most samples record temperatures between ~ 800 and $900\text{ }^{\circ}\text{C}$ (~ 850 and $950\text{ }^{\circ}\text{C}$, T_{BK90}) (Fig. 4.3). This suggests that the low temperature (i.e. shallow) mantle lithosphere is better represented than the deep lithosphere. The bias towards low temperature xenoliths may reflect more efficient sampling of the shallow mantle lithosphere by the dike. However, to the author's knowledge none of the mantle xenolith suites collected and described from the Canadian Cordillera were collected from a dike. It is possible that the suite represents a concentration of samples from a limited range of the mantle lithosphere due to pulsed sampling (e.g. created by magma supply variations) combined with the effect of laminar dike flow. This could result in xenoliths being transported without sorting or mixing. During such transport little intermingling of xenoliths from different depths would occur.

Harder (2004) conducted thermometry by determining xenolith equilibration temperatures in sequential batches of 5 xenoliths each; eventually several batches would pass without changing the current minimum or maximum temperature. Harder argued that this represented a full and statistically valid range of temperatures reflecting the entire temperature range of mantle lithosphere sampled by the magma. For Harder's suite this was obtained between 25 and 30 samples; in the Mt. Preston suite, the maximum range was obtained at the 47th of 50 samples (Fig. 4.3). Because of the comprehensive sampling program (over 150 xenoliths collected),

deliberate selection of xenoliths to capture representative mineral modes, textures, and grain sizes, and the analysis of several more xenoliths than Harder (2004), it is argued that this temperature range reflects a representative range of the temperatures of xenoliths sampled by the dike.

The temperature range for the mantle lithosphere represented by the Mt. Preston xenolith suite is typical for hot mobile belts like the Canadian Cordillera (Hyndman et al., 2005) and is consistent with results from other xenolith suites in British Columbia (Harder (2004) and references therein) when compared using equilibration temperatures calculated with the same thermometer. Note that the Taylor (1998) thermometer applied to the highest temperature xenolith in the Mt. Preston suite, for example, results in an equilibration temperature of 1044 °C, while the Brey and Köhler (1990) thermometer results in a temperature of 1119 °C; temperature estimates may be significantly different depending on the geothermometer used.

Because of the lack of evidence for crustal-scale tectonic activity since the dike intruded at 19 Ma—magmatism of the Cheslatta Lake suite is interpreted to be related to Eocene faulting and the extensional tectonic regime (Anderson et al., 2001)—it is argued that the temperatures obtained for this sample suite are applicable to present-day mantle lithosphere under Mt. Preston.

Mineral compositions in individual xenoliths are presented against temperature (i.e. depth) in Figure 4.4. There appear to be no systematic changes in xenolith mineral composition with depth.

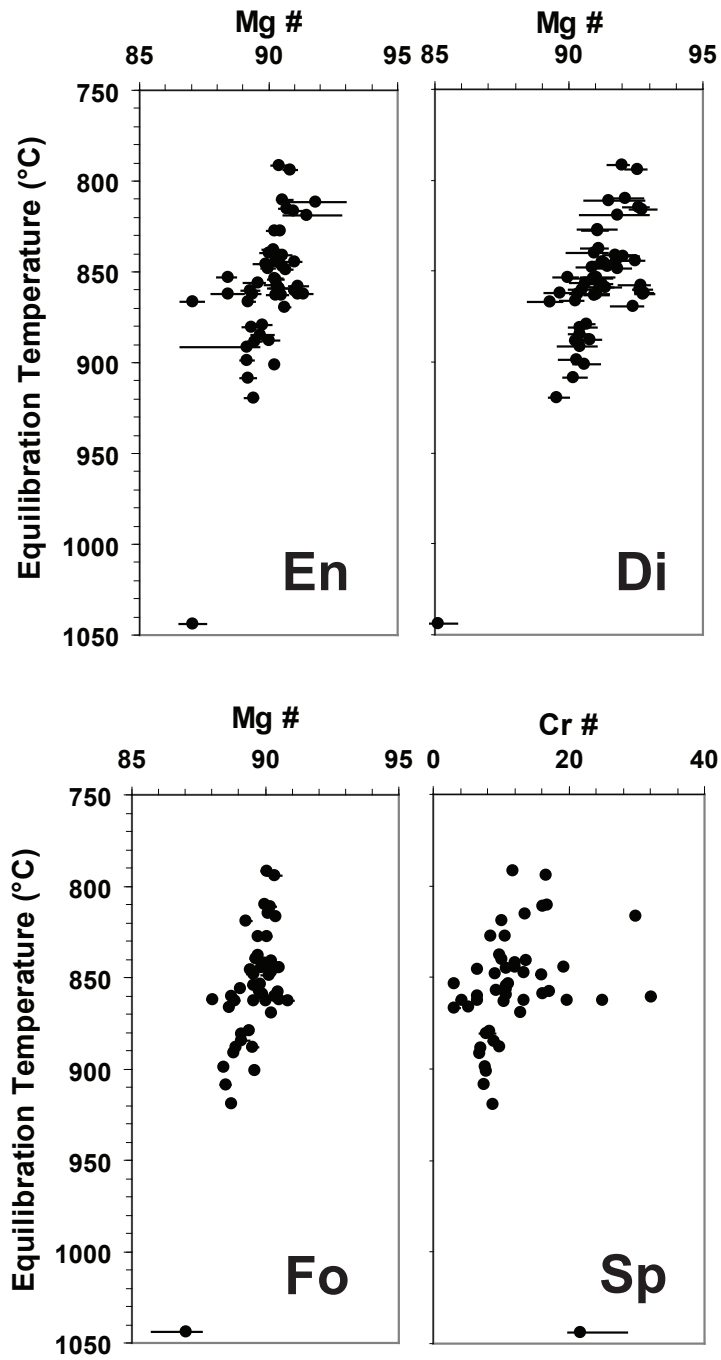


Figure 4.4 Average mineral compositions within mantle xenoliths, versus xenolith equilibration temperature (ie. relative mantle position). Range of compositions within each xenolith indicated by bars. En = enstatite, Di = diopside, Fo = forsterite, Sp = spinel.

4.4 Geotherm

Adopting a geotherm for the lithosphere beneath Mt. Preston allows the xenolith equilibration temperatures to be plotted against depth and pressure, and allows for estimates of mantle lithosphere thickness to be made. Harder (2004) and Harder and Russell (2006) used a one dimensional model for the lithosphere (derived from Russell and Kopylova (1999) and Russell et al. (2001)) that comprises a crust of known thickness (Z_M), with constant surface temperature (T_0), radiogenic heat production (A_0), thermal conductivity (K_1), density (ρ_1), and surface heat flow (q_0). Using earthquake-generated P and S waves collected from 2005-2006 as part of the BATHOLITHS program, a Moho depth (i.e. crustal thickness Z_M) of approximately 32 km was determined for the arc-parallel region just south of Mt. Preston (Calkins et al., 2010). Surface temperature (T_0) was set at 10 °C. For a heat production (A_0) estimate for the crust, measurements by Lewis et al. (2003) estimated $1.6 \pm 0.8 \mu\text{W}/\text{m}^3$ for Cordillera south of 59 °N; this value was used. Thermal conductivity (K_1) was set at 2.5 W/m·K, and density (ρ_1) was set at 2700 kg/m³ (Harder, 2004). Hyndman et al. (2005) estimated surface heat flow (q_0) values of $76 \pm 21 \text{ mW}/\text{m}^2$ for the northern Canadian Cordillera and 75 ± 15 for the southern; a surface heat flow of $80 \text{ mW}/\text{m}^2$ was calculated from other variables and used (equation 2 of Harder and Russell (2006)).

For the lithospheric mantle, a thermal conductivity constant (K_2) of 3.2 and a density (ρ_2) of 3300 kg/m³ (by pycnometry; see Appendix I) are used for the model. Heat production (A) is negligible. Using the equilibration temperatures of the mantle-derived xenolith suite, the temperature at the base of the crust (i.e. the xenolith equilibrated at the lowest temperature, thus representing the maximum temperature at the base of the crust) is set at 792 °C, and the temperature at the base of the mantle lithosphere (i.e. the xenolith equilibrated at the highest

temperature, thus representing the minimum temperature at the base of the mantle lithosphere) is set at 1044 °C.

The crustal portion of the geotherm is calculated using equation 1 of Harder and Russell (2006); the mantle lithosphere portion uses equation 3. A rigorous treatment of the range of input variables would result in a family of plausible geotherms.

A model geotherm is presented in Fig. 4.5. With the parameters used, the thickness of the mantle lithosphere determined by the geotherm is approximately 17 km, with the lithosphere/asthenosphere boundary at 49 km depth. Assuming the accuracy of all other variables, this is a minimum thickness, due to the use of the lowest and highest equilibration temperatures of the xenoliths sampled and analyzed to define the temperatures of the crust/mantle and lithosphere/asthenosphere boundaries, respectively. The pressure range for the lithospheric mantle sampled is approximately 8.5 to 14.0 kbar. On this geotherm, the highest temperature xenolith, which is used to define the lithosphere/asthenosphere boundary temperature, was from 8 km deeper than the next highest.

For comparison, a family of geotherms determined for the Llangorse Mtn. area in the NCVP resulted in a lithospheric mantle 16-30 km thick with a Moho fixed at 36 km depth, for a total lithospheric thickness of 52-66 km (Harder and Russell, 2006). Data gathered during the BATHOLITHS geophysical program (e.g. surface heat flow data) near Mt. Preston will refine more variables, resulting in better estimates of the thermal profile beneath the area.

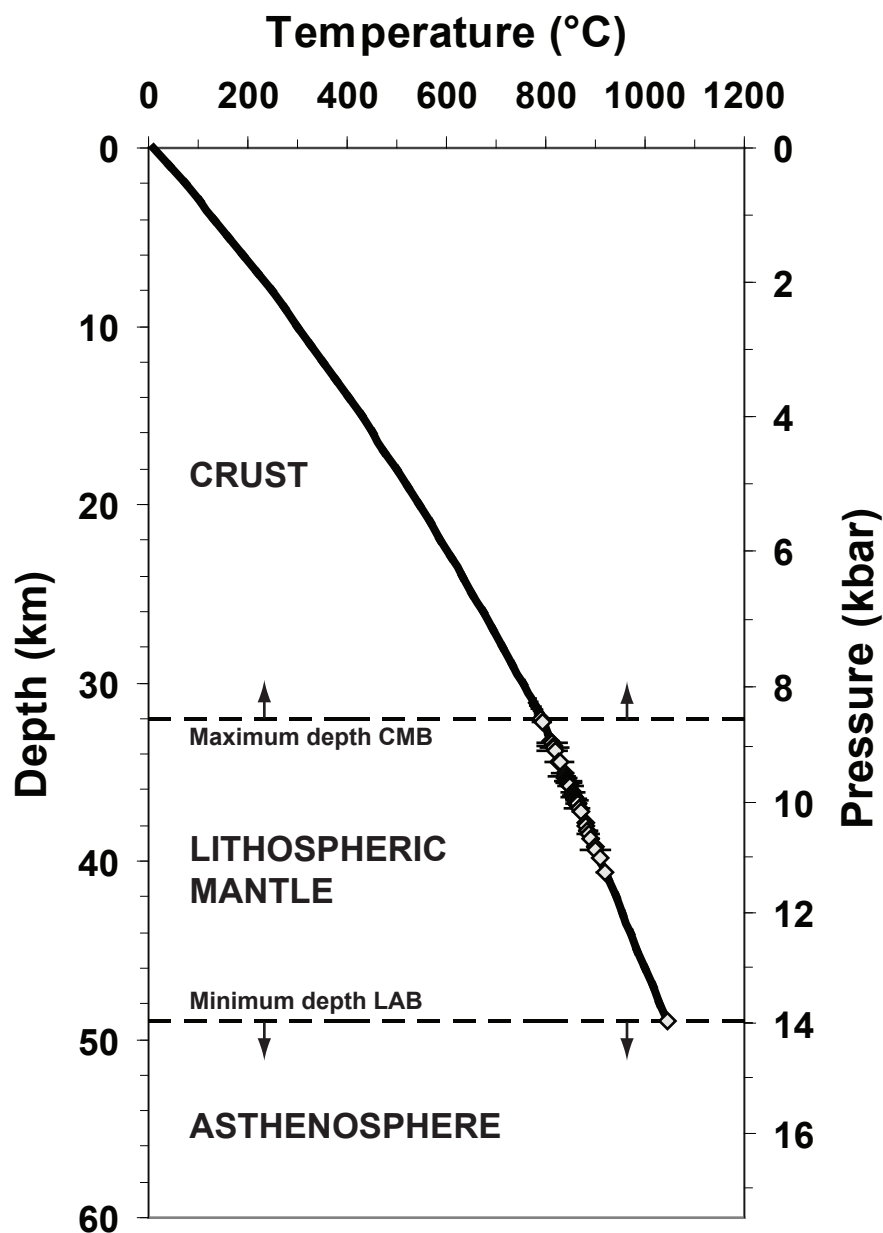


Figure 4.5 Model geotherm for the Mt. Preston area, based on one dimensional model of the crust and mantle (Harder and Russell, 2006). Mantle-derived xenoliths are plotted according to their equilibration temperatures. If model variables are accurate, the lowest temperature xenolith defines the maximum temperature for the crust/mantle boundary (CMB), and the highest temperature xenolith defines the minimum temperature for the lithosphere/asthenosphere boundary (LAB). Moho depth is fixed by geophysics; L/A boundary changes depending on input values (see text).

4.5 Chemistry

Major element chemical compositions of mantle xenoliths are summarized in Table 4.3. Mg# varies from 87 to 91; Al₂O₃ content has a mean of ~3.0 wt.%, and varies from 0.2 wt.% (dunite) to 11.9 (websterite), and 1.2 to 4.7 wt.% for lherzolites. Major element chemical compositions are similar to those of other mantle xenolith suites in the Canadian Cordillera (Fig. 4.6, Fig. 4.7). Trace and rare earth element (REE) compositions are presented in Table 4.4. Rare earth element patterns are light rare earth element (LREE; La to Sm) depleted to flat (Fig. 4.8). Many patterns show a ‘spoon-shaped’ profile of LREE depletion, with slight enrichment of the lightest REEs; only one pattern (the harzburgite) is weakly LREE enriched relative to the middle (MREE; Eu to Ho) and heavy (HREE; Er to Lu) rare earth elements. The MREEs and HREEs of the dunite are below detection, while the LREEs show similar concentrations to some of the other xenoliths. There are no pronounced single element anomalies present.

The lithospheric mantle of the Canadian Cordillera is relatively homogeneous; it is dominated by fertile lherzolite (including the Mt. Preston suite), with rare harzburgites except in northwestern BC, where harzburgites are more abundant (Shi et al., 1998). The Mt. Preston xenolith suite is unique in that it contains modal evidence of metasomatic enrichment (carbonate and sulfides; see Chapter 5). In terms of major element chemistry, the Mt. Preston suite is similar to the rest of the Cordillera, and other continental spinel-bearing peridotites worldwide (Peslier et al., 2002).

Mg number and Al₂O₃ content (and mean) are very similar to other unimodal mantle xenolith localities in British Columbia (Shi et al., 1998; Peslier et al., 2002). Major element contents versus MgO (Fig. 4.6) can be considered to reflect degrees of basaltic melt extraction from fertile (i.e. low MgO) peridotite, leaving more depleted (i.e. high MgO) peridotite as

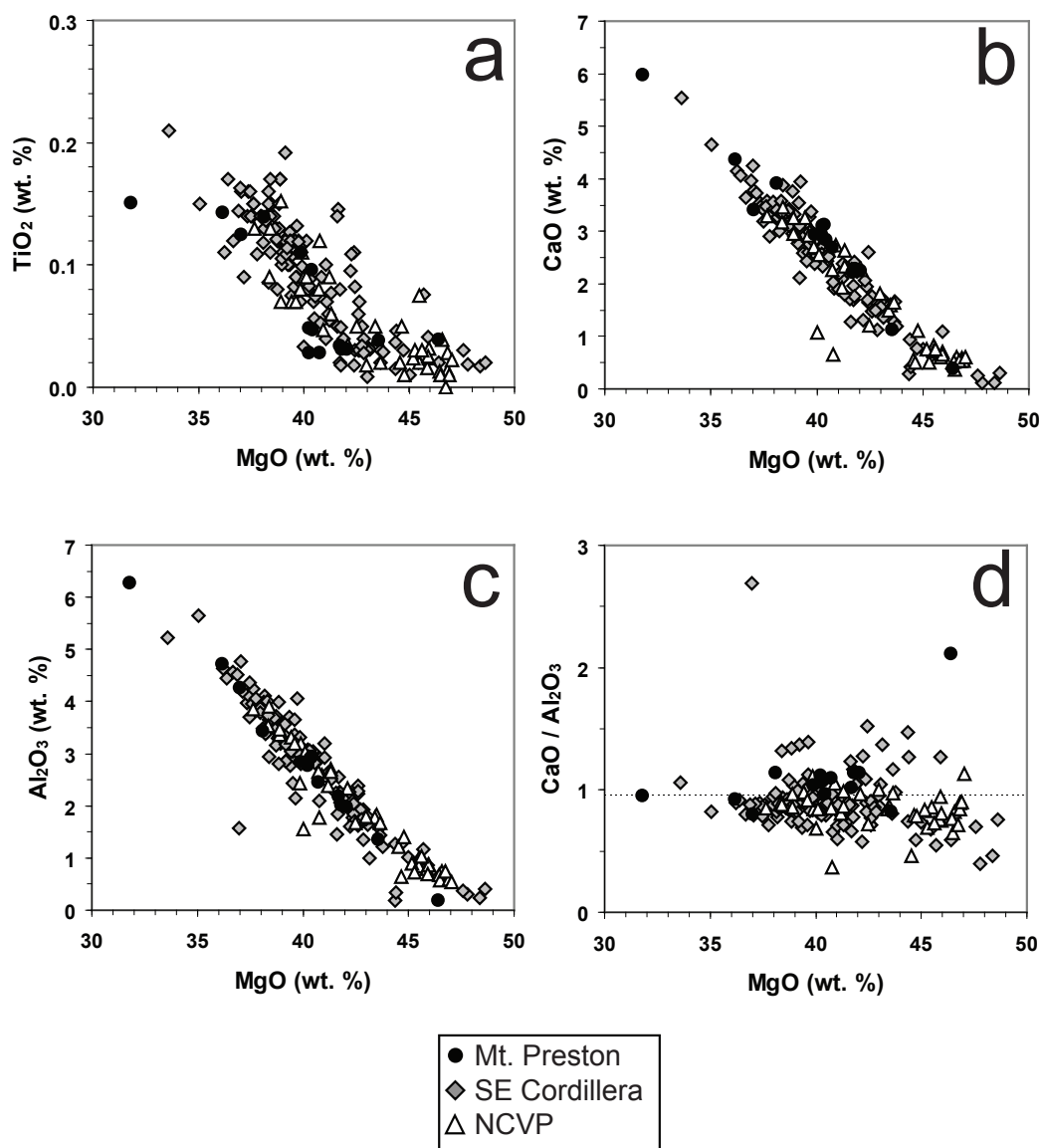


Figure 4.6 Major elements (a, b, c) and major element ratio (d) vs. MgO (as an indicator of depletion) for mantle xenoliths (lherzolites, harzburgites, and dunites) from Mt. Preston, southeast Canadian Cordillera (Peslier et al., 2002), and the NCVP (Francis, 1987; Shi et al., 1998; Harder, 2004). Horizontal line indicates average global CaO/Al₂O₃ ratio for subcontinental spinel lherzolite mantle (McDonough, 1990).

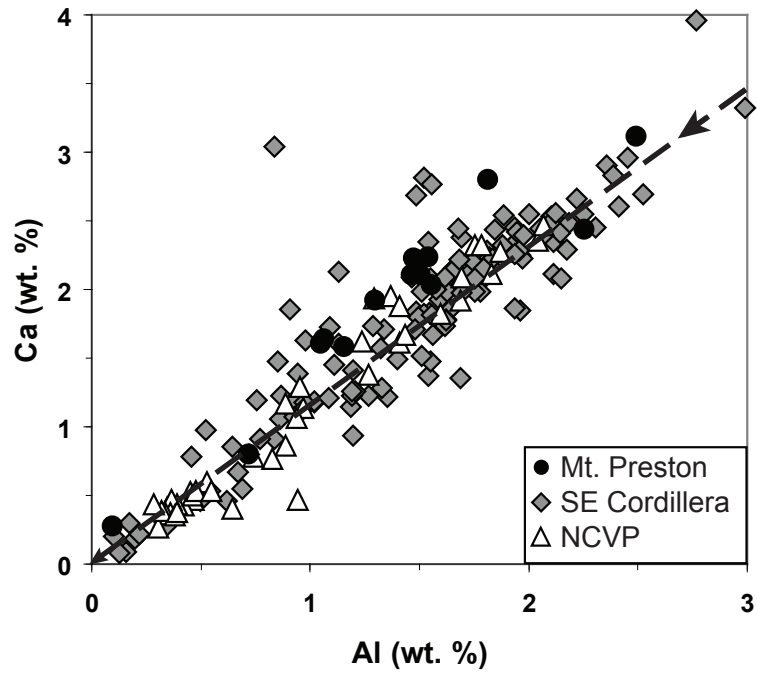


Figure 4.7 Plot of cations Ca vs. Al (wt.%) concentrations in mantle xenoliths from the Canadian Cordillera. Data sources as in Figure 4.6. Dashed line with arrows denotes the expected trend for depletion of oceanic peridotite (Boyd, 1989).

Table 4.3 Whole rock major element compositions (wt.%) of xenoliths from Mt. Preston.

Sample	31	31 ¹	35	35 ²	44	50	69	70A	78	79A	139
Rock Type	lherzolite	lherzolite	lherzolite	lherzolite	lherzolite	lherzolite	websterite	lherzolite	lherzolite	ol-websterite	lherzolite
SiO ₂	44.21	44.24	44.11	44.26	44.29	44.61	48.07	44.40	43.53	46.12	44.38
TiO ₂	0.047	0.048	0.031	0.031	0.034	0.028	0.057	0.028	0.139	0.151	0.143
Al ₂ O ₃	2.94	2.79	2.01	1.98	2.18	2.45	11.90	2.77	3.43	6.27	4.71
Fe ₂ O ₃	1.53	1.75	1.63	1.76	1.68	1.23	1.54	1.51	1.94	2.14	2.01
FeO	6.68	6.47	6.35	6.27	6.34	6.84	3.27	6.47	6.91	5.36	6.49
MnO	0.119	0.120	0.112	0.113	0.113	0.116	0.179	0.115	0.139	0.119	0.132
MgO	40.42	40.25	41.80	42.07	41.70	40.74	18.40	40.24	38.10	31.80	36.16
CaO	2.84	3.11	2.29	2.25	2.21	2.68	14.73	2.94	3.91	5.98	4.36
Na ₂ O	0.19	0.20	0.12	0.12	0.13	0.13	0.89	0.15	0.29	0.47	0.33
K ₂ O	0.01	0.01	0.01	0.01	0.01	<d/1	0.01	0.01	0.03	0.01	0.02
P ₂ O ₅	0.017	0.017	0.017	0.017	0.017	0.016	0.017	0.016	0.031	0.021	0.024
H ₂ O ⁺	0.48	0.46	0.62	0.63	0.66	0.65	0.49	0.63	0.77	0.61	0.59
H ₂ O ⁻	0.25	0.28	0.22	0.23	0.19	0.17	0.12	0.15	0.26	0.22	0.21
CO ₂	0.33	0.40	0.33	0.33	0.33	0.26	0.11	0.29	0.26	0.33	0.26
Total	99.81	99.87	99.43	99.84	99.69	99.75	99.66	99.57	99.48	99.38	99.61
FeO _{Total}	8.06	8.04	7.82	7.85	7.85	7.95	4.66	7.83	8.66	7.29	8.30
LOI	0.37	0.47	0.48	0.49	0.49	0.34	0.36	0.35	0.57	0.61	0.41

All sample numbers prefixed by "NP-MP05-"

¹ Duplicate analysis.

² Replicate sample based on splitting of sample before powdering.

Table 4.3 (cont'd)

Sample	159A	160A	160B	161D	162A	164A
Rock Type	lherzolite	lherzolite	dunite	harzburgite	ol-websterite	lherzolite
SiO ₂	44.45	44.60	39.83	44.06	46.54	43.95
TiO ₂	0.110	0.125	0.039	0.038	0.073	0.096
Al ₂ O ₃	2.84	4.26	0.18	1.36	5.75	2.91
Fe ₂ O ₃	1.44	1.69	1.99	1.48	1.98	1.71
FeO	6.86	6.87	9.98	6.90	5.70	6.44
MnO	0.119	0.126	0.146	0.116	0.126	0.118
MgO	39.89	37.03	46.42	43.57	33.17	40.37
CaO	2.94	3.41	0.38	1.12	5.11	3.13
Na ₂ O	0.26	0.30	0.03	0.08	0.36	0.26
K ₂ O	0.01	0.01	0.01	0.01	<d/l	<d/l
P ₂ O ₅	0.023	0.025	0.026	0.018	0.017	0.019
H ₂ O ⁺	0.61	0.43	0.38	0.60	0.63	0.59
H ₂ O ⁻	0.20	0.18	0.17	0.25	0.13	0.15
CO ₂	0.33	0.33	0.29	0.26	0.26	0.29
Total	99.88	99.21	99.70	99.61	99.72	99.88
FeO _{Total}	8.16	8.39	11.77	8.23	7.48	7.98
LOI	0.38	0.23	<d/l	0.34	0.39	0.33

All sample numbers prefixed by "NP-MP05-"

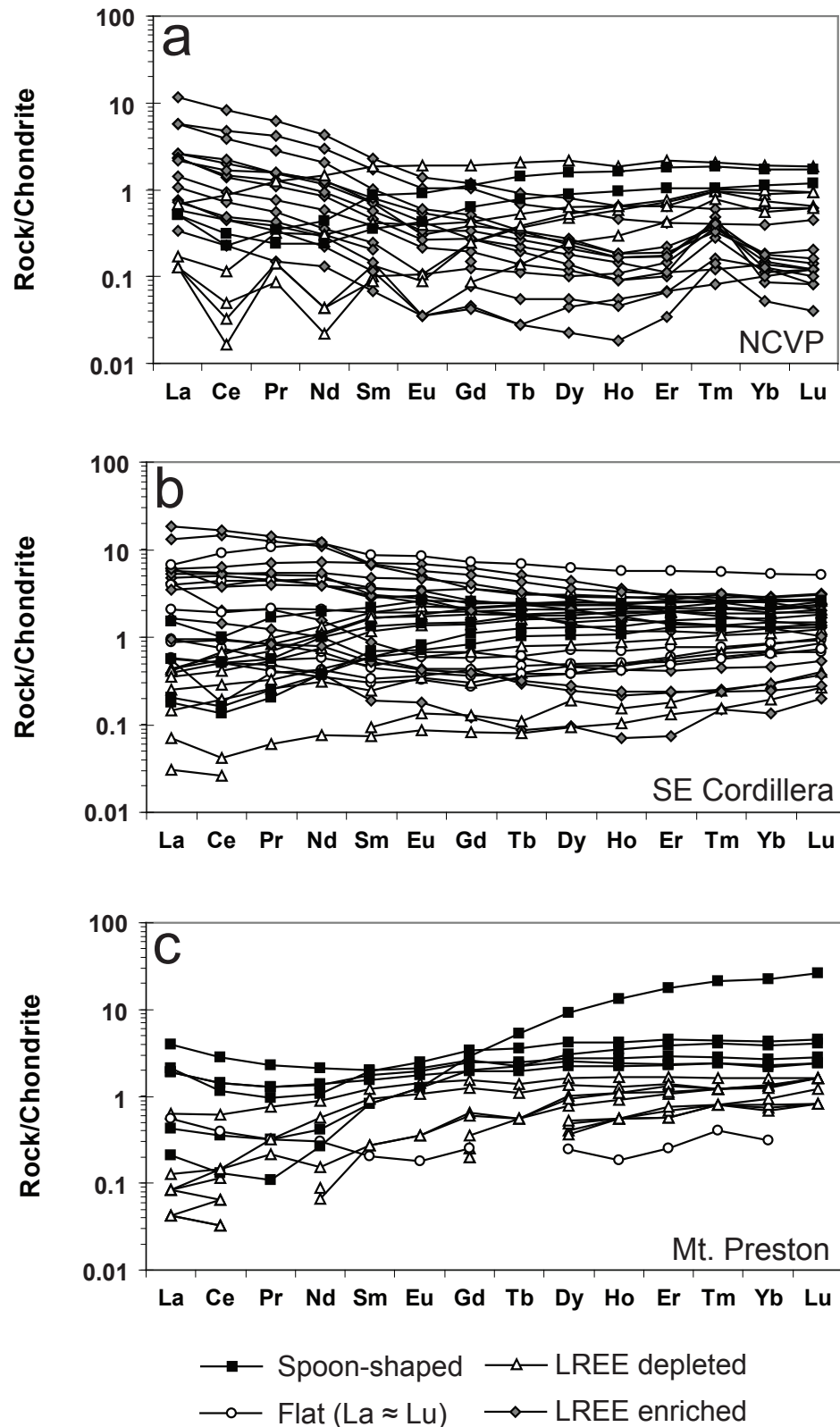


Figure 4.8 Rare earth element (REE) concentrations for British Columbia mantle xenolith suites, normalized to chondrite (McDonough and Sun, 1995) and subdivided by pattern shape. NCVP data from Harder (2004), southeast Cordillera data from Peslier et al. (2002).

Table 4.4 Whole rock trace and rare earth element concentrations (ppm) of mantle xenoliths from Mt. Preston.

Sample	31	31 ¹	35	35 ²	44	50	69	70A	78	79A	139
Rock Type	lherzolite	lherzolite	lherzolite	lherzolite	lherzolite	lherzolite	websterite	lherzolite	lherzolite	ol-websterite	lherzolite
Ba	2.04	0.86	1.28	2.05	1.33	1.22	2.80	0.85	7.00	3.03	7.56
Sc	<d/l	10	<d/l	<d/l	<d/l	12	83	<d/l	15	20	13
V	61	63	46	48	50	61	401	62	73	120	89
Cr	2662	2636	2844	2885	2825	2859	1534	2651	1889	3203	2442
Co	109	100	107	114	111	110	43	107	115	82	107
Ni	2252	2322	2374	2399	2382	2275	474	2246	2145	1636	1983
Zn	9	4	8	6	6	8	<d/l	10	<d/l	35	11
Cu	11	26	2	6	4	14	3	<d/l	30	26	35
Y	1.52	1.54	0.69	0.68	0.86	0.89	20.2	1.35	3.24	6.24	3.83
La	0.03	<d/l	0.02	0.01	0.01	0.02	0.10	0.01	0.94	0.50	0.45
Ce	0.09	0.02	0.07	0.04	0.02	0.04	0.22	0.02	1.71	0.71	0.88
Pr	0.02	<d/l	<d/l	<d/l	<d/l	<d/l	0.03	<d/l	0.21	0.09	0.12
Nd	0.07	0.03	0.04	<d/l	<d/l	<d/l	0.19	<d/l	0.96	0.49	0.62
Sm	0.04	0.04	<d/l	<d/l	<d/l	<d/l	0.12	<d/l	0.30	0.29	0.26
Eu	0.02	0.02	<d/l	<d/l	<d/l	<d/l	0.07	<d/l	0.12	0.14	0.11
Gd	0.12	0.13	0.05	0.04	0.05	0.04	0.57	0.07	0.52	0.67	0.49
Tb	0.02	0.02	<d/l	<d/l	<d/l	<d/l	0.19	0.02	0.08	0.13	0.09
Dy	0.23	0.25	0.10	0.09	0.12	0.13	2.24	0.19	0.62	1.03	0.68
Ho	0.06	0.06	0.03	0.03	0.03	0.03	0.73	0.05	0.13	0.23	0.15
Er	0.18	0.21	0.09	0.09	0.11	0.12	2.84	0.17	0.38	0.72	0.46
Tm	0.03	0.03	0.02	0.02	0.02	0.02	0.52	0.03	0.06	0.11	0.07
Yb	0.20	0.22	0.12	0.11	0.13	0.15	3.64	0.21	0.37	0.69	0.43
Lu	0.04	0.04	0.02	0.02	0.02	0.03	0.64	0.04	0.06	0.11	0.07

All sample numbers prefixed by "NP-MP05-"

All trace elements except Ba and Y by X-ray fluorescence.

¹ Duplicate analysis.

² Replicate sample based on splitting of sample before powdering.

Table 4.4 (cont'd)

Sample	159A	160A	160B	161D	162A	164A
Rock Type	lherzolite	lherzolite	dunite	harzburgite	ol-websterite	lherzolite
Ba	3.96	1.75	1.97	3.19	1.12	1.54
Sc	12	10	<d/l	<d/l	12	11
V	60	75	<d/l	36	101	53
Cr	2755	2835	318	2751	2395	2433
Co	113	113	153	119	93	105
Ni	2207	1984	2901	2514	1691	2310
Zn	7	15	53	9	18	6
Cu	9	21	<d/l	<d/l	<d/l	19
Y	2.30	3.18	0.12	0.37	4.94	1.76
La	0.15	0.45	0.09	0.13	0.05	0.02
Ce	0.38	0.87	0.18	0.24	0.08	0.09
Pr	0.07	0.12	0.02	0.03	0.01	0.03
Nd	0.41	0.63	0.10	0.14	0.12	0.26
Sm	0.18	0.23	<d/l	0.03	0.12	0.14
Eu	0.08	0.10	<d/l	0.01	0.07	0.06
Gd	0.31	0.39	<d/l	0.05	0.40	0.25
Tb	0.05	0.07	<d/l	<d/l	0.08	0.04
Dy	0.40	0.55	<d/l	0.06	0.76	0.33
Ho	0.09	0.12	<d/l	0.01	0.19	0.07
Er	0.27	0.37	<d/l	0.04	0.61	0.22
Tm	0.04	0.06	<d/l	0.01	0.10	0.03
Yb	0.26	0.35	<d/l	0.05	0.62	0.21
Lu	0.04	0.06	<d/l	<d/l	0.10	0.04

All sample numbers prefixed by "NP-MP05-"

All trace elements except Ba and Y by X-ray fluorescence.

residue. Similarly, on a Ca-Al diagram the oceanic trend of Boyd (1989) defines the evolution of compositions as melt is extracted, from fertile to depleted compositions (Fig. 4.7). In both Figures 4.6 and 4.7, the major element composition of the xenoliths in the Mt. Preston suite show a range of compositions representing varying degrees of melt extraction from a fertile mantle source. Most of the xenoliths show calcium enrichment relative to aluminum, possibly relating to carbonation. Some southeast Canadian Cordilleran xenoliths show the same compositions and although modal carbonate has not been reported in those rocks, past carbonate metasomatism is considered a plausible explanation for their chemical compositions (Peslier et al., 2002).

In the plagioclase-bearing websterite, CaO and Al₂O₃ are highly enriched, consistent with the abundance of clinopyroxene and presence of plagioclase. The extremely fertile composition of these websterites is consistent with an origin including enrichment by mantle melts which crystallized within the mantle and eventually equilibrated and recrystallized, forming equilibrium textures similar to other mantle rocks (Canil et al., 1987). The fact that carbonates with intrusive textures are also found in this xenolith indicates that carbonate enrichment postdated these events.

A flat, near unity chondrite normalized REE pattern in peridotite generally indicates little to no previous melt extraction, while a depleted trace element pattern with decreasing depletion from LREEs to HREEs is indicative of past melt extraction, depleting the residue in more incompatible elements. Peslier et al. (2002) considered these patterns indicative of a lack of metasomatic disturbance. While the Mt. Preston suite follows these trends broadly, the lightest LREEs (e.g. La, Ce) are commonly enriched slightly, resulting in “spoon-shaped” REE patterns with the lowest relative abundances at Pr or Nd. The dunite is especially demonstrative of LREE enrichment; the LREE contents are similar to that of some other xenoliths from the suite, while the MREE and HREE concentrations are below detection. Takazawa et al. (1992) found that

migrating LREE-rich melts affect spinel lherzolite in the lightest REEs progressively, beginning with La then Ce then Nd. The abundances of the MREEs and HREEs are consistent with melting indices (MgO, Al₂O₃), i.e. enriched in lherzolites relative to harzburgite or dunite. Websterites were not chosen for REE analysis in previous studies of Cordilleran xenoliths (Peslier et al., 2002; Harder, 2004); the highly enriched MREEs and HREEs in the websterite are likely the result of the dominance of clinopyroxene as a phase (63 wt.%; Table 4.1). Rare earth elements are more compatible in clinopyroxene than orthopyroxene or olivine (Takazawa et al., 1992).

Metasomatised xenoliths with carbonate commonly show LREE to MREE enriched patterns (e.g. Delpech et al., 2004). The rare earth element abundances show the overprinting of metasomatism in the Mt. Preston xenoliths, following varying degrees of melt extraction from fertile mantle (least depleted lherzolite to most depleted dunite).

Tb/Yb ratios for peridotites can indicate whether melt extraction has occurred in the spinel or garnet stability field, as Yb partitions strongly into garnet as a residual phase, resulting in strong Tb/Yb decreases even at small degrees of melting (Bodinier et al., 1988). The Mt. Preston peridotite compositions are consistent with melt extraction in the spinel stability field (Fig. 4.9), as with other suites in the Cordillera (Peslier et al., 2002). Tb enrichment has been interpreted as the result of strong enough metasomatism to affect the MREEs (Fig. 4.9; Peslier et al., 2002). None of the Mt. Preston xenoliths analyzed show Tb enrichment over Yb relative to chondrite, suggesting that metasomatic processes did not disturb the MREEs or if so, very little.

In summary, there is bulk chemical evidence for metasomatism within the Mt. Preston xenoliths. Some Ca enrichment may be inferred from the major elements, where Ca is enriched relative to Al when compared to expected depletions derived from extraction of melts from the fertile parents of these rocks. The REEs commonly show some enrichment in the lightest LREEs, even in a dunite with highly depleted MREEs and HREEs, indicating that metasomatic processes

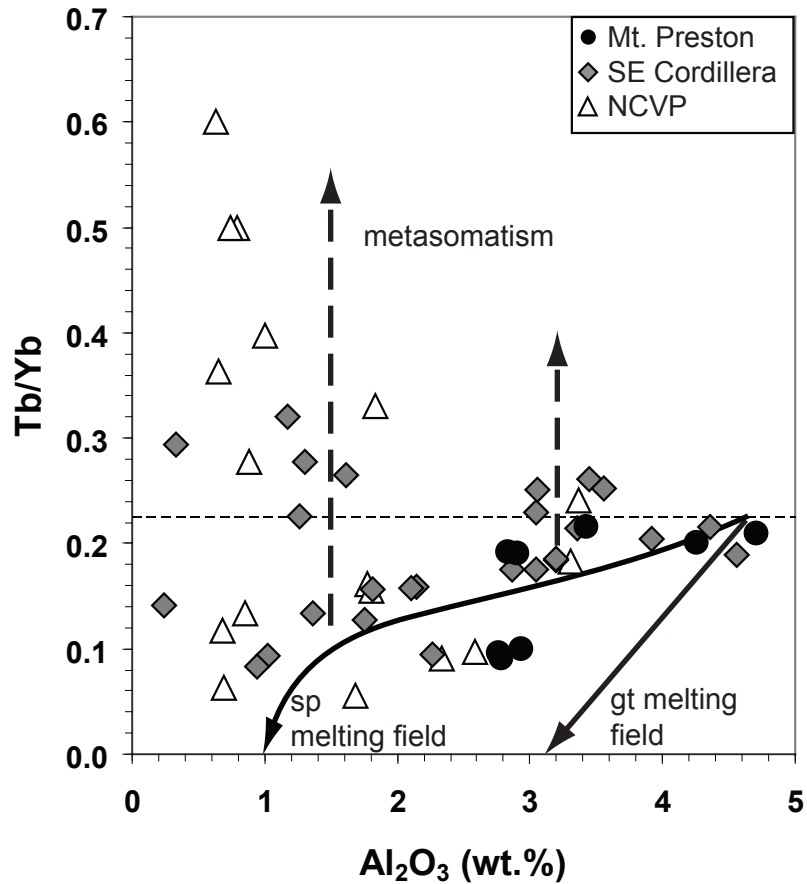


Figure 4.9 Tb/Yb vs. Al₂O₃ for Canadian Cordillera lherzolites, harzburgites, and dunites. Data sources as in Figure 4.8. Solid arrows show melting trends for spinel stable and garnet stable assemblages (Bodinier et al., 1988; McDonough and Frey, 1990). Chondrite Tb/Yb (McDonough and Sun, 1995) is also shown (horizontal dashed line). Figure after Peslier et al. (2002).

enriched the LREEs, following the depletion of incompatible elements during variable degrees of melting of fertile mantle, likely in the spinel stability field.

4.6 Re-Os Isotopes

Rhenium-osmium isotopic results are shown in Table 4.5. Generally during mantle melting Re is moderately incompatible, while Os is highly compatible. This is the basis behind the Re depletion age (T_{RD}), which is a minimum age for Re depletion, normally applied to mantle rocks which have experienced melt depletion. It assumes that all Re in the rock was extracted during melting, halting the growth of ^{187}Os . The model age (T_{MA}) is the model age of separation of the rock from a mantle reservoir that follows chondritic isotopic evolution (e.g. stabilization of mantle lithosphere from convecting mantle); this assumes that the sample's Re/Os reflects its long term history within the mantle.

Re-Os isotopes are often used to date the depletion event that caused the conversion of fertile peridotite into depleted, as Os is compatible during melting. However, sulfides complicate those model ages, as Os is highly soluble in sulfides and sulfides are mobile in the mantle; the Os isotope budget in mantle rocks is controlled by sulfides (Powell and O'Reilly (2007) and references therein). Alard et al. (2002) also noted that different powder aliquots from the same sample resulted in different Re-Os isotopic compositions. This is indicative of a perturbation in Re-Os system, and a consequence of the 'nugget effect'; the low abundance but high degree of control the sulfides have on the Re-Os system led to erroneous results.

Unfortunately Re-Os analyses were conducted on the Mt. Preston samples despite the presence of sulfides. The appearance of a 'future' Re depletion age (NP-MP05-160A) is an indication that the Re/Os ratio has been disturbed. The whole rock Re-Os results for the Mt.

Table 4.5 Rhenium-osmium isotopic and related data for mantle xenoliths, from Mt. Preston (NP) and Llangorse Mtn. (MH, LM). Ages are Re depletion age (T_{RD}) and model age (T_{MA}). Errors are 2σ .

Sample Name	Rock Type	Re (ppb)	Os (ppb)	$^{187}\text{Os}/^{188}\text{Os}$	$^{187}\text{Re}/^{188}\text{Os}$	T_{MA} (Ga)	T_{RD} (Ga)	S (ppm)	Al_2O_3 (wt.%)
NP-MP05-31	Lherzolite	0.3264 ± 0.007	4.7349 ± 0.0436	0.1270 ± 0.0007	0.3322 ± 0.003	1.24	0.28	200	2.94
NP-MP05-160A	Lherzolite	0.2474 ± 0.006	2.9246 ± 0.0269	0.1295 ± 0.0005	0.4077 ± 0.004	<0	<0	200	4.26
MH-02-116	Harzburgite	0.0086 ± 0.002	0.0440 ± 0.0004	0.1224 ± 0.0025	0.9392 ± 0.257	<0	0.92	<d/1 (40)	0.54
MH-02-121	Lherzolite	0.0312 ± 0.003	2.6408 ± 0.0243	0.1262 ± 0.0005	0.0568 ± 0.004	0.45	0.39	<d/1 (40)	2.34^1
95LM1	Harzburgite	0.0029 ± 0.002	0.1982 ± 0.0018	0.1233 ± 0.0011	0.0703 ± 0.057	0.95	0.79	<d/1 (40)	0.68

¹Average of 4 replicate samples.

Preston xenoliths cannot be interpreted, as they represent mixed results for the metasomatic sulfides and the peridotite hosts, and the sample aliquots themselves may have been subject to the nugget effect. However, recent advances in in situ Re-Os analysis of sulfides (e.g. Alard et al., 2000; 2002) present an excellent opportunity for future work on the Mt. Preston samples.

5. MANTLE CARBONATE

Carbonate was found in all of the mantle xenoliths examined, as well as the host dike and the dike wall rocks. Below the occurrence and composition of the carbonate are described.

5.1 Occurrence

The occurrence of carbonate in mantle xenoliths was investigated using a Cambridge Image Technology™ CL8200 Mk4 cold cathodoluminescence (CL) system attached to a petrographic microscope. Operating conditions included an excitation voltage of 15 kV and a current of 350 μ A. Granular carbonate (intergranular or inclusions) and/or carbonate veins are found in all mantle xenoliths (Fig. 5.1, Table 4.2). Mg-calcite grains were noted in 4 xenoliths (840 to 867 °C; 850 to 892 °C by T_{BK90}), veins in 10 xenoliths (792 to 885 °C; 826 to 924 °C by T_{BK90}), and both occurrences in 37 xenoliths (794 to 1044 °C; 815 to 1119 °C by T_{BK90}).

Intergranular carbonate (≤ 0.3 mm) is found as discrete grains exhibiting uniform extinction, or as patches with crystallographically distinct internal subdomains (Fig. 5.2, 5.3). Texturally the intergranular carbonate appears to be in equilibrium with coexisting silicate and oxide phases, as suggested by shared triple-point grain boundaries (Fig. 5.2b). Intergranular carbonate sometimes shows concentric zones of Mg-enrichment (Fig. 5.4b, d). Intergranular carbonate can be found in association with any combination of the other mantle silicate or oxide phases. In one peridotitic xenolith a small rutile inclusion was found within a carbonate grain (Fig. 5.2c). Some intergranular carbonate patches are associated with carbonate veins (Fig. 5.5a).

Carbonate also occurs as ≤ 0.2 mm inclusions (Fig. 5.4) hosted by all other mantle minerals. The carbonate inclusions are distinct from and appear unrelated to the carbonate veins, but some inclusions define trails that cross host grains (Fig. 5.5c).

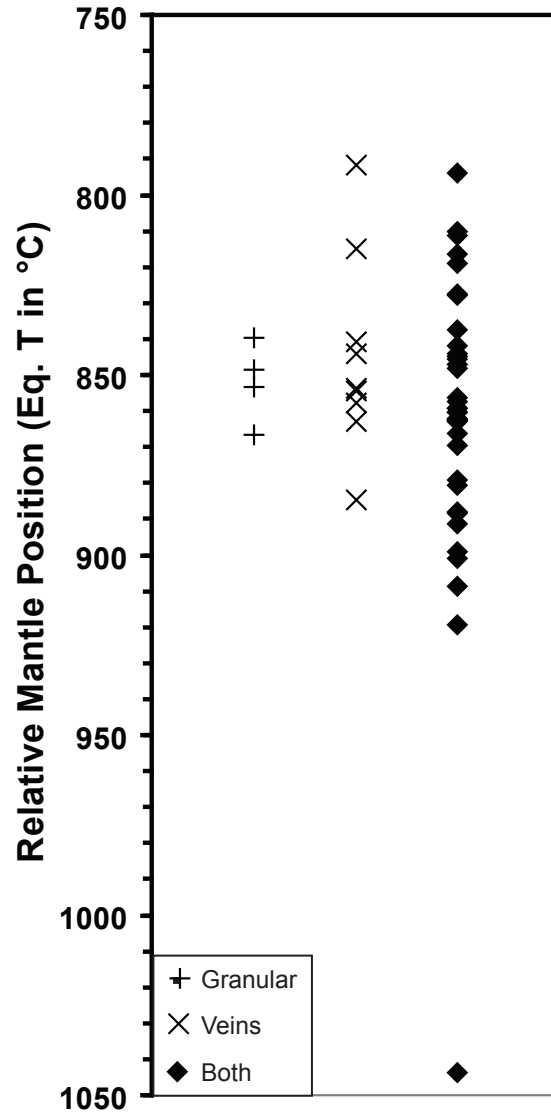


Figure 5.1 Occurrence and habits of carbonate in mantle xenoliths versus mantle position inferred by geothermometry. All xenoliths with calculated equilibration temperatures are plotted, as carbonate occurs in all samples examined.

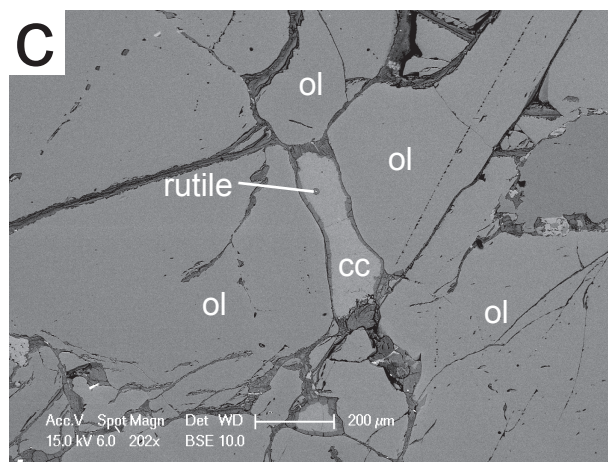
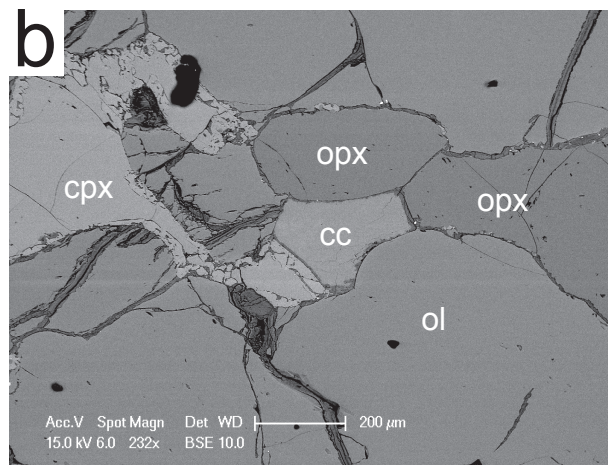
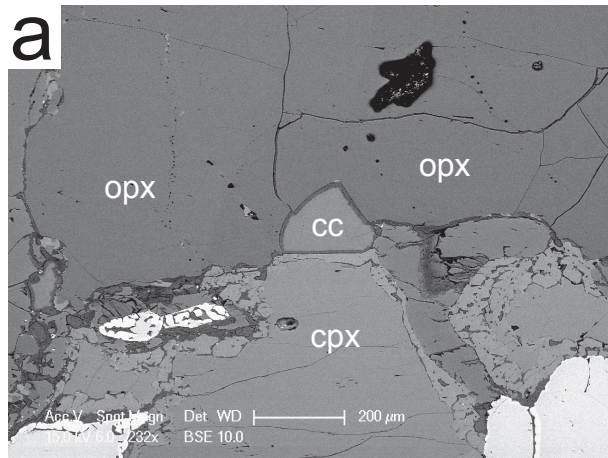


Figure 5.2 Backscattered electron SEM images of carbonate from mantle xenoliths, illustrating equilibrium textures with coexisting phases. (a) and (b) Granoblastic texture of carbonate in equilibrium with pyroxenes and olivine. (c) Calcite in textural equilibrium with olivine; carbonate has an inclusion of rutile. Phase label abbreviations as in Figure 3.1.

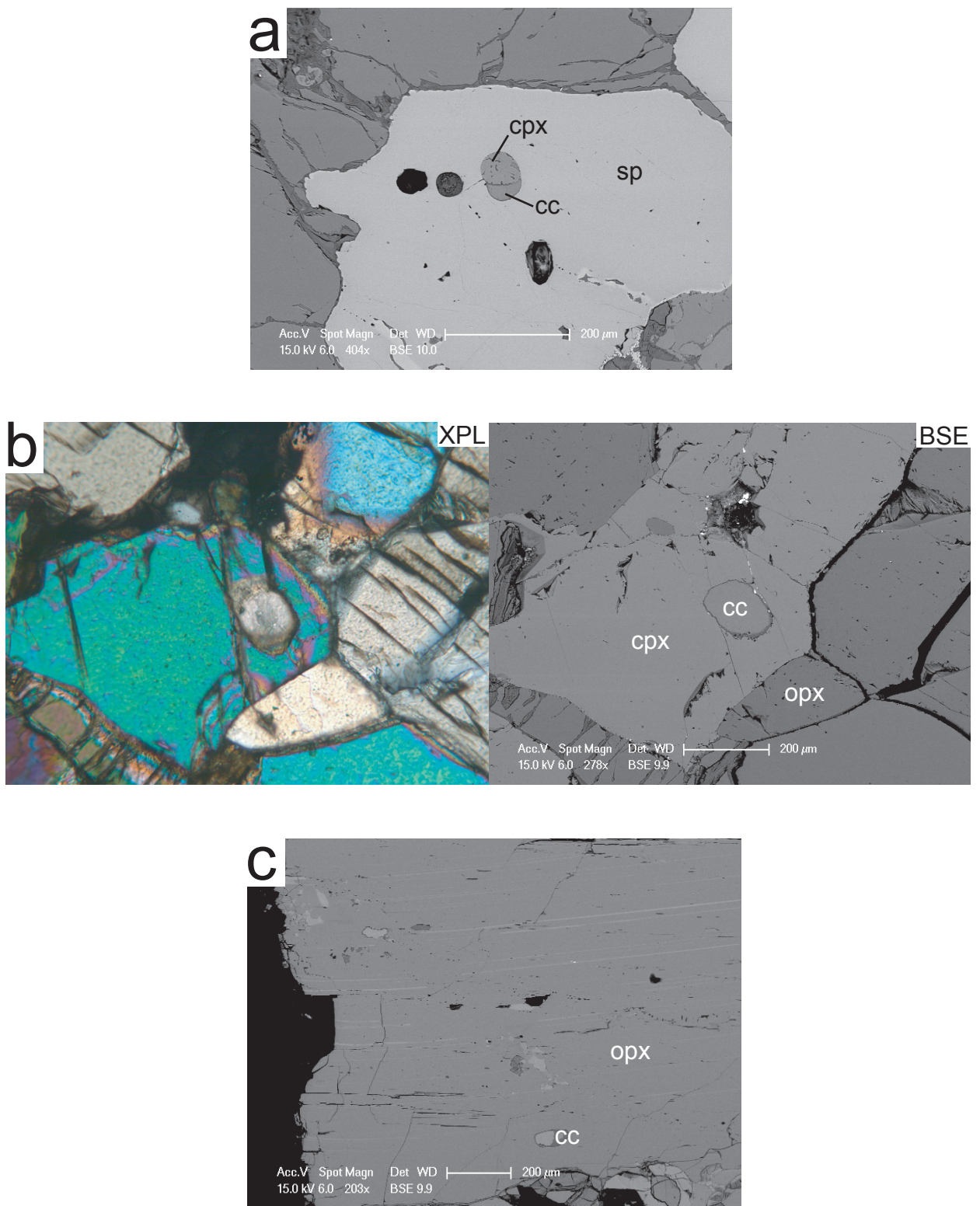


Figure 5.3 Backscattered electron (BSE) SEM images and a crossed polarized (XPL) photomicrograph of carbonate inclusions in other mantle xenolith minerals, including spinel (a), clinopyroxene (b), and orthopyroxene (c). Carbonate in (c) is part of a discontinuous linear inclusion trail that spans multiple host pyroxenes.

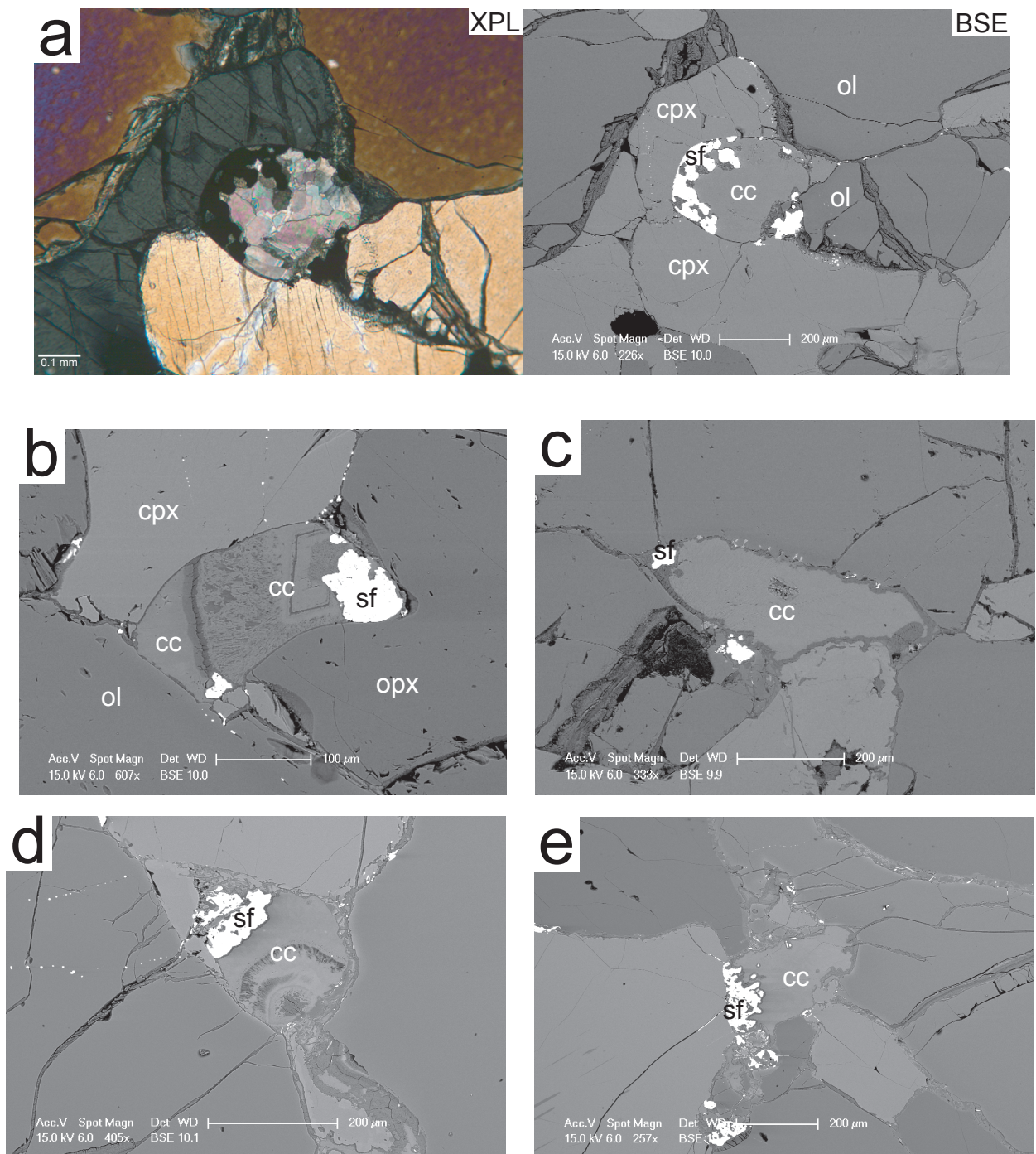


Figure 5.4 BSE SEM images and a crossed polarized photomicrograph illustrating the occurrence of sulfides (sf) and the common coexistence of sulfides and carbonate (cc).

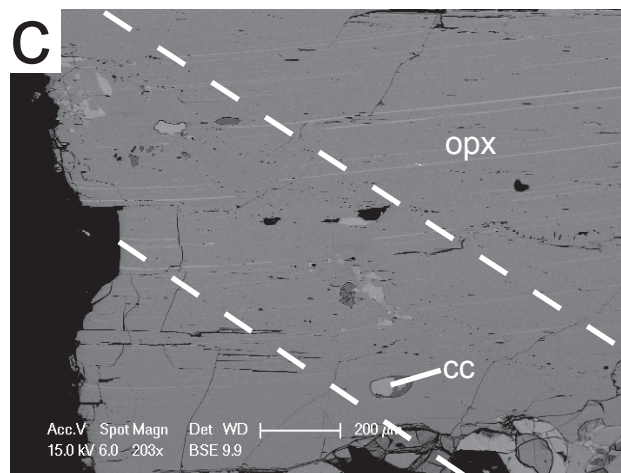
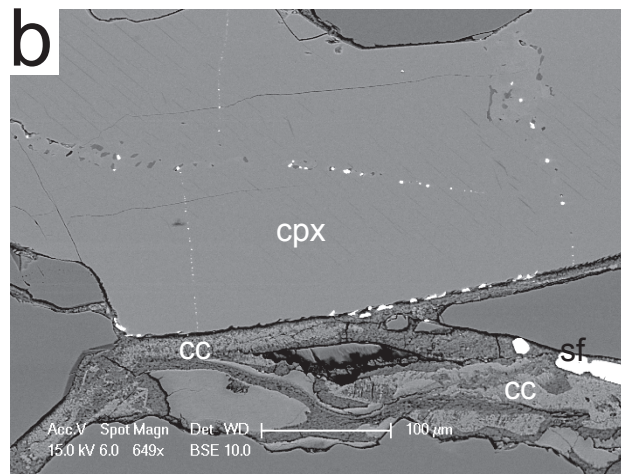
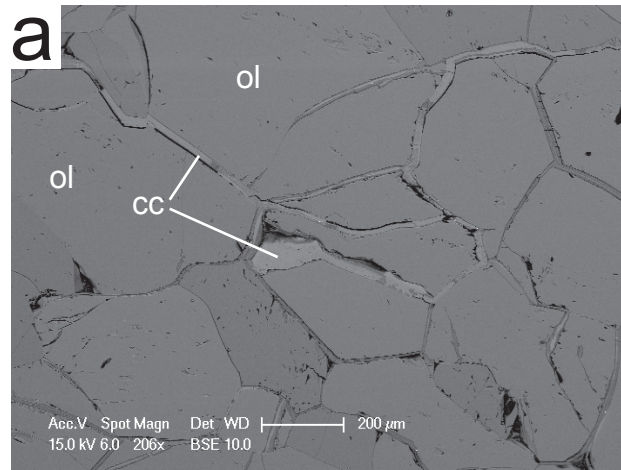


Figure 5.5 BSE SEM images illustrating carbonate veins, (a) and (b), and inclusion trails in grains, (b) and (c). Dashed lines in (c) mark the margins of a wide discontinuous inclusion trail.

Carbonate veins (≤ 0.1 mm wide) appear as intergranular and crosscutting features (Fig. 5.5). Occasionally carbonate veins are seen to merge with larger grains of carbonate (Fig. 5.5a). At least one host magma vein was observed to crosscut carbonate veins.

Electron microprobe-derived compositions range from X_{Ca} 86-94 for intergranular and vein carbonate, with an Mg# range of 79-92. Carbonates defining an inclusion trail (Fig. 5.5c) are more calcic (X_{Ca} 92-98) and more iron-rich (Mg# 50-72) in composition. All carbonate analysed within these mantle xenoliths are classified as Mg-bearing calcite. Quoted compositions exclude the Mg-rich bands in some carbonates; the compositions of these could not be measured precisely during microprobe analysis.

Rietveld analysis conducted on the XRD data of 15 mantle xenoliths was able to resolve calcite in all but three (Table 4.1). Errors on phases with such low abundance can be up to 100 %, although an abundance of 1 wt.% or less is corroborated by CL microscope observations of the 51 xenoliths.

Two crustal xenoliths (NP-MP05-26 and -27) from the basanite dike were examined on the CL microscope; neither sample contained carbonate. In addition, xenoliths from two sample suites from different parts of British Columbia were also examined. The Llangorse Mtn. xenolith suite of Harder (2004; Harder and Russell, 2006) and the xenolith suite of Resnick et al. (1999), from the Cheslatta Lake volcanics. Neither study had reported carbonate as a constituent in their rocks. Both the xenoliths and host lava were examined by CL microscopy but no carbonate was found.

Carbonate occurs in every xenolith in the Mt. Preston suite, including lherzolites, websterites, and dunites. A study of mantle xenoliths from New Mexico (Perkins et al., 2006) reported carbonate mainly in websterites and only rarely in lherzolites; no harzburgites were studied. In a study from the East African Rift in Tanzania (Lee et al., 2000), carbonate only

occurred in 2 of over 50 xenolith samples from the Labait volcano lavas, and in 4 of 7 samples from Monduli volcano lavas.

Intergranular carbonate has been reported in mantle-derived xenoliths from numerous localities in varied tectonic environments, such as Argentina (Laurora et al., 2001), Hungary (Demeny et al., 2004), the Kerguelen Islands (Delpech et al., 2004; Moine et al., 2004), Spitzbergen (Ionov et al., 1993; Ionov et al., 1996), the East African Rift (Lee et al., 2000), South Africa (Berg, 1986), and the southwest United States (Ducea et al., 2005; Perkins et al., 2006). Intergranular carbonates in these mantle xenoliths are usually associated with silicate glass (e.g. quenched melt). The carbonate commonly is globular in shape, showing curved menisci, partially coalesced globules, and intermingling with silicate glass (e.g. Demeny et al., 2004). This presence of glass in association with carbonate is interpreted as a primary mantle feature (i.e. unrelated to sampling; Perkins et al. (2006) and references therein); the fact that the glass has not crystallized and texturally equilibrated limits the duration between infiltration and transport to the surface. No glass was observed in the Mt. Preston suite, which is consistent with complete equilibration of the metasomatic carbonate within the mantle.

The intergranular carbonate textures in the Mt. Preston suite strongly suggest textural equilibrium between carbonate and the host peridotite was attained in the mantle. However, this does not imply long term equilibration; in at least one other suite (Perkins et al., 2006), carbonates appeared texturally equilibrated although isotopic disequilibrium between carbonate and the host mantle minerals required carbonate enrichment to have occurred shortly before sampling.

In other xenolith suites containing carbonate there is a common association with products of secondary crystallization (i.e. crystallization of infiltrating metasomatic fluid/melt or products of reaction with the host) such as amphibole, apatite, sulfides, and rutile, as well as secondary clinopyroxene and spinel, which have distinct compositions compared to those of the host rock

(e.g. Delpech et al., 2004). In the Mt. Preston xenoliths only sulfides and one small ($\sim 1 \mu\text{m}$) crystal of rutile were observed in association with carbonate. As reported for a suite of carbonated xenoliths from the East African Rift, there is no evidence of orthopyroxene replacement by clinopyroxene, as seen in many carbonatite-modified rocks (Lee et al. (2000) and references therein). In the Mt. Preston suite the absence of secondary silicate phases argues against silicate melt infiltration, while the absence of hydrous minerals argues against hydrous metasomatic agents.

Carbonate veins intrude grain fractures and along grain boundaries persistently; this feature is commonly noted in carbonated xenoliths (e.g. Lee et al., 2000) and has been attributed to low viscosity carbonate melt infiltration (Demeny et al., 2004). Sulfide melts also have low viscosities at mantle conditions (Gaetani and Groves, 1999).

While the presence of isolated carbonate inclusions is strong evidence for a mantle source for the carbonate, it cannot be used to argue for long-term carbonate equilibration in the mantle. Their presence is an indication of how quickly silicate phases can heal at mantle conditions; monomineralic inclusions of carbonate in host silicate phases have been described in other xenolith suites (e.g. Lee et al., 2000; Perkins et al., 2006) in which evidence indicated that carbonate introduction occurred shortly before or during host magma eruption.

Carbonate compositions in other xenolith suites (e.g. Lee et al. (2000) and references therein; Moine et al., 2004) are similar to those of the Mt. Preston suite (i.e. Mg-bearing calcite). Dalton and Wood (1993a) determined that Mg-calcite is stable in lherzolitic compositions at mantle temperatures and pressures; the stability field coincides with the temperature range from the Mt. Preston xenoliths, coupled with model pressure estimates (see Section 4.4). Different compositions of xenolith carbonate relative to primary carbonate from the entraining magma provide further support for the primary nature of the carbonate within the xenoliths, rather than infiltration from the volatiles of the entraining magma. The Mg-rich bands in some intergranular

carbonates from the Mt. Preston suite are similar to the Mn-rich bands found in a suite in New Mexico, which were interpreted to be growth-related (Perkins et al., 2006). Mg-calcite and dolomite could also occur together from subsolvus dissociation from disordered carbonate (Dalton and Wood, 1993a).

In summary, petrographic observations confirm these carbonates and sulfides are derived from the mantle lithosphere. Carbonate compositions are similar to other reports of mantle-derived carbonate, and are different from the composition of carbonate in the dike. The presence of apparently isolated carbonate inclusions in the xenoliths' phases is strong evidence for a mantle source. Carbonate veins and Mg-rich zones in intergranular carbonate are consistent with other reports of mantle-derived carbonate. The lack of carbonate in crustal xenoliths, the lack of secondary silicate phases related to the carbonate, and the fact that veins of host basanite crosscut carbonate veins argues against any relation to the host magma. There are also indications that the carbonate in the xenoliths attained equilibrium in the mantle: some textures suggest textural equilibrium, and the lack of glass and quench textures is consistent with long term equilibration within the mantle.

5.2 Sulfides

Sulfides (≤ 0.1 mm) were noted in eight of the xenoliths examined by CL. They commonly occur at the edges of carbonate grains, in contact with silicates (Fig. 5.3) or at the margins of carbonate veins (Fig. 5.5b). They also appear in inclusion trails, with or without associated carbonate (Figs. 5.3d, 5.5b). By EMP analysis, the sulfides are pentlandite and chalcopyrite (Fig. 5.6, 5.7). The sulfides are not sufficiently abundant volumetrically to be resolved by Rietveld analysis ($\ll 1$ %).

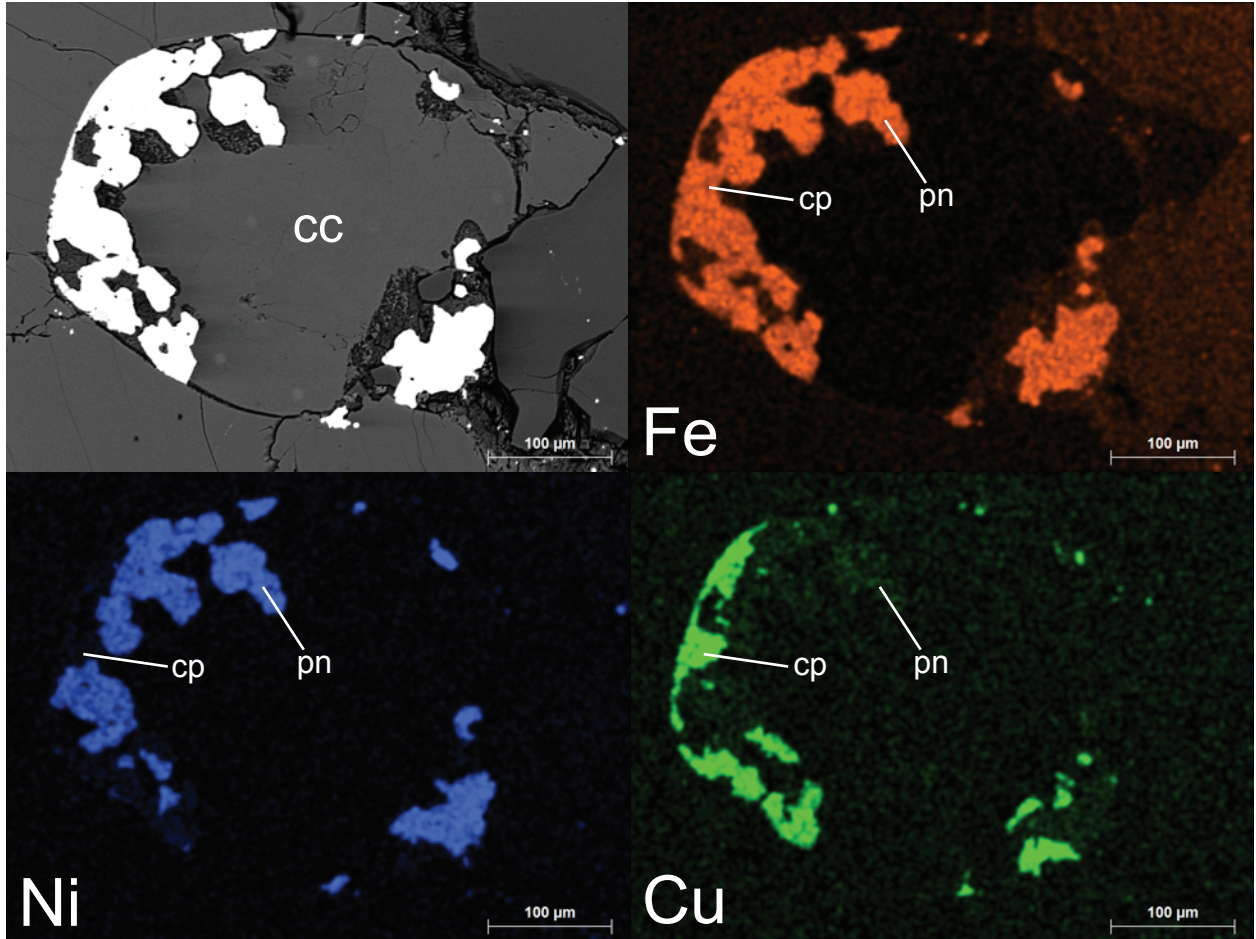


Figure 5.6 BSE image (top left) and false colour single element intensity maps, showing an example occurrence of coexisting sulfides pentlandite (pn) and chalcopyrite (cp), alongside calcite (cc) in a mantle xenolith. All images have the same field of view. See Figure 5.4a for coexisting phases and a photomicrograph.

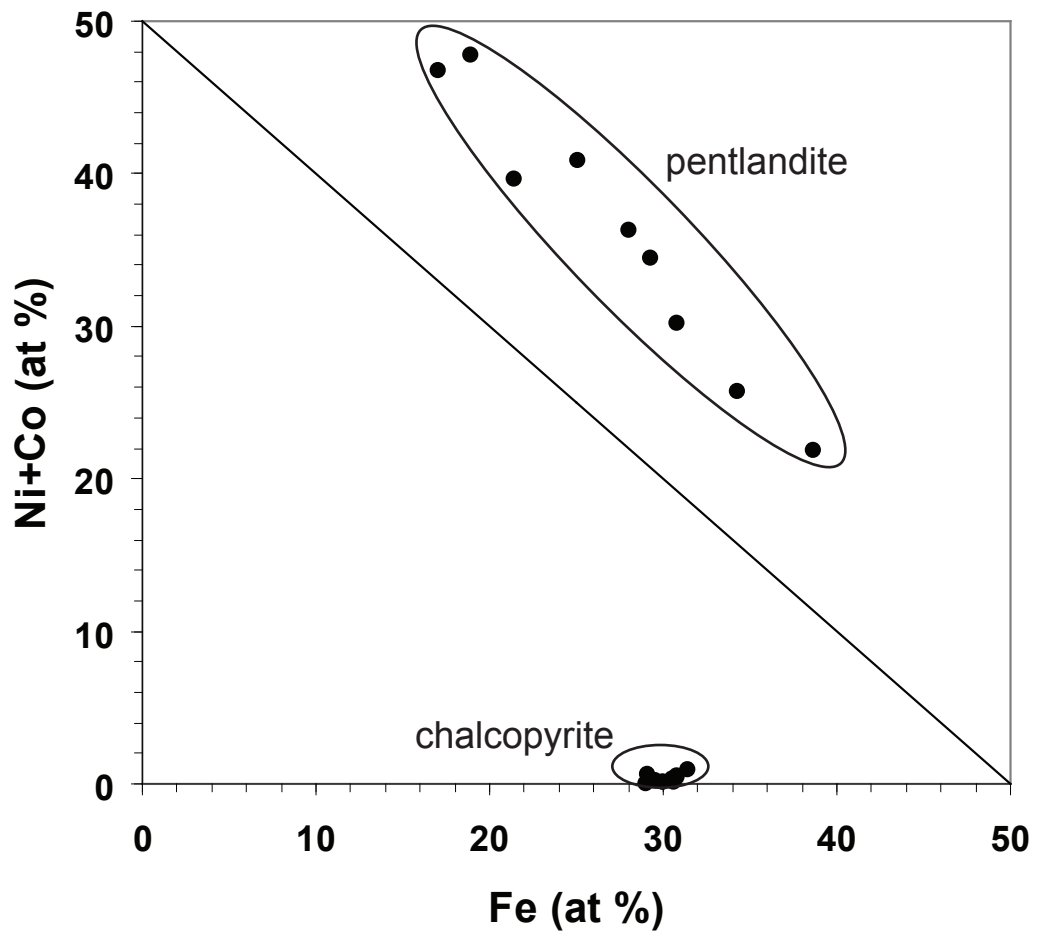


Figure 5.7 Compositions of coexisting sulfides analyzed in mantle xenoliths, plotted by atomic percentages of elements.

Sulfide occurrence spans the range of xenolith equilibration temperatures, and does not correlate with carbonate stable isotope composition (see Section 5.3). Pentlandite and chalcopyrite commonly occur together due to unmixing from an Fe, Cu, Ni mono-sulfide solution (Kogarko et al 1995; Ducea and Park, 2000). Sulfides are a common accessory in mantle-derived rocks, with carbonate (e.g. Ionov et al., 1996; Ionov, 1998) or without (e.g. Alard et al., 2002; Griffin et al., 2002). Like carbonate, sulfides have a low melting temperature relative to other phases within peridotites (Kogarko et al., 1995). However, for MSS of typical composition in the mantle ($\text{Fe}_6\text{Ni}_4\text{S}$), the solidus would be above the equilibration temperature of any of the Mt. Preston xenoliths (Lorand and Conquere, 1983), indicating that the sulfides would have been crystalline at equilibrium in the mantle lithosphere. Sulfides have been postulated as a common component of carbonate melts (Ionov et al., 1996) or carbonate-silicate melts (Kogarko et al., 1995). The sulfides in these xenoliths are unaltered; chalcopyrite and pentlandite would oxidize readily if exposed at or near surface. This is further support for the interpreted unaltered condition of the xenoliths from Mt. Preston.

5.3 Stable Isotopes

Carbon and oxygen isotope compositions are plotted in Figure 5.8 and shown in Tables 5.1, 5.2, and 5.3. To discriminate between carbonate sources, wall rock and dike carbonate was analyzed as well as carbonate from the xenoliths. Wall rock and dike analyses include microdrilled (i.e. targeted) as well as leached whole rock samples; see Appendix E for methods. Carbonates from the dike (includes vesicles and groundmass), wall rock, and mantle xenoliths all have distinct carbon-oxygen isotopic compositions. The wall rock carbonate has $\delta^{18}\text{O}$ compositions of -1.7 to -2.6 ‰ relative to Vienna Standard Mean Ocean Water (VSMOW), and $\delta^{13}\text{C}$ compositions of -5.4 to -5.9 ‰ relative to Vienna Peedee Belemnite (VPDB). Dike

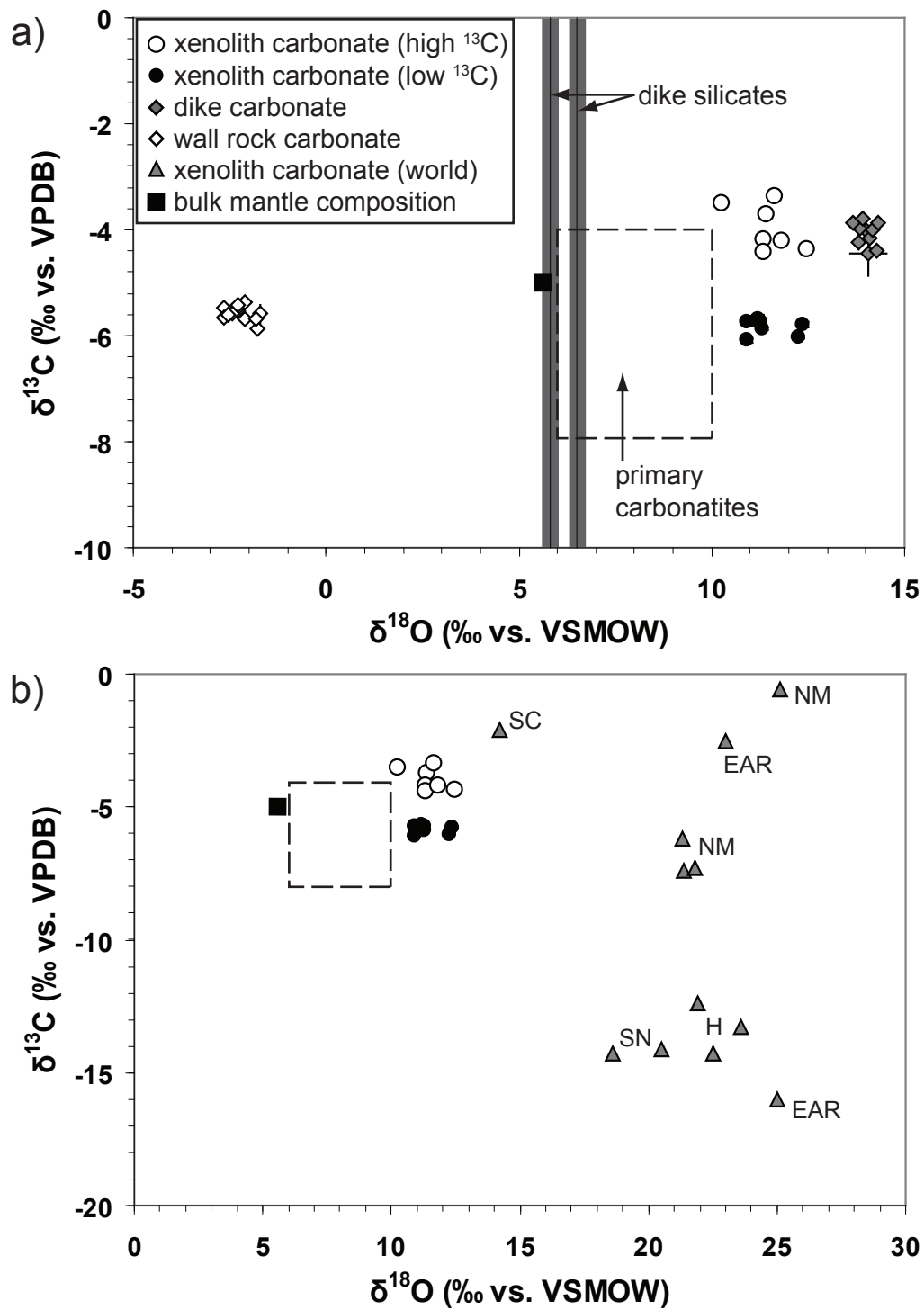


Figure 5.8 Carbon and oxygen isotope compositions for carbonates in mantle xenoliths, wall rock, and dike from Mt. Preston, and mantle xenoliths worldwide. Primary carbonatite and bulk mantle included for reference. (a) Samples from Mt. Preston. (b) Xenolith-hosted carbonate, including worldwide samples: NM New Mexico (Perkins et al., 2006); SN Sierra Nevada (Ducea et al., 2005); H Hungary (Demeny et al., 2004); SC Slave Craton (van Achterbergh et al., 2002); EAR East African Rift (Lee et al., 2000). Analysis errors are generally smaller than symbols, or unreported. Primary carbonatite field from Taylor et al. (1967) and Keller and Hoefs (1995); bulk mantle value from Harmon and Hoefs (1995) and Deines (2002).

Table 5.1 Carbon and oxygen isotopic compositions of carbonate within the basanite dike. Errors are 1σ .

Sample	$\delta^{13}\text{C}$ (‰ vs. VPDB)	$\delta^{18}\text{O}$ (‰ vs. VSMOW)
NP-MP05-1 ^(a)	-4.23 ± 0.13	13.82 ± 0.09
NP-MP05-1 ^(a)	-4.00 ± 0.09	13.98 ± 0.10
NP-MP05-1 ^(a)	-3.97 ± 0.10	13.83 ± 0.07
NP-MP05-1 ^(b)	-3.88 ± 0.07	13.67 ± 0.05
NP-MP05-1 ^(b)	-3.79 ± 0.05	13.90 ± 0.06
NP-MP05-1 ^(c)	-4.14 ± 0.14	14.08 ± 0.14
NP-MP05-1 ^(d)	-3.99 ± 0.08	14.17 ± 0.14
NP-MP05-1 ^(d)	-3.86 ± 0.07	14.30 ± 0.10
NP-MP05-1 ^(e)	-4.46 ± 0.41	14.05 ± 0.47
NP-MP05-1 ^(e)	-4.39 ± 0.06	14.29 ± 0.07

Carbonate fractions extracted from: (a) whole rock powders; (b, c, d, e) carbonate-rich patches by microdrilling.

Table 5.2 Carbon and oxygen isotopic compositions of carbonate within low grade metamorphic rocks of the Hazelton Group. Errors are 1σ .

Sample	$\delta^{13}\text{C}$ (‰ vs. VPDB)	$\delta^{18}\text{O}$ (‰ vs. VSMOW)
NP-MP05-4 ^(a)	-5.47 ± 0.00	-2.64 ± 0.00
NP-MP05-4 ^(a)	-5.53 ± 0.08	-2.43 ± 0.05
NP-MP05-4 ^(a)	-5.67 ± 0.05	-2.64 ± 0.05
NP-MP05-4 ^(a)	-5.53 ± 0.05	-2.28 ± 0.06
NP-MP05-4 ^(b)	-5.58 ± 0.09	-2.43 ± 0.05
NP-MP05-4 ^(b)	-5.88 ± 0.07	-1.76 ± 0.13
NP-MP05-4 ^(c)	-5.45 ± 0.03	-2.27 ± 0.03
NP-MP05-4 ^(c)	-5.36 ± 0.04	-2.11 ± 0.04
NP-MP05-4 ^(d)	-5.62 ± 0.05	-2.53 ± 0.07
NP-MP05-4 ^(d)	-5.43 ± 0.05	-2.29 ± 0.05
NP-MP05-4 ^(e)	-5.59 ± 0.17	-1.72 ± 0.11
NP-MP05-4 ^(e)	-5.68 ± 0.06	-2.09 ± 0.06
NP-MP05-4 ^(e)	-5.69 ± 0.08	-1.83 ± 0.10

Carbonate fractions extracted from: (a) whole rock powders; (b, c, d, e) carbonate-rich patches by microdrilling.

Table 5.3 Carbon and oxygen isotopic compositions of carbonate from mantle-derived xenoliths. Errors are 1σ .

Sample	$\delta^{13}\text{C}$ (‰ vs. VPDB)	$\delta^{18}\text{O}$ (‰ vs. VSMOW)
NP-MP05-31	-4.36 ± 0.10	12.46 ± 0.08
NP-MP05-35	-5.67 ± 0.06	11.20 ± 0.06
NP-MP05-35 ¹	-6.09 ± 0.04	10.92 ± 0.05
NP-MP05-44	-5.72 ± 0.04	11.17 ± 0.03
NP-MP05-50	-5.74 ± 0.07	10.91 ± 0.11
NP-MP05-69	<d/l	<d/l
NP-MP05-70A	-4.41 ± 0.06	11.35 ± 0.06
NP-MP05-78	-6.03 ± 0.03	12.26 ± 0.05
NP-MP05-79A	-4.20 ± 0.05	11.82 ± 0.05
NP-MP05-139	-5.75 ± 0.07	11.26 ± 0.09
NP-MP05-159A	-5.79 ± 0.05	12.35 ± 0.05
NP-MP05-160A	-3.72 ± 0.04	11.41 ± 0.04
NP-MP05-160B	-3.37 ± 0.06	11.64 ± 0.07
NP-MP05-161D	-3.51 ± 0.08	10.26 ± 0.09
NP-MP05-162A	-4.19 ± 0.05	11.34 ± 0.04
NP-MP05-164A	-5.87 ± 0.03	11.30 ± 0.06

¹ Replicate sample based on splitting of sample before powdering.

carbonate has $\delta^{18}\text{O}$ compositions of 13.7 to 14.3 ‰ (VSMOW), and $\delta^{13}\text{C}$ compositions of -3.8 to -4.5 ‰ (VPDB). Carbonates from the 14 mantle xenoliths analyzed fall into two separate groups identified by different ^{13}C compositions. The ^{13}C -enriched group (7 xenoliths) has $\delta^{13}\text{C}$ compositions between -3.4 and -4.4 ‰ (VPDB), while the ^{13}C -depleted group (7 xenoliths) has $\delta^{13}\text{C}$ compositions between -5.7 and -6.1 ‰ (VPDB). In terms of oxygen isotopes both groups have similar compositions; total $\delta^{18}\text{O}$ range is 10.3 to 12.5 ‰ (VSMOW). The two isotopic groups occur in an overlapping range of the mantle lithosphere recorded by paleo-equilibration temperatures (816 to 1044 °C (851 to 1119 °C, T_{BK90}) for the seven xenoliths in the ^{13}C enriched group, 811 to 888 °C (849 to 940 °C, T_{BK90}) for the seven in the ^{13}C depleted group).

All but two of the xenolith samples used for stable isotope analysis contained both granular carbonate and carbonate veins. The other two contained only vein carbonate and they are part of the ^{13}C -depleted group. There appears to be no correlation between carbon isotope composition and equilibration temperature (i.e. mantle position), carbonate abundance, sulfide occurrence, or bulk composition.

The $\delta^{18}\text{O}$ composition of wall rock carbonate (~2 ‰ less than VSMOW) is consistent with equilibration with meteoric or formation water. In the dike, $\delta^{18}\text{O}$ values are ~14 ‰ greater than VSMOW, which is 8 ‰ higher than the associated silicates in the dike (Fig. 5.8a; Tables 3.6, 5.1). These results indicate that the sources for the carbonate in the dike and the wall rock were isotopically distinct. The whole rock and microdrilled samples within each lithology also show no significant isotopic variation within each rock, indicating that (a) neither rock experienced crystallization of carbonate from multiple isotopic sources, or (b) complete overprinting of isotopic signatures from previous events occurred. It also validates the process of acid leaching in these rocks during analysis, as microdrilled and leached samples had similar compositions. It is important to note that the samples from the dike and wall rock were separated by <20 m in the

field. The distinct isotopic compositions for dike and wall rock carbonate which exist in close spatial association is strong evidence against overprinting by post-dike emplacement (~19 Ma) processes.

The carbonate within the dike no signs of isotopic exchange with meteoric waters; isotopic exchange with these fluids would deplete the carbonate in ^{18}O , and with enough exchange eventually to compositions representative of meteoric water. Carbonates are sensitive to isotopic exchange relative to most silicates, though at low temperatures ordered calcite is essentially closed to alteration (O'Neil, 1987), suggesting that low temperatures have prevailed since the dike emplaced. These observations add confidence to interpretations based on the unaltered nature of the dike and its xenoliths.

The isotopic compositions of the carbonates from the dike are consistent with primary magmatic carbonate described from other basaltic dikes (e.g. Demény and Harangi, 1996). At magmatic temperatures (1000-1200 °C) oxygen isotopic fractionation should be less than 2 ‰ between calcite and the dike silicates such as forsterite and diopside (Chiba et al., 1989). This is evidence of isotopic exchange between minerals and fluids during cooling. In a suite of carbonate-bearing basaltic dikes with similar carbonate isotopic compositions, Demény and Harangi (1996) attributed enrichment of ^{18}O in the carbonates to isotopic exchange with the magmatic fluid phase during cooling and degassing.

All the mantle lithosphere sampled and analyzed is carbonated. Thus it is very likely the dike magma mechanically and chemically scavenged carbonate from entrained and disaggregated xenoliths to produce a melt phase richer in CO_2 that could be induced to exsolve a CO_2 -rich fluid during ascent from depressurization. The C-O isotopic compositions of the dike and xenolith carbonate are consistent with this hypothesis. The additional CO_2 volatile content in the melt would assist magma ascent, creating higher rise velocities, thus aiding in preserving other xenoliths.

The carbonates from the Mt. Preston xenoliths are closer to primary mantle isotopic compositions than any other mantle-hosted carbonates reported (Fig. 5.8b; Lee et al., 2000; van Achterbergh et al., 2002; Demeny et al., 2004; Ducea et al., 2005; Perkins et al., 2006). The Mt. Preston xenoliths host carbonate having $\delta^{18}\text{O}$ compositions less than 3 ‰ greater than the field established to date for primary mantle-derived carbonatites (Fig. 5.8; Taylor et al., 1967; Keller and Hoefs, 1995). In other studies, authors report enriched $\delta^{18}\text{O}$ compositions in mantle-derived carbonate in xenoliths (Lee et al., 2000; van Achterbergh et al., 2002; Demeny et al., 2004; Ducea et al., 2005; Perkins et al., 2006) that are taken to indicate isotopic disequilibrium between carbonate and host silicates, and explained by short durations between enrichment and eruption. The global mantle average for the $\delta^{18}\text{O}$ composition of the silicate and oxide phases in spinel peridotite xenoliths is approximately 5-5.7 ‰ relative to VSMOW depending on the phase (Mattey et al., 1994). If oxygen isotope compositions in the Mt. Preston xenoliths' silicates are similar to those compositions, the carbonate in the xenoliths is ^{18}O enriched by approximately 4 to 7 ‰ above coexisting silicate compositions. In the range of equilibration temperatures of the Mt. Preston xenoliths, $\Delta^{18}\text{O}_{\text{cc-di}}$ fractionations are expected to be ~1.5-2 ‰, and $\Delta^{18}\text{O}_{\text{cc-fo}}$ fractionations 2-3 ‰ (Chiba et al., 1989). To explain this potential difference of up to 5.5 ‰ isotopic compositions of the silicates would be needed. If an oxygen isotopic gradient between carbonates and coexisting silicates exists that indicates disequilibrium, that information can be used to estimate residence times of the carbonate within the mantle and thus the age of metasomatic enrichment. However, while melts in the mantle may retain their oxygen isotopic composition over relatively long time scales (e.g. Perkins et al., 2006), once crystallized and diffused in small pockets at low modal proportions as in the Mt. Preston xenoliths, equilibration is attained rapidly via diffusion. For a 0.3 mm calcite grain under anhydrous conditions (Labotka et al., 2000) at 1100 °C equilibrating with diopside (Chiba et al., 1989) having a $\delta^{18}\text{O}$ of 5 ‰, calcite of a $\delta^{18}\text{O}$ composition of 25 ‰ would reach the compositions measured in the Mt. Preston

xenoliths (10.3 to 12.5 ‰) in just 4 to 10 years (Perkins et al. (2006), following Crank (1975)). The existence of distinct ^{13}C -depleted and -enriched groups suggests that at least two enrichment events are recorded in the suite of xenoliths analyzed from Mt. Preston. If this is the case, either the xenoliths were sampled shortly after these episodes of enrichment (by a source that crystallized carbonates of dissimilar $\delta^{18}\text{O}$ and $\delta^{13}\text{C}$ compositions, coincidentally sampling and halting the $\delta^{18}\text{O}$ equilibration process at a point when they recorded similar compositions) before the carbonates equilibrated their oxygen isotopic compositions with the host silicates, or the carbonate products of these enrichment events isotopically equilibrated in the mantle.

5.4 Strontium Isotopes

Strontium isotopes record the composition of the carbonate source, as they are insensitive to fractionation during phase changes such as melting and crystallization. In addition, calcium carbonates readily accept strontium while excluding rubidium. Results are presented in Figure 5.9 on an Sr-O isotope diagram, and in Tables 5.4 and 5.5. The $^{87}\text{Sr}/^{86}\text{Sr}$ ratio of the dike carbonate is 0.7040, while the country rock carbonate ratio is approximately 0.7047. The bulk rock $^{87}\text{Sr}/^{86}\text{Sr}$ ratio (0.7036) for the dike is also different from the carbonate separated from the dike. In addition, carbonates from the mantle xenoliths fall into two different composition groups ($^{87}\text{Sr}/^{86}\text{Sr}$ ratios of approximately 0.7044 and 0.7046).

Strontium isotope compositions show excellent agreement with the carbon and oxygen isotopic compositions. The strontium isotopes reveal different source compositions for the carbonate in the country rock and the dike, and for the ^{13}C -enriched and ^{13}C -depleted groups of xenolith carbonate, which is consistent with the carbon and oxygen isotope results. The strontium isotope compositions also show the interesting result that the carbonate from the dike

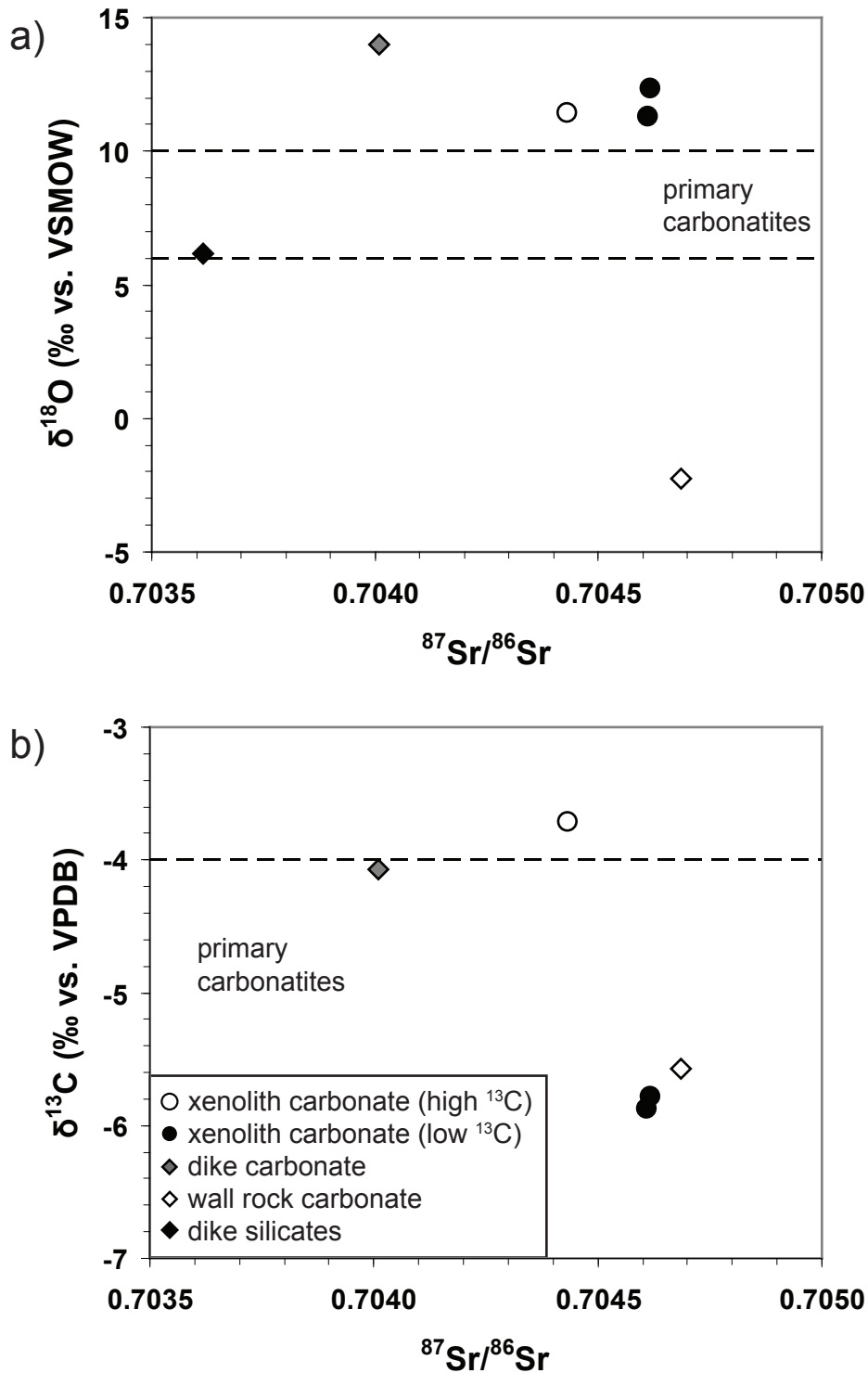


Figure 5.9 Strontium isotope composition of dike, wall rock, and peridotite carbonate, and dike silicates, plotted against (a) oxygen and (b) carbon (without dike silicate) isotopic compositions. Low and high ^{13}C groups (Fig. 5.8) correspond to high and low $^{87}\text{Sr}/^{86}\text{Sr}$ compositions, respectively. For dike silicates, Sr composition is represented by whole rock Sr data (Table 3.3). Composition range for primary carbonatites (last 500 Ma) from Taylor et al. (1967), Keller and Hoefs (1995), and Barker (1996).

Table 5.4 Strontium isotopic compositions of carbonate extracted from whole rock powders of the basanite dike and surrounding metamorphic rocks, and standards used in analyses. Errors are 2σ .

Dike sample	$^{87}\text{Sr}/^{86}\text{Sr}$	Cycles	$^{86}\text{Sr}/^{88}\text{Sr}$
NP-MP05-1	0.704010 ± 0.000007	145	0.1191
NP-MP05-1 ¹	0.704025 ± 0.000007	145	0.1191
Wall rock sample			
NP-MP05-4	0.704685 ± 0.000007	142	0.1191
NP-MP05-4 ¹	0.704676 ± 0.000007	145	0.1195
Standard			
SRM987 (600ng)	0.710242 ± 0.000006	141	0.1198
SRM987 (600ng)	0.710245 ± 0.000007	143	0.1194
SRM987 (600ng)	0.710242 ± 0.000008	114	0.1188

¹ Duplicate analysis.

Table 5.5 Strontium isotopic composition of carbonate from mantle xenoliths, and standards used in analyses. Errors are 2σ .

Sample	$^{87}\text{Sr}/^{86}\text{Sr}$	Cycles	$^{86}\text{Sr}/^{88}\text{Sr}$
NP-MP05-159A	0.704618 ± 0.000008	146	0.1198
NP-MP05-160A	0.704432 ± 0.000008	144	0.1196
NP-MP05-164A	0.704610 ± 0.000008	147	0.1196
NP-MP05-164A ¹	0.704607 ± 0.000009	139	0.1199
Standard			
SRM987 (600ng)	0.710220 ± 0.000008	130	0.1195
SRM987 (300ng)	0.710233 ± 0.000008	148	0.1200
SRM987 (600ng)	0.710232 ± 0.000007	142	0.1192

¹ Duplicate analysis.

does not have the same $^{87}\text{Sr}/^{86}\text{Sr}$ composition as the silicates in the melt it was associated with. All Sr isotopic compositions are consistent with a mantle source (Zindler and Hart, 1986).

The $^{87}\text{Sr}/^{86}\text{Sr}$ composition of the dike carbonate (0.7040) is different from the dike whole rock (0.7036), suggesting a different or contaminated source for the carbonate in the dike. If a CO_2 -rich volatile phase had already exsolved during dike emplacement, and it absorbed volatilized carbonate from mantle xenoliths and/or crustal xenoliths, it may explain this unique Sr composition. Mixing between a carbonate phase with the composition of the dike whole rock (0.7036) and carbonates from disaggregated mantle xenoliths similar to those analyzed (0.7044-0.7046) is a plausible origin for the Sr composition of the carbonates in the dike (0.7040). Enrichment of CO_2 in a host magma by the assimilation of carbonate from xenoliths was also suggested by Ionov et al. (1993), who noted carbonate in the host basanite of a suite of carbonate-bearing xenoliths. Importantly, the carbonates in the xenoliths have a more radiogenic Sr composition (0.7044-0.7046) than the dike whole rock or its associated carbonate, ruling out either as the contributor for the carbonate in the xenoliths.

The strontium isotope compositions for the xenoliths indicate that the ^{13}C -enriched carbonates have low $^{87}\text{Sr}/^{86}\text{Sr}$ compositions, and vice versa. This supports the hypothesis of multiple enrichment events with different carbon and strontium isotope compositions (oxygen isotopes cannot be commented on as they are indistinguishable between groups, and may represent equilibrium compositions in the xenoliths rather than source compositions). Note that because strontium isotopes in carbonate were analyzed using acid leaches, separate carbonate populations within single xenoliths (if they exist) cannot be resolved. However, the fact that the carbonates from individual xenoliths record two isolated groups in $\delta^{13}\text{C}$ and $^{87}\text{Sr}/^{86}\text{Sr}$ space, rather than recording a spectrum of mixing between end members, suggests that is not an issue.

6. DISCUSSION

6.1 Cordilleran Mantle Lithosphere as Host

In terms of many thermal, mineralogical, petrological, and chemical properties, the mantle sampled from beneath Mt. Preston is not distinct from other samples of BC mantle lithosphere. Instead, it is made unique by the presence of carbonate and sulfides in the mantle sampled, and features attributable to metasomatic enrichment by a carbonate-bearing agent.

6.1.1 Thermal properties and depth

The low temperature (i.e. shallow) mantle lithosphere is better represented than the deep lithosphere in the suite (~ 800 to 900 °C; ~ 850 and 950 °C, T_{BK90}). This has been noted in other BC suites (e.g. Prescott, 1983; Harder, 2004). The lowest equilibration temperature from the suite (792 °C; 826 °C, T_{BK90}) among other data was used in a one dimensional crustal model (Harder, 2004; Harder and Russell, 2006), which produced a model geotherm for the Mt. Preston area. On the model geotherm (Fig. 4.5), the highest temperature (1044 °C; 1119 °C, T_{BK90}) xenolith sits at 49 km depth, which is 8 km deeper than the next highest temperature xenolith; the most sampled interval of temperatures corresponds to a depth range of ~ 32 to 40 km. Thus using an average model geotherm the mantle lithosphere under Mt. Preston is at least 17 km thick, for a total lithospheric thickness of at least 49 km. For comparison, a rigorous family of geotherms determined for the Llangorse Mtn. area in the NCVP resulted in a lithospheric mantle 16 - 30 km thick with a Moho fixed at 36 km depth, for a total lithospheric thickness of 52 - 66 km (Harder and Russell, 2006). The temperature range for the mantle lithosphere represented by the Mt. Preston xenolith suite is typical for hot mobile belts like the Canadian Cordillera (Hyndman et al., 2005) and is consistent with results from other xenolith suites in British Columbia (Harder

(2004) and references therein). Using the Brey and Köhler (1990) thermometer for comparison purposes, the Mt. Preston suite records an equilibration temperature range of 815-1119 °C; using this thermometer suites in the NCVP record an overall temperature range of ~780-1220 °C (Harder (2004) and references therein). The estimation of similar depths to the Moho by geophysical surveys in other parts of the province (e.g. Hammer and Clowes, 2004) contributes to similar calculated geotherms for those xenolith suites, indicating similar temperature-depth profiles for the mantle lithosphere in BC.

6.1.2 Modal mineralogy

In addition to ranges of paleotemperatures and lithospheric depths, other properties of the Mt. Preston suite are conformable with other reported Cordilleran xenolith suites. The suite is modally dominated by lherzolites (i.e. ‘unimodal’) in composition (Fig. 4.2, Table 4.1), which is typical of Canadian Cordilleran suites except several from northwest British Columbia to southwest Yukon, which contain higher proportions of harzburgites (Shi et al., 1998). With the exception of two plagioclase-spinel websterites, all the Mt. Preston xenoliths are only spinel-bearing, consistent with the interpreted lithospheric mantle depths and temperatures and other Cordilleran suites; plagioclase peridotites are rarely found (e.g. Prescott, 1983).

Of the 51 xenoliths studied in detail, 48 have olivine (ol), clinopyroxene (cpx), orthopyroxene (opx), spinel (sp), as in most other Cordilleran xenolith suites (e.g. Littlejohn and Greenwood, 1974). Of the other three, two are websterites that lack olivine and contain plagioclase (Fig. 4.1b), and one is a dunite that does not contain orthopyroxene. Although equilibrated plagioclase-spinel websterites similar to the two from the Mt. Preston suite have not been reported elsewhere, plagioclase-spinel websterite has been reported in at least one other suite (Canil et al., 1987). Dunites are a minor but common component in Cordilleran suites.

6.1.3 Textures

All xenoliths exhibit equilibrium (i.e. granoblastic) texture and show no signs of shearing, similar to Canadian Cordilleran mantle lithosphere described elsewhere (Littlejohn and Greenwood, 1974). The lack of hydrous minerals or glass is consistent with other sites; hydrous minerals are a rare and minor phase in Canadian Cordilleran xenoliths (Brearley and Scarfe, 1984; Canil and Scarfe, 1989; Peslier et al., 2002).

6.1.4 Major element compositions

Mineral compositions are Mg-rich and Cr-rich, consistent with mantle-derived samples (Frey and Prinz, 1978). The suite's Mg numbers and Al_2O_3 contents (and mean) are very similar to other unimodal mantle xenolith localities in British Columbia (Shi et al., 1998; Peslier et al., 2002). Major element chemical compositions are broadly similar to those of other mantle xenolith suites in the Canadian Cordillera (Fig. 4.6, Fig. 4.7; Peslier et al., 2002; Francis, 1987; Shi et al., 1998; Harder, 2004) and other continental spinel-bearing peridotites worldwide (Peslier et al., 2002). On indices of depletion (Figs. 4.6, 4.7) with the exception of the websterites the xenoliths show compositions reflecting varying degrees of melt extraction from a fertile mantle source. However, most of the xenoliths show calcium enrichment relative to aluminum; this is not unique, but may relate to carbonation. Some southeast Canadian Cordilleran xenoliths show Ca enrichment and although modal carbonate has not been reported in those rocks, past carbonate metasomatism is considered a plausible explanation for their chemical compositions (Peslier et al., 2002). The websterites are highly enriched in components such as CaO and Al_2O_3 , and are extremely fertile; their compositions indicate previous enrichment by melts (e.g. Canil et al., 1987).

6.1.5 Trace and rare earth element compositions

Trace and rare earth element (REE) compositions (Table 4.4, Fig. 4.8) are similar to some other BC suites (Peslier et al., 2002; Harder, 2004). Many of the xenolith suite's REE patterns show a 'spoon-shaped' profile of broad LREE depletion, with enrichment of the lightest REEs. This feature is consistent with metasomatism by LREE-rich melts (Takazawa et al., 1992) and has been observed in other carbonate-bearing xenolith suites (e.g. Delpech et al., 2004). While not unique to the Cordillera (e.g. Peslier et al., 2002; Harder, 2004) these features may relate to the enrichment event producing the carbonates and sulfides seen in the xenoliths.

6.1.6 Summary

The similarities in properties such as thermal character, depth profile, modal mineralogy, textures, and chemistry across BC indicates the mantle lithosphere beneath Mt. Preston has experienced similar processes as elsewhere in the Canadian Cordillera. Exceptions to this are features directly attributable to metasomatic enrichment. Reaction rims on clinopyroxene may be related to high temperature carbonate enrichment (Laurora et al., 2001). Inclusion trails in the Mt. Preston xenoliths, preferentially affecting pyroxenes, are similar to other metasomatized suites (e.g. Perkins et al., 2006). Other features such as Ca enrichment relative to Al and inflected REE patterns showing LREE enrichment distinguish the Mt. Preston suite from some (but not all) suites in the Canadian Cordillera. These properties have been interpreted as representing cryptic metasomatism in other suites from BC (Peslier et al., 2002), and are consistent with metasomatic enrichment producing the carbonates and sulfides and inclusion trails seen in the Mt. Preston suite.

6.2 Mantle-Sourced Carbonate

The carbonates found in the Mt. Preston xenolith suite are mantle sourced and their occurrence spans the range of mantle lithosphere sampled. A manifestation of metasomatism within the mantle, the carbonates and sulfides are interpreted to have equilibrated within the mantle lithosphere, and are preserved in pristine form.

6.2.1 Occurrence and source in the mantle lithosphere

Magnesian calcite occurs as intergranular patches, as inclusions, or as veins in all of the mantle xenoliths from Mt. Preston (Fig. 5.1), indicating pervasive carbonation of the suite. Carbonate is present as intergranular patches (Figs. 5.2, 5.4) associated with all phases and carbonate veins, with textures such as triple-point grain boundaries indicating textural equilibration with associated silicate phases rather than intrusive space filling (Fig. 5.2; Perkins et al., 2006). Carbonate is also found as inclusions which are isolated in silicate or oxide phases with no veins leading to crystal margins, indicating healing of the host crystal occurred around the inclusion (Fig. 5.3). Some inclusions are part of linear trails that cross multiple host grains (Fig. 5.5b, c), which are similar to those reported from other metasomatised xenolith suites (e.g. Perkins et al., 2006) in which carbonate enrichment was interpreted to occur in the mantle. Veins of Mg-calcite appear as intergranular and crosscutting features; sparse veinlets of basanite crosscut all features (Fig. 4.1e) including these carbonate veins, indicating that the carbonate veins predated the intrusions of host magma and thus intruded the host within the mantle.

Carbonates from grains and veins within the xenoliths are categorized as magnesian calcite (Mg-calcite), while carbonate from the dike is nearly pure calcite. The differing compositions of the carbonate from the xenoliths and the dike suggest different sources for these carbonates; in addition, the xenolith carbonate compositions are consistent with those reported from other

carbonate-bearing xenolith suites (e.g. Lee et al. (2000) and references therein; Moine et al., 2004). Coexisting pentlandite and chalcopyrite grains were noted in eight of the xenoliths, commonly at the edges of carbonate grains or veins (Fig. 5.3, 5.5b) or in inclusion trails, with or without carbonate (Figs. 5.3d, 5.5b). These sulfides are a common accessory in carbonate-bearing mantle-derived rocks (e.g. Ionov et al., 1996; Ionov, 1998) and occur together due to unmixing from an Fe, Cu, Ni mono-sulfide solution within the mantle (Kogarko et al 1995; Ducea and Park, 2000).

Several other samples were examined for the presence of carbonate using CL. Two crustal xenoliths from the Mt. Preston dike had no carbonate, suggesting that the Mt. Preston dike did not infiltrate and precipitate carbonate within the mantle xenoliths. Mantle xenoliths from the Llangorse Mtn. suite (Harder, 2004; Harder and Russell, 2006), and mantle xenoliths from the Cheslatta lake volcanics (Resnick et al., 1999) were also inspected. No carbonate was reported by these authors and none was found in the samples examined, suggesting that the carbonate from the mantle-derived xenoliths at Mt. Preston are a unique occurrence rather than an overlooked phase in other suites.

Reaction zones occur in the margins of some clinopyroxene or (rarely) spinel grains, appearing related to carbonate grain or vein contact; in the highest temperature sample there are coronae around the margins of entire grains, commonly without observable vein contacts (Fig. 4.1d). These reaction zones are unlikely to be related to the reaction of peridotite with the host basanite magma (e.g. Francis, 1987; Shaw et al., 2006), as the carbonates and sulfides preserved in the xenolith would have been volatilized, no melt contacts were observed, and thermometry results were uniform within the sample. Rather, the reaction zones are likely related to high temperature carbonate enrichment (e.g. Laurora et al., 2001).

Carbonates from the dike, dike wall rock and xenoliths each have distinct carbon-oxygen isotopic compositions (Fig. 5.8, Tables 5.1, 5.2, 5.3), which suggests different carbonate sources.

Strontium isotopic compositions determined for the same carbonate occurrences show distinct sources for the carbonate in the dike, wall rock, and xenoliths (Fig. 5.9, Tables 5.4, 5.5), consistent with C-O isotopic compositions. The carbonates in the xenoliths have a more radiogenic Sr composition than the dike whole rock or its associated carbonate, ruling out either as the contributor for the carbonate in the xenoliths. The isotopic compositions of all of the carbonate occurrences are distinct and show no signs of isotopic exchange with other sources or each other, despite their close spatial association (all sampled within 20 m of each other). Thus the xenolith carbonates' isotopic compositions are distinct and consistent with a source within the mantle.

In summary, the carbonates and sulfides observed in the mantle-derived xenoliths are derived from the mantle lithosphere, and were intrusively added to the sampled mantle. All mantle xenoliths contain carbonate, as discrete grains and/or crosscutting veins and inclusion trails, while none of the crustal xenoliths show these features. Sulfides were found associated with carbonate that are consistent with crystallization from mantle-derived sulfide melt (e.g. Ionov et al., 1996; Ionov, 1998). Intergranular carbonate morphology indicates textural equilibration with surrounding phases. Inclusions of carbonate and sulfide, some included in trails spanning multiple host grains, indicate host phases annealed after carbonate and sulfide enrichment, consistent with other carbonated xenolith suites (e.g. Perkins et al., 2006). Basanite veins were observed crosscutting carbonate veins. Reaction zones in the margins of grains in an equilibrated high temperature xenolith are consistent with metasomatic enrichment within the mantle (Laurora et al., 2001). Calcite from the xenoliths is magnesian in composition, similar to carbonates from other metasomatised xenolith suites (e.g. Lee et al. (2000) and references therein; Moine et al., 2004) and dissimilar from calcite in the host basanite. Xenoliths examined from two other mantle-derived xenolith suites from BC contained no carbonate, suggesting the

carbonate from the Mt. Preston xenoliths is a product of its mantle source. Finally, carbon, oxygen, and strontium isotopic compositions indicate that carbonate from the dike, its wall rock, and the mantle-derived xenoliths have distinct compositions and sources.

The presence of carbonate in every xenolith examined from the Mt. Preston suite is notable compared to other carbonated suites (Lee et al., 2000; Perkins et al., 2006) and argues for pervasive metasomatism of the mantle lithosphere.

6.2.2 Stability of calcite and sulfides in the mantle lithosphere

The mantle-derived xenoliths from Mt. Preston contain magnesian calcite and coexisting chalcopyrite and pentlandite. To interpret the history of enrichment in the xenoliths, the stability of these phases in the mantle-derived xenoliths must be evaluated.

Using an average crustal density of 2700 kg/m^3 for the crust and a density of 3300 kg/m^3 (by pycnometry; Appendix I) for the lithospheric mantle, the model geotherm calculated using the suite of xenoliths from Mt. Preston results in a range of pressure-temperature conditions ranging from $792 \text{ }^\circ\text{C}$ at 8.5 kbar to $1044 \text{ }^\circ\text{C}$ at 14.0 kbar for the xenolith suite. This P-T range broadly correlates with the stability field of magnesian calcite in lherzolitic compositions, indicating that experimental results are consistent with the appearance of stable Mg-calcite in these rocks (Dalton and Wood, 1993a).

Sulfides have a low melting temperature relative to other phases within peridotites (Kogarko et al., 1995). However, for monosulfide solution (MSS) of typical composition in the mantle ($\text{Fe}_6\text{Ni}_4\text{S}$) which crystallizes into chalcopyrite and pentlandite, its solidus would be above the equilibration temperature of any of the Mt. Preston xenoliths (Lorand and Conquere, 1983), indicating that the sulfides would have been crystalline at equilibrium in the mantle lithosphere.

6.2.3 Equilibration within the mantle

There is strong evidence the carbonates present in the mantle-derived xenoliths equilibrated within in the mantle lithosphere before sampling by the basanite magma.

When present as intergranular patches the carbonate commonly shows textures consistent with attainment of equilibrium between carbonate and the host peridotite, such as triple-point grain boundaries (Fig. 5.2). These textures do not imply equilibration, however; carbonates have appeared texturally equilibrated in another xenolith suite when isotopic disequilibrium required carbonate enrichment to have occurred shortly before sampling (Perkins et al., 2006). Isolated inclusions of carbonate and sulfide in host silicate and oxide phases (Figs. 5.3, 5.5) are also consistent with equilibration but do not imply it, as observed in other suites interpreted to be metasomatised shortly before eruption (e.g. Lee et al., 2000; Perkins et al., 2006).

The lack of glass observed in the xenoliths is significant. Previous studies have almost always associated carbonate in mantle xenoliths with silicate glass, and used it and/or isotopic data to postulate a short duration between enrichment in the mantle and eruption, since the glass had not crystallized yet (e.g. Laurora et al., 2001; Demeny et al., 2004; Ducea et al., 2005; Perkins et al., 2006). The petrographic observations of the carbonates in these xenoliths do not necessitate that interpretation, which is consistent with the attainment of complete equilibration in the mantle.

Carbon and oxygen isotope compositions (Fig. 5.8, Tables 5.1, 5.2, 5.3) indicate that the carbonates from the 14 mantle xenoliths analyzed fall into two distinct groups (7 xenoliths each) identified by different $\delta^{13}\text{C}$ compositions. Strontium isotopes (Fig. 5.9, Tables 5.4, 5.5) also show that the xenolith carbonates fall into two different composition groups, and thus had distinct sources. All carbonates from the Mt. Preston xenoliths are closer to primary mantle isotopic compositions than any other mantle-hosted carbonates reported (Fig. 5.8b; Lee et al., 2000; van Achterbergh et al., 2002; Demeny et al., 2004; Ducea et al., 2005; Perkins et al.,

2006). These authors invoked short durations between enrichment and eruption based on textural and/or isotopic data to preserve the oxygen isotopic disequilibrium recorded by the carbonates (oxygen rapidly attains isotopic equilibrium with coexisting phases within the mantle). The carbonates' $\delta^{18}\text{O}$ compositions are less than 3 ‰ greater than the composition field considered indicative of primary mantle compositions for carbonatites, but are enriched ≤ 5.5 ‰ above average mantle silicate compositions when fractionations are taken into account, raising the question of whether the carbonates are isotopically equilibrated. Isotopic exchange proceeds rapidly (on the order of a decade) via diffusion at mantle conditions for carbonates similar to those in the Mt. Preston suite. Because the xenolith carbonates record at least two enrichment events, which both affected a large and overlapping range of the mantle lithosphere (recorded by paleo-equilibration temperatures), two possibilities arise: either (a) the xenoliths were enriched shortly before sampling in two separate but nearly contemporaneous episodes of enrichment, by sources that crystallized carbonates of dissimilar $^{87}\text{Sr}/^{86}\text{Sr}$, $\delta^{13}\text{C}$, and $\delta^{18}\text{O}$ compositions (differing initial $\delta^{18}\text{O}$ compositions are inferred due to the recording of similar compositions at the time of sampling despite having differing durations of isotopic exchange with the mantle host) and the carbonates' oxygen isotopic compositions did not equilibrate with the host silicates, or (b) the isotopically dissimilar carbonate products of these enrichment events, separated in time by an unrestricted duration, isotopically equilibrated in the mantle and their $\delta^{18}\text{O}$ records equilibrium compositions in the xenoliths, though they may be ^{18}O enriched relative to expected fractionation with mantle silicates of average isotopic composition. Given the available data, the latter option is considered more plausible.

6.2.4 Comments on preservation

In order to preserve the carbonate and sulfides in the xenoliths, transport of the xenoliths must have been a process that minimized the effects of high and long term heat. Multiple features of the dike and xenoliths attest to this.

Fast ascent is the first inferred feature. There are several large xenoliths in the suite; the largest measured was approximately 40 cm in diameter. This indicates rapid transport of at least some of the xenoliths (Spera, 1984). Because the dike is aphyric and mafic in composition the magma would have had a high temperature and a low Newtonian viscosity (i.e. no yield strength) during flow, requiring a high upward component to flow velocity to buoy the xenoliths. The dike is also inferred to have been charged with significant volatiles, aiding ascent. It commonly appears vesicular (Fig. 2.7a), indicating a significant fluid/vapour component was present. The very minor amount of hydrous minerals and the abundance of calcite in the groundmass and vesicles suggests that the volatile components of the dike were H₂O-poor and CO₂-rich. Xenocrysts of olivine and large Mg-rich clinopyroxene or orthopyroxene crystals commonly occur in the dike rock (Fig. 3.1). They are interpreted to be xenocrysts from mechanical breakdown of Mg-rich mantle xenoliths, which likely contained carbonate since all the xenoliths examined had modal carbonate. In other xenolith suites that contained mantle-derived carbonate (Ionov et al., 1993; Lee et al., 2000; Laurora et al., 2001), the lavas xenoliths were collected from also contained carbonate. This suggests that as the magmas transit carbonated mantle lithosphere they scavenge carbonate to become significantly more CO₂ enriched (Ionov et al., 1993). All the mantle lithosphere sampled and analyzed from Mt. Preston is carbonated, thus it is very likely the dike magma scavenged carbonate from plucked and disaggregated xenoliths, and/or volatilized CO₂ from depressurization (Canil, 1990) to become richer in CO₂. The carbon, oxygen, and strontium isotopic compositions of the dike and xenolith carbonate are consistent with a contaminated source for the calcite in the dike with compositions resembling the sampled

xenoliths. Enrichment in CO₂ would further charge the dike magma and assist ascent, aiding the preservation of remaining xenoliths.

The dike's emplacement history also suggests favourable conditions for preservation. The concentration of peridotite xenoliths in a short interval in the dike is very unusual and has not been reported previously in the Cordillera. Isolation from surface processes until erosional unloading exposed the xenoliths may have contributed to their preservation. The basanite dike is fairly young and post-dates any major tectonic events. Parrish (1983) calculated approximately 1 km of uplift in the area in the last 10 Ma based on fission track data; as the dike exposure is already in a high altitude area (over 2000 m above sea level), the xenoliths must have been emplaced into a relatively shallow low temperature environment. This would expedite cooling of the dike magma itself, and a low temperature emplacement environment would result in the carbonates being resistant to isotopic alteration processes (O'Neil, 1987). Xenoliths constitute 50–80 vol.% of the dike over the short interval where the dike narrows to 1 m in width (Fig. 2.8); this accumulation of xenoliths may have isolated many of the nodules from thermal effects beyond that caused by interstitial melt between xenoliths. The mean diameter of xenoliths at this locality is ~15 cm, with the largest approximately 40 cm in diameter; larger xenoliths require longer exposure to high temperature melt to experience the same thermal effects as small xenoliths.

6.3 Carbonate Enrichment Events

While the timing of the metasomatic enrichments cannot be empirically constrained, the occurrence of modal carbonate and sulfides in these mantle-derived xenoliths, previously unreported in the Canadian Cordillera, is geographically unique. Coupled with other observations a plausible metasomatic agent, source, and time frame can be postulated.

6.3.1 Timing of enrichment

In many other studies, isotopic disequilibrium (Perkins et al., 2006) or textural and chemical disequilibrium (Lee et al., 2000; Delpech et al., 2004; Demeny et al., 2004; Moine et al., 2004; Ducea et al., 2005; Ionov et al., 2006) between carbonates and host peridotites indicated that carbonate enrichment occurred shortly before sampling by the host magma. However, in the Mt. Preston suite there is no immediate restriction on when the enrichment events occurred. No glass was observed in the mantle xenoliths, the Mg-calcite and the sulfides observed in the suite are crystalline and stable in the temperatures and pressure ranges interpreted for the xenolith suite, and the xenolith carbonates' oxygen isotopic compositions are interpreted to represent equilibrium conditions in the mantle. Without an isotopic gradient between the carbonate and host silicates the enrichment age cannot be constrained. The host dike is also essentially identical to other mafic volcanic centres in the Cheslatta Lake volcanic suite, thus there is no apparent reason to relate the timing of the enrichment of the xenoliths with the eruption of the dike as interpreted in other suites (e.g. Ionov et al., 2006; Perkins et al., 2006).

However, the data do constrain relative timing of events. The fact that intrusively textured carbonate and sulfides are observed in all xenoliths, including depleted dunites and enriched websterites, indicates that the carbonate enrichment events post-dated all melt extraction and enrichment processes. Enrichment also post-dates any texture-destructive processes such as recrystallization, as many linear inclusion trails span multiple mineral grains within the xenoliths, and reaction zones are preserved in some xenoliths' minerals.

6.3.2 Metasomatic agent

The metasomatic events enriched a coincident and wide range of mantle lithosphere as determined by paleoequilibration temperatures. Sulfides are associated with carbonates from

both the ^{13}C -enriched and ^{13}C -depleted groups. The close association of carbonate and sulfides both intergranularly (Fig. 5.4) and in veins and inclusion trails (Fig. 5.5) indicates that these phases were part of the same enrichment events and the result of a single enrichment agent. The absence of secondary silicate phases (i.e. crystallization of infiltrating metasomatic agents) such as amphibole or apatite, as well as secondary clinopyroxene and spinel, argues against silicate melt infiltration. The absence of hydrous minerals also argues against hydrous metasomatic agents. Given these observations a carbonate melt with associated monosulfide solution (MSS) is the most plausible enrichment agent.

Carbonate-bearing melts have been invoked numerous times as metasomatic agents in mantle xenoliths (e.g. Ionov et al., 1993, 1996; Ionov, 1998; Lee et al., 2000; Demeny et al., 2004). None of the classic features of carbonatite metasomatism were observed in the Mt. Preston xenoliths, but this is consistent with at least one other carbonate-bearing xenolith suite interpreted to be the result of carbonatite melt precipitation (Lee et al., 2000). Volatile-bearing minerals such as apatite and amphibole have also been considered indicators of carbonate metasomatism (Green and Wallace, 1988; Yaxley et al., 1991). However, Ionov et al. (1996) interpreted carbonate melts as precipitating no volatile-bearing minerals in xenoliths from Spitsbergen. Sulfides are a common accessory in carbonate-bearing mantle-derived rocks (e.g. Ionov et al., 1996; Ionov, 1998), and may be a typical component of the carbonate melts (Ionov et al., 1996), possibly occurring as sulphide liquid (Kogarko et al., 1995). Carbonate veins intrude grain fractures and along grain boundaries persistently in the Mt. Preston suite; this feature is often noted in carbonated xenoliths (e.g. Lee et al., 2000) and has been attributed to low viscosity carbonate melt infiltration (Demeny et al., 2004). Sulfide melts also have low viscosities at mantle conditions (Gaetani and Groves, 1999).

Compositional features of the xenoliths are also consistent with a carbonate agent. Most of the xenoliths show calcium enrichment relative to aluminum, which has been attributed to

cryptic carbonate metasomatism (Peslier et al., 2002). Many rare earth element patterns from the Mt. Preston xenoliths show slight enrichment of the lightest REEs, consistent with the effects of a migrating LREE-rich melt such as carbonatite (Takazawa et al., 1992). Metasomatic features similar to those caused by carbonatite melts can be derived from other processes, such as hydrous silicate melts (e.g. Laurora et al. (2001) and references therein), though the Mt. Preston xenoliths lack any hydrous minerals.

Experiments (Lee and Wyllie, 1996; 1998) have shown that carbonatitic melts cannot have >80 % CaCO₃ whether they are primary or evolved melts, or products of immiscibility. However, they can precipitate carbonates more Ca-enriched than this. The relatively Ca-rich carbonate compositions (X_{Ca} 86-94 for intergranular and vein carbonate) are consistent with representing crystal cumulates from a carbonate melt rather than a quenched carbonate melt (Lee et al., 2000).

The xenolith-derived carbonate compositions are consistent with carbonatites in $\delta^{13}\text{C}$ composition (Fig. 5.8; Keller and Hoefs, 1995) and in Sr isotope composition, though carbonatites are variable in $^{87}\text{Sr}/^{86}\text{Sr}$ (~0.703 to 0.706 for those in the last 500 Ma) as a result of their varied sources (Barker (1996) and references therein).

The metasomatic agent is interpreted to have been a carbonate melt with associated MSS. Consistent with other authors (Dalton and Wood, 1993b; Ionov et al., 1993; Ionov et al., 1996) the more general term carbonate melt is used rather than carbonatite, as the composition of the carbonate melt is not known.

6.3.3 Metasomatic source

The metasomatised xenoliths from Mt. Preston are unique in the Canadian Cordillera, and are geographically restricted. The Mt. Preston xenolith suite occupies a solitary position within the Cordillera, on the western margin of the Intermontane Belt in central BC within 40 km of

Coast Belt rocks (Figs. 2.2, 2.3). In central and southern British Columbia, other occurrences of mantle xenoliths are situated well within or east of the Intermontane Belt (e.g. Edwards and Russell, 2000). Accompanying this position is the fact that carbonated mantle has not been reported from other mantle xenolith localities in the Canadian Cordillera. Xenoliths from two other suites from BC were inspected (Resnick et al., 1999; Harder, 2004), of which one was collected approximately 50 km east of Mt. Preston in the Cheslatta Lake volcanics (Fig. 2.2; Resnick et al., 1999), and neither appeared to contain carbonate. Both of these sites (and others) are located in the Intermontane Belt, specifically in Stikinia. Thus the origin and long term history of the mantle lithosphere should be of no consequence, as the uncarbonated mantle lithosphere sampled to the east of Mt. Preston would have the same origin as that beneath Mt. Preston with either interpretation. While the Mt. Preston dike shows some features that may have aided preservation of the carbonates, the dike itself is not significantly different from other Cheslatta Lake volcanic centres in any parameter but carbonate enrichment, which is due to assimilation of carbonated xenoliths as interpreted based on isotopic data.

Due to Mt. Preston's unique geographic location and presence of metasomatic carbonate and sulfides, while sharing other characteristics with other xenolith occurrences, it is argued that the enrichment process was a geographically constrained feature, likely related to metasomatic agents derived from subducted oceanic crust. As the mantle lithospheric samples in other regions of BC represent mantle lithosphere that has experienced similar histories (i.e. tectonic accretions with potential enrichment by subduction in the process) and do not display modal carbonate and/or sulfides, a more recent event is postulated. This is consistent with the observation that the carbonate and sulfides appear to be the undisturbed last event recorded by the xenoliths.

Subducting slab-related enrichment agents have been interpreted in other carbonate-bearing xenolith suites (e.g. Laurora et al., 2001; Demeny et al., 2004; Ducea et al., 2005; Perkins et al., 2006). Decarbonation reactions in subducting plates can occur at greater

temperatures than dehydration reactions, based on experimental and thermodynamic data (Yaxley and Green, 1994; Ducea et al. (2005) and references therein), or the silicate and carbonate melts may be immiscible resulting in separation (Lee and Wyllie, 1997). Mt. Preston occupied an arc to back arc location during the duration of Coast Plutonic Complex magmatism history (Gehrels et al., 2009). Based on tectonic models (van der Heyden 1992; Monger et al., 1994; Madsen et al., 2006; Gehrels et al., 2009), this would restrict the timing of the enrichment event(s) from at earliest, Jurassic time to ~50 Ma when Coast Belt magmatism waned; subduction ended ~40 Ma, although the margin of the subducted slab persisted to ~35 Ma beneath the area (Madsen et al., 2006). However, for enrichment to have occurred before 90-85 Ma the mantle lithosphere under Mt. Preston would have had to be thermally and texturally unaffected by the accretion of terranes of the Insular Belt into Stikinia-Yukon Tanana (Monger and Price, 2002; Gehrels et al., 2009).

Subduction related metasomatism has been considered for xenolith suites from northwest BC and southwest Yukon based on incompatible trace element enrichments, although no metasomatic phases were observed in those rocks (Carignan et al., 1996; Shi et al., 1998; Peslier et al., 2000). If subduction-related enrichment during Coast Plutonic Complex magmatism is postulated as the source for the carbonates and sulfides in the Mt. Preston suite, the sites in northwest BC and southwest Yukon could be expected to show this as well. However, several of these sites are interpreted to overlie anomalously hot asthenosphere interpreted as a Tertiary to recent thermal event (Frederiksen et al., 1998; Shi et al., 1998); at the interpreted P-T range for these rocks little isobaric heating (≤ 50 °C) is required to make crystalline calcite unstable (Dalton and Wood, 1993a).

As the carbonates in the xenoliths are interpreted to have isotopically equilibrated with coexisting phases, in terms of oxygen isotopes there is no information on the ultimate origin of the carbonate. However, carbon isotopes are not subject to isotopic exchange with neighbouring

silicates, thus they should reflect the carbon source. The $\delta^{13}\text{C}$ compositions of the xenolith carbonates range between -3 and -6 vs. VPDB. There are several sources of carbon derived from the subduction of oceanic crust. Marine sedimentary carbonates have a $\delta^{13}\text{C}$ range of approximately +4 to -2, and -10 to -30 for organic reduced carbon (Faure, 1986). Ophicarbonates (carbonate veins in serpentinites) have a range of -4 to -21 (Jedrysek and Sachanbinski (1994) and references therein). With these constraints, both the ^{13}C -enriched and -depleted groups could have resulted from a combination of carbonate sources. In carbonatites $\delta^{13}\text{C}$ compositions are generally homogenized to intermediate values between sedimentary and organic carbon (Deines, 1989). Although Sr isotopes are useful in determining differing sources, in this case all Sr isotopic compositions from the carbonates in the xenoliths, dike, and wall rock are consistent with a mantle source (Zindler and Hart, 1986).

CONCLUSION

The dike at Mt. Preston is located north of Bella Coola in west central British Columbia. It is hosted by Hazelton Group rocks of the western Intermontane Belt, within 40 km of Coast Belt rocks. The dike is a primitive basanite that erupted at 19 Ma, and is considered part of the Cheslatta Lake volcanic suite. Calcite occurs in the dike groundmass and vesicles, indicating the dike was enriched in CO₂ during emplacement. The dike contains abundant unaltered peridotite xenoliths, which represent samples of the lithospheric mantle beneath Mt. Preston sampled by the dike.

A total of 51 xenoliths have been studied in detail. Properties not attributable to metasomatic enrichment are similar to other mantle xenolith suites from the Cordillera. All are spinel-bearing, and the suite is dominated by lherzolitic compositions, with fewer harzburgites, dunites, and websterites. Two-pyroxene thermometry (Taylor, 1998) is used to determine paleoequilibrium temperatures for individual xenoliths; the minimum temperature (792 °C; 826 °C, T_{BK90}) represents the maximum temperature at the crust-mantle boundary and the maximum temperature (1044 °C; 1119 °C, T_{BK90}) represents the minimum temperature of the lithosphere-asthenosphere boundary at 19 Ma. On a model geotherm this represents a thickness of approximately 17 km. Chemical properties of the xenoliths are consistent with mantle lithosphere that has experienced various degrees of melt depletion in the spinel stability field and in some cases melt enrichment, followed by the addition of carbonates and sulfides by metasomatism. Major element compositions show an enrichment of Ca relative to Al and enrichment of the LREEs, indicative of metasomatism.

Magnesian calcite occurs in all of the xenoliths examined, occurring as intergranular patches, veins, and isolated inclusions or discontinuous inclusion trails, commonly in association with sulfides pentlandite and chalcopyrite. Textures indicate the carbonate was in textural

equilibrium with the host peridotites, and there are no indications of disequilibrium such as interstitial glass. Carbon-oxygen isotopic compositions of carbonates from the dike, wall rock, and mantle xenoliths indicate that each have distinct compositions. Oxygen isotopic compositions of the xenoliths' magnesian calcite indicates that, consistent with textural observations, the carbonates have equilibrated with the host mantle, having $\delta^{18}\text{O}$ compositions less than 3 ‰ greater than the compositions established for primary mantle-derived carbonatites. In addition, carbonates from the mantle xenoliths fall into two separate groups identified by different $\delta^{13}\text{C}$ compositions, suggesting different source compositions. Strontium isotopic compositions also indicate different sources for carbonate in the two xenolith groups, indicating that multiple enrichment events must have occurred, enriching the mantle with carbonates of different sources and compositions. Strontium isotopic ratios also show that the dike scavenged carbonate from disaggregated mantle xenoliths, becoming enriched in CO_2 . Timing of enrichment is not constrained to shortly before eruption, and no relationship between the host magma and mantle-derived xenoliths is required. A plausible metasomatic agent is a carbonate melt with associated monosulfide solution, derived from the subduction of oceanic crust beneath North America during Coast Plutonic Belt magmatism, when Mt. Preston was in an arc to back arc position. Textural features and tectonic reconstructions suggest enrichments may have occurred between ~90 and 35 Ma.

REFERENCES

- Abraham A., Francis D. and Polve M. (2001) Recent alkaline basalts as probes of the lithospheric mantle roots of the Northern Canadian Cordillera. *Chemical Geology* **175**, 361-386.
- Abraham A., Francis D. and Polve M. (2005) Origin of Recent alkaline lavas by lithospheric thinning beneath the northern Canadian Cordillera. *Can. J. Earth Sci.* **42**, 1075-1095.
- Alard O., Griffin W. L., Lorand J. P., Jackson S. E., and O'Reilly S. Y. (2000) Non-chondritic distribution of the highly siderophile elements in mantle sulfides. *Nature*, **407**, 891–894.
- Alard, O., Griffin W. L., Pearson N. J., Lorand J. P., and O'Reilly S. Y. (2002) New insights into the Re-Os systematics of sub-continental lithospheric mantle from in situ analysis of sulfides. *Earth Planet. Sci. Lett.* **203**, 651-663.
- Anderson R. G., Snyder L. D., Wetherup S., Struik L. C., Villeneuve M. E., and Haskin M. (1998) Mesozoic to Tertiary volcanism and plutonism in southern Nechako NATMAP area. Part 1: Influence of Eocene tectonics and magmatism on the Mesozoic arc and orogenic collapse: New developments in the Nechako River map area. In *New geological constraints on Mesozoic to Tertiary metallogeny and on mineral exploration in central British Columbia: Nechako NATMAP Project* (eds. L. C. Struik and D. G. MacIntyre). Geological Association of Canada, Cordilleran Section, March 27, 1998, Short Course Notes.
- Anderson R. G., Resnick J., Russell J. K., Woodsworth G. J., Villeneuve M. E. and Grainger N. C. (2001) The Cheslatta Lake suite: Miocene mafic, alkaline magmatism in central British Columbia. *Can. J. Earth Sci.* **38**, 697-717.
- Andronicos C. L. and Ducea M. (2004): BATHOLITHS: An integrated geological, geochemical and geophysical study of the formation of continents. In *Geological Society of America, Abstracts with Programs* **36**, 5, 343 p.
- Asimow P. D. and Ghiorso M. S. (1998) Algorithmic modifications extending MELTS to calculate subsolidus phase relations. *Am. Min.* **83**, 1127-1131.
- Baer A.J. (1973) Bella Coola—Laredo Sound map-areas, British Columbia. *Geological Survey of Canada*, Memoir 372, 122 p.
- Barker D. S. (1996) Consequences of recycled carbon in carbonatites. *Can. Min.* **34**, 373-387.
- Berg G. W. (1986) Evidence for carbonate in the mantle. *Nature* **324**, 50-51.
- Bevier M.L. (1978) Field relations and petrology of the Rainbow Range shield volcano, west-central British Columbia. MSc Thesis, unpub, Vancouver, University of British Columbia, 100 p.

- Bevier M. L. (1989) A lead and strontium isotopic study of the Anahim volcanic belt, British Columbia: Additional evidence for widespread suboceanic mantle beneath western North America. *Geological Society of America Bulletin* **101**, 973-981.
- Bevier M. L., Armstrong R. L. and Souther J. G. (1979) Miocene peralkaline volcanism in west-central British Columbia—Its temporal and plate-tectonics setting. *Geology* **7**, 389-392.
- Bevier M.L. (1983a) Regional stratigraphy and age of Chilcotin Group basalts, south-central British Columbia. *Can. J. Earth Sci.* **20**, 515–524.
- Bevier M.L. (1983b) Implications of chemical and isotopic composition for petrogenesis of Chilcotin Group basalts, British Columbia. *Journal of Petrology* **24**, 207–226.
- Bodinier J. L., Dupuy C. and Dostal J. (1988) Geochemistry and petrogenesis of Eastern Pyrenean peridotites. *Geochimica et Cosmochimica Acta.* **52**, 2893-29.
- Boyd F. R. (1989) Compositional distinction between oceanic and cratonic lithosphere. *Earth Planet. Sci. Lett.* **96**, 15-26.
- Brearley M. and Scarfe C. M. (1984) Amphibole in a spinel lherzolite xenolith: evidence for volatiles and partial melting in the upper mantle beneath southern British Columbia. *Can. J. Earth Sci.* **21**, 1067-1072.
- Breitsprecher K., Thorkelson D. J., Groome W. G. and Dostal J. (2003) Geochemical confirmation of the Kula-Farallon slab window beneath the Pacific Northwest in Eocene time. *Geology* **31**, 4, 351-354.
- Brey G. P. and Köhler T. (1990) Geothermobarometry in Four-phase Lherzolites II. New Thermobarometers, and Practical Assessment of Existing Thermobarometers. *Journal of Petrology* **31**, 6, 1353-1378.
- Brey G. P., Kohler T. and Nickel K.G. (1990) Geothermobarometry in Four-phase Lherzolites I. Experimental Results from 10 to 60 kb. *Journal of Petrology* **31**, 6, 1313-1352.
- Calkins J. A., Zandt G., Girardi J., Dueker K., Gehrels G. E., and Ducea M. N. (2010) Characterization of the crust of the Coast Mountains Batholith, British Columbia, from P to S converted seismic waves and petrologic modeling. *Earth and Planetary Science Letters* **289**, 145-155.
- Canil D. (1990) Experimental study bearing on the absence of carbonate in mantle-derived xenoliths. *Geology* **18**, 1011-1013.
- Canil D. and Fedortchouk Y. (1999) Garnet dissolution and the emplacement of kimberlites. *Earth Planet. Sci. Lett.* **167**, 227–237.
- Canil D. and Scarfe C.M. (1989) Origin of Phlogopite in Mantle Xenoliths from Kostal Lake, Wells Gray Park, British Columbia. *Journal of Petrology* **30**, 5, 1159-1179.

- Cashman K. V., Sturtevant B., Papale P. and Navon O. (2000) *Magmatic fragmentation; in Encyclopedia of Volcanoes* (ed. H. Sigurdsson). Academic Press, San Diego, pp. 421–430.
- Chiba H., Chacko T., Clayton R. N. and Goldsmith J. R. (1989) Oxygen isotope fractionations involving diopside, forsterite, magnetite, and calcite: Application to geothermometry. *Geochimica et Cosmochimica Acta*. **53**, 2985-2995.
- Clinton R. N. and Mayeda T. K. (1963) The use of bromine pentafluoride in the extraction of oxygen from oxides and silicates for isotopic analysis. *Geochimica et Cosmochimica Acta* **27**, 43-52.
- Clowes R. M., Cook F. A. and Ludden J. N. (1998) Lithoprobe Leads to New Perspectives on Continental Evolution. *GSA Today* **8**, 1-7.
- Connolly J. A. D. (1990) Multivariable phase diagrams: An algorithm based upon generalized thermodynamics. *American Journal of Science* **290**, 666–718.
- Cook F. A. and Erdmer P. (2005) An 1800 km cross section of the lithosphere through the northwestern North American plate: lessons from 4.0 billion years of Earth's history. *Can. J. Earth Sci.* **42**, 1295-1311.
- Cook F. A., Clowes R. M., Snyder D. B., Van der Velden A. J., Hall K. W., Erdmer P. and Evenchick C. A. (2004) Precambrian crust beneath the Mesozoic northern Canadian Cordillera discovered by Lithoprobe seismic reflection profiling. *Tectonics* **23**, TC2010, doi:10.1029/2002TC001412.
- Cook F. A., Hall K. W. and Lynn E. (2005) The edge of northwestern North America at ~1.8 Ga. *Can. J. Earth Sci.* **42**, 983-997.
- Cousens B. L. and Bevier M. L. (1995) Discerning asthenospheric, lithospheric, and crustal influences on the geochemistry of Quaternary basalts from the Iskut-Unuk rivers area, northwestern British Columbia. *Can. J. Earth Sci.* **32**, 1451-1461.
- Crank J. (1975) *The Mathematics of Diffusion*. Clarendon Press, Oxford.
- Dalton J. A. and Wood B. J. (1993a) The partitioning of Fe and Mg between olivine and carbonate and the stability of carbonate under mantle conditions. *Contrib. Mineral. Petrol.* **114**, 501-509.
- Dalton J. A. and Wood B. J. (1993b) The compositions of primary carbonate melts and their evolution through wallrock reaction in the mantle. *Earth Planet. Sci. Lett.* **119**, 511-525.
- Deines P. (1989) Stable isotope variations in carbonatites. In *Carbonatites: Genesis and Evolution* (ed. K. Bell). Unwin Hyman, London. pp. 301-359.
- Deines, P. (2002) The carbon isotope geochemistry of mantle xenoliths. *Earth-Science Reviews* **58**, 247-278.

- Delpech G., Gregoire M., O'Reilly S. Y., Cottin J. Y., Moine B., Michon G. and Giret A. (2004) Feldspar from carbonate-rich silicate metasomatism in the shallow oceanic mantle under Kerguelen Islands (South Indian Ocean). *Lithos* **75**, 209-237.
- Demeny A. and Harangi S. (1996) Stable isotope studies and processes of carbonate formation in Hungarian alkali basalts and lamprophyres: evolution of magmatic fluids and magma-sediment interactions. *Lithos* **37**, 335-349.
- Demeny A., Vennemann T. W., Hegner E., Nagy G., Milton J. A., Embey-Isztin A., Homonnay Z. and Dobosi G. (2004) Trace element and C–O–Sr–Nd isotope evidence for subduction-related carbonate–silicate melts in mantle xenoliths (Pannonian Basin, Hungary). *Lithos* **75**, 89-113.
- Diakow L. J., Mahoney J. B., Haggart J. W., Woodsworth G. J., Gordee S. M., Snyder L. D., Poulton T. P., Friedman R. M., Villeneuve M. (2003) Geology of the Eastern Bella Coola Map Area (93 D), West-Central British Columbia. In Geological Fieldwork 2002, BC Ministry of Energy and Mines, Paper 2003-1, pp. 65-76.
- Dingwell D.B. (1996) Volcanic dilemma: flow or blow? *Science* **273**, 1054–1055.
- Dostal J., Hamilton T. S. and Church B. N. (1996) The Chilcotin basalts, British Columbia (Canada): Geochemistry, petrogenesis and tectonic significance. *N. Jb. Miner. Abh.* **170**, 207-229.
- Dostal J., Robichaud D. A., Church B. N. and Reynolds P. H. (1998) Eocene Challis–Kamloops volcanism in central British Columbia: an example from the Buck Creek basin. *Can. J. Earth Sci.* **35**, 915-963.
- Dostal J., Church B. N., Reynolds P. H. and Hopkinson L. (2001) Eocene volcanism in the Buck Creek basin, central British Columbia (Canada): transition from arc to extensional volcanism. *Journal of Volcanology and Geothermal Research* **107**, 149-170.
- Dostal J., Keppie J. D., Church B. N., Reynolds P. H. and Reid C. R. (2008) The Eocene-Oligocene magmatic hiatus in the south-central Canadian Cordillera: a capture of the Kula Plate by the Pacific Plate? *Can. J. Earth Sci.* **45**, 69-82.
- Ducea M. N. and Park S. K. (2000) Enhanced mantle conductivity from sulfide minerals, southern Sierra Nevada, California. *Geophysical Research Letters* **27**, 16, 2405-2408.
- Ducea M. N., Saleeby J., Morrison J. and Valencia V. A. (2005) Subducted carbonates, metasomatism of mantle wedges, and possible connections to diamond formation: An example from California. *American Mineralogist* **90**, 864-870.
- Edwards B. and Russell J. K. (1998) Time scales of magmatic processes: new insights from dynamic models for magmatic assimilation. *Geology* **26**, 12, 1103–1106.
- Edwards B. R. and Russell J. K. (1999) Northern Cordilleran volcanic province: A northern Basin and Range? *Geology* **27**, 3, 243-246.

- Edwards B. and Russell J. K. (2000) Distribution, nature, and origin of Neogene-Quaternary magmatism in the northern Cordilleran volcanic province, Canada. *Geological Society of America Bulletin* **112**, 8, 1280–1295.
- Evenchick C. A. and Thorkelson D. J. (1993) Geology, Spatsizi River, British Columbia (104H). Geological Survey of Canada, Open File 2719, scale 1:250 000.
- Evenchick C. A., Gabrielse H. and Snyder D. (2005) Crustal structure and lithology of the northern Canadian Cordillera: alternative interpretations of SNORCLE seismic reflection lines 2a and 2b. *Can. J. Earth Sci.* **42**, 1149-1161.
- Falloon T. J. and Green D. H. (1990) Solidus of carbonated fertile peridotite under fluid saturated conditions. *Geology* **18**, 195-199.
- Faure G. (1986) *Principles of Isotope Geology (2nd ed.)*. John Wiley & Sons, New York.
- Francis D. (1987) Mantle-Melt Interaction Recorded in Spinel Lherzolite Xenoliths from the Alligator Lake Volcanic Complex, Yukon, Canada. *Journal of Petrology* **28**, 3, 569-597.
- Francis D. and Ludden J. (1990) The Mantle Source for Olivine Nephelinite, Basanite, and Alkaline Olivine Basalt at Fort Selkirk, Yukon, Canada. *Journal of Petrology* **31**, 2, 371-400.
- Francis D. and Ludden J. (1995) The Signature of Amphibole in Mafic Alkaline Lavas, a Study in the Northern Canadian Cordillera. *Journal of Petrology* **36**, 5, 1171-1191.
- Frederiksen A. W., Bostock M. G., VanDecar J. C. and Cassidy J. F. (1998) Seismic structure of the upper mantle beneath the northern Canadian Cordillera from teleseismic travel-time inversion. *Tectonophysics* **294**, 43-55.
- Frey F. A. and Prinz M. (1978) Ultramafic inclusions from San Carlos, Arizona: Petrologic and geochemical data bearing on their petrogenesis. *Earth Plan. Sci. Lett.* **38**, 129-176.
- Fujii T. and Scarfe C. M. (1982) Petrology of ultramafic nodules from West Kettle River, near Kelowna, British Columbia. *Contrib. Mineral. Petrol.* **80**, 297–306.
- Gabrielse H., Monger J. W. H., Wheeler J. O. and Yorath C. J. (1991) Part A. Morphogeological belts, tectonic assemblages, and terranes. In *Geology of the Cordilleran Orogen in Canada* (eds. H. Gabrielse and C. Yorath). Geological Survey of Canada, Geology of Canada, no. 4. pp. 15-28.
- Gaetani G. A. and Groves T. L. (1999) Wetting of mantle olivine by sulfide melt: implications for Re/Os ratios in mantle peridotite and late stage core formation. *EPSL* **169**, 147-163.
- Garcia M. O., Ito E., Eiler J. M. and Pietruszka A. J. (1998) Crustal Contamination of Kilauea Volcano Magmas Revealed by Oxygen Isotope Analyses of Glass and Olivine from Puu Oo Eruption Lavas. *Journal of Petrology* **39**, 5, 803-817.

- Gehrels G., Rusmore M., Woodsworth G., Crawford M., Andronicos C., Hollister L., Patchett J., Ducea M., Butler R., Klepeis K., Davidson C., Friedman R., Haggart J., Mahoney B., Crawford W., Pearson D. and Girardi J. (2009) U-Th-Pb geochronology of the Coast Mountains batholith in north-coastal British Columbia: constraints on age and tectonic evolution. *GSA Bulletin*, **121**, 9/10, 1341-1361.
- Ghiorso M. S. and Sack R. O. (1995) Chemical mass transfer in magmatic processes. IV. A revised and internally consistent thermodynamic model for the interpolation and extrapolation of liquid-solid equilibria in magmatic systems at elevated temperatures and pressures. *Contrib. Mineral. Petrol.* **119**, 197-212.
- Gordee S. M., Mortensen J. K., Mahoney J. B. and Hooper R. L. (2005) Volcanostratigraphy, litho-geochemistry and U-Pb geochronology of the upper Hazelton Group, west-central British Columbia: implications for Eskay Creek – type VMS mineralization in southwest Stikinia. In Geological Fieldwork, 2004, British Columbia Ministry of Energy, Mines and Petroleum Resources, Paper 2005-1, pp. 311–322.
- Grainger N. C. and Anderson R. G. (1999) Geology of the Eocene Ootsa Lake Group in northern Nechako River and southern Fort Fraser map areas, central British Columbia. In Current Research 1999-A, Geological Survey of Canada, Paper 1999-A, pp. 139-148.
- Grainger N. C., Villeneuve M. E., Heaman L. M. and Anderson R. G. (2001) New U–Pb and Ar/Ar isotopic age constraints on the timing of Eocene magmatism, Fort Fraser and Nechako River map areas, central British Columbia. *Can. J. Earth Sci.* **38**, 679-696.
- Green D. H. and Wallace M. E. (1988) Mantle metasomatism by ephemeral carbonatite melts. *Nature* **336**, 459-462.
- Griffin W. L., Spetsius Z. V., Pearson N. J. and O'Reilly S. Y. (2002) In situ Re-Os analysis of sulfide inclusions in kimberlitic olivine: New constraints on depletion events in the Siberian lithospheric mantle. *Geochemistry Geophysics Geosystems* **3**, 11, 1-25.
- Haeussler P. J., Bradley D. C., Wells R. E. and Miller M. L. (2003) Life and death of the Resurrection plate: Evidence for its existence and subduction in the northeastern Pacific in Paleocene-Eocene time. *GSA Bulletin* **115**, 7, 867-880.
- Harder M. C. (2004) The Llangorse volcanic field: volcanology and mantle petrology. M. Sc. thesis, University of British Columbia.
- Harder M. and Russell J. K. (2006) Thermal state of the upper mantle beneath the Northern Cordilleran Volcanic Province (NCVP), British Columbia, Canada. *Lithos* **87**, n. 1-2, 1-22.
- Harder M. and Russell J. K. (2007) Basanite glaciovolcanism at Llangorse mountain, northern British Columbia, Canada. *Bull Volcanology* **69**, 329-340.
- Harmon R. S. and Hoefs J. (1995) Oxygen isotope heterogeneity of the mantle deduced from global ¹⁸O systematics of basalts from different geotectonic settings. *Contrib. Mineral. Petrol.* **120**, 95-114.

- Hart S. R. (1984) A large-scale isotope anomaly in the Southern Hemisphere mantle. *Nature* **309**, 753-757.
- Haskin M. L., Snyder L. D. and Anderson R.G. (1998) Tertiary Endako Group volcanic and sedimentary rocks at four sites in the Nechako River and Fort Fraser map area, central British Columbia. In Current Research 1998-A, Geological Survey of Canada, Paper 1998-A, pp. 155-164.
- Hauri E. H., Shimizu N., Dieu J. J. and Hart S. R. (1993) Evidence for hotspot-related carbonatite metasomatism in the oceanic upper mantle. *Nature* **365**, 221-227.
- Hyndman R. D., Currie C. A. and Mazzotti S. P. (2005) Subduction zone backarcs, mobile belts, and orogenic heat. *GSA Today* **15**, 2, 4-10.
- Ickert R. B., Thorkelson D. J., Marshall D. D. and Ullrich T. D. (2009) Eocene adakitic volcanism in southern British Columbia: Remelting of arc basalt above a slab window. *Tectonophysics* **464**, 164-185.
- Ionov D. (1998) Trace Element Composition of Mantle derived Carbonates and Coexisting Phases in Peridotite Xenoliths from Alkali Basalts. *Journal of Petrology* **39**, 11-12, 1931-1941.
- Ionov D. A., Dupuy C., O'Reilly S. Y., Kopylova M. G. and Genshaft Y. S. (1993) Carbonated peridotite xenoliths from Spitsbergen: implications for trace element signature of mantle carbonate metasomatism. *Earth Planet. Sci. Lett.* **119**, 283-297.
- Ionov D. A., O'Reilly S. Y., Genshaft Y. S. and Kopylova M. G. (1996) Carbonate-bearing mantle peridotite xenoliths from Spitsbergen: phase relationships, mineral compositions and trace-element residence. *Contrib. Mineral. Petrol.* **125**, 375-392.
- Ionov D. A., Shirey S. B., Weis D. and Brugmann G. (2006) Os–Hf–Sr–Nd isotope and PGE systematics of spinel peridotite xenoliths from Tok, SE Siberian craton: Effects of pervasive metasomatism in shallow refractory mantle. *Earth Planet. Sci. Lett.* **241**, 47-64.
- Irvine T. N. and Baragar W. R. A. (1971) A Guide to the Chemical Classification of the Common Volcanic Rocks. *Can. J. Earth Sci.* **8**, 523-548.
- Jedrysek M. O. and Sachanbinski M. (1994) Stable isotope and trace element studies of vein ophicarbonates at Gogolow-Jordanow serpentinite massif (Poland)—a contribution to the origin of ophiaragonite and ophimagnesite. *Geochem J.* **28**, 341–350.
- Keller J. and Hoefs J. (1995) Stable isotope characteristics of recent natrocarbonatites from Oldoinyo Lengai. In: *Carbonatite volcanism: Oldoinyo Lengai and the petrogenesis of natrocarbonatites*. (eds. K. Bell and J. Keller). Springer, Berlin. pp. 113-123.
- Kogarko L. N., Henderson C. M. B. and Pacheco H. (1995) Primary Ca-rich carbonatite magma and carbonate-silicate-sulphide liquid immiscibility in the upper mantle. *Contrib. Mineral. Petrol.* **121**, 267-274.

- Kohlstedt D. L. and Holtzman B. K. (2009) Shearing melt out of the Earth: An experimentalist's perspective on the influence of deformation on melt extraction. *Annu. Rev. Earth Planet. Sci.* **37**, 561–593.
- Kopylova M. G. and Russell J. K. (2000) Chemical stratification of cratonic lithosphere: constraints from the Northern Slave craton, Canada. *Earth Plan. Sci. Lett.* **181**, 71-87.
- Labotka T. C., Cole D. R. and Riciputi L. R. (2000) Diffusion of C and O in calcite at 100 MPa. *American Mineralogist* **85**, 488–494.
- Laurora A., Mazzucchelli M., Rivalenti G., Vannucci R., Zanetti A., Barbieri M. A. and Cingolani C. A. (2001) Metasomatism and Melting in Carbonated Peridotite Xenoliths from the Mantle Wedge: The Gobernador Gregores Case (Southern Patagonia). *Journal of Petrology* **42**, 1, 69-87.
- Le Bas M. J., Le Maitre R. W., Streckeisen A. and Zanettin B. (1986) A chemical classification of volcanic rocks based on the total alkali-silica diagram. *Journal of Petrology* **27**, 745-750.
- Le Bas M. J. (1989). Nephelinitic and basanitic rocks. *Journal of Petrology* **30**, 1299-1312.
- Lee C., Rudnick R. L., McDonough W. F. and Horn I. (2000) Petrologic and geochemical investigation of carbonates in peridotite xenoliths from northeastern Tanzania. *Contrib. Mineral. Petrol.* **139**, 470-484.
- Lee W. J. and Wyllie P. J. (1996) Liquid immiscibility in the join NaAl-Si₃O₈ -CaCO₃ to 2.5 GPa and the origin of calciocarbonatite magmas. *Journal of Petrology* **37**, 1125– 1152.
- Lee W. J. and Wyllie P. J. (1997) Liquid immiscibility between nephelinite and carbonatite from 1.0 to 2.5 GPa compared with mantle melt compositions. *Contrib. Mineral Petrol.* **127**, 1–16.
- Lee W. and Wyllie P. J. (1998) Processes of Crustal Carbonatite Formation by Liquid Immiscibility and Differentiation, Elucidated by Model Systems. *Journal of Petrology* **39**, no. 11-12, 2005-2013.
- Lee W., Wyllie P. J. and Rossman G. R. (1994) CO₂-rich glass, round calcite crystals, and no liquid immiscibility in the system CaO-SiO₂-CO₂ at 2.5 GPa. *American Mineralogist* **79**, 1135-1144.
- Lewis T. J., Hyndman R. D. and Fluck P. (2003) Heat flow, heat generation, and crustal temperatures in the northern Canadian Cordillera: Thermal control of tectonics. *J. Geophys. Res.* **108**, B6, 16-1 – 16-18.
- Littlejohn A. L. and Greenwood H. J. (1974) Lherzolite nodules in basalts from British Columbia, Canada. *Can. J. Earth Sci.* **11**, 1288–1308.

- Lorand J. P. and Conquere F. (1983) Contribution a l'etude des sulfures dans les enclaves de lherzolite a spinelle des basaltes alcalins (Massif Central et Languedoc, France). *Bulletin de mineralogy* **106**, 5, 585-605.
- Ludwig K. R. (2003) Isoplot 3.09 A Geochronological Toolkit for Microsoft Excel. Berkeley Geochronology Center, Special Publication No. 4.
- Macdonald G. A. and Katsura T. (1964). Chemical composition of Hawaiian lavas. *Journal of Petrology* **5**, 82-133.
- Mathews W. H. (1989) Neogene Chilcotin basalts in south-central British Columbia: geology, ages, and geomorphic history. *Can. J. Earth Sci.* **26**, 969-982.
- McDonough W. F. (1990) Constraints on the composition of the continental lithospheric mantle. *Earth Planet. Sci. Lett.* **101**, 1-18.
- McDonough W. F. and Frey F. A. (1990) Rare earth elements in upper mantle rocks. In *Geochemistry and mineralogy of rare earth elements* (eds. B. R. Lipin and G. A. McKay) Reviews in Mineralogy, Mineralogical Society of America, **21**, 100-145.
- McDonough W. F. and Sun S. -s. (1995). The composition of the Earth. *Chemical Geology* **120**, 223-253.
- Madsen J. K., Thorkelson D. J., Friedman R. M. and Marshall D. D. (2006) Cenozoic to Recent plate configurations in the Pacific Basin: Ridge subduction and slab window magmatism in western North America. *Geosphere* **2**, 1, 11-34.
- Mahoney J. B., Hooper R. L., Gordee S. M., Haggart J. W. and Mortensen J. K. (2005) Initial evaluation of bedrock geology and economic mineralization potential of southern Whitesail Lake map area (NTS 093E/02, 03), west-central British Columbia. In Geological Fieldwork, 2004, British Columbia Ministry of Energy, Mines and Petroleum Resources, Paper 2005-1, pp. 291–299.
- Mahoney J. B., Haggart J. W., Hooper R. L., Snyder L. D. and Woodsworth G. (2006) Geological setting and mineralization potential of the southwestern Whitesail Lake map area (NTS 93E), western British Columbia: preliminary assessment. In Geological Fieldwork, 2005, BC Ministry of Energy, Mines and Petroleum Resources, Paper 2006-1, pp. 313-322.
- Marsden, H. and Thorkelson, D. J. (1992) Geology of the Hazelton Volcanic Belt in British Columbia: Implications for the Early to Middle Jurassic Evolution of Stikinia. *Tectonics* **11**, 6, 1266-1287.
- Massol H. and Jaupart C. (1999) The generation of gas overpressure in volcanic eruptions. *Earth Planet. Sci. Lett.* **166**, 57–70.
- Mattey D., Lowry D. and Macpherson C. (1994) Oxygen isotope composition of mantle peridotite. *Earth Planet. Sci. Lett.* **128**, 231–241.

- Michol K. A. (2006) Analysis of strain in a welded block and ash flow deposit, Mount Meager, Southwestern British Columbia. M. Sc. thesis, University of British Columbia.
- Mitchell R. H. (1987) Mantle-derived xenoliths in Canada. In *Mantle Xenoliths* (ed. P. H. Nixon). John Wiley and Sons, New York, pp. 33–40.
- Moine B. N., Gregoire M., O'Reilly S. Y., Delpech G., Sheppard S. M. F., Lorand J. P., Renac C., Giret A. and Cottin J. Y. (2004) Carbonatite melt in oceanic upper mantle beneath the Kerguelen Archipelago. *Lithos* **75**, 239-252.
- Monger J. and Price R. (2002) The Canadian Cordillera: Geology and Tectonic Evolution. *CSEG Recorder*, February 2002, 17-36.
- Monger J. W. H., Price R. A. and Tempelman-Kluit D. J. (1982) Tectonic accretion and the origin of the two major metamorphic and plutonic belts in the Canadian Cordillera. *Geology* **10**, 70–75.
- Monger J. W. H., van der Heyden P., Journeay J. M., Evenchick C. A. and Mahoney J. B. (1994) Jurassic-Cretaceous basins along the Canadian Coast Belt: Their bearing on pre-mid-Cretaceous sinistral displacements. *Geology* **22**, 175-178.
- Morelli R. M., Creaser R. A., Selby D., Kontak D. J. and Horne, R. J. (2005) Rhenium-Osmium Geochronology of Arsenopyrite in Meguma Group Gold Deposits, Meguma Terrane, Nova Scotia, Canada: Evidence for Multiple Gold-Mineralizing Events. *Economic Geology* **100**, 1229-1242.
- Nicholls J., Stout M. Z. and Fiesinger D. W. (1982) Petrologic variations in Quaternary volcanic rocks, British Columbia, and the nature of the underlying upper mantle. *Contrib. Mineral. Petrol.* **79**, 201–218.
- O'Neil J. R. (1987) Preservation of H, C, and O isotopic ratios in the low temperature environment. In *Stable Isotope Geochemistry of Low Temperature Fluids* (ed. T. K. Kyser). Short Course Volume, Mineralogical Association of Canada, **13**, 85-128.
- Parrish R. R. (1983) Cenozoic thermal evolution and tectonics of the Coast Mountains of British Columbia: 1. Fission track dating, apparent uplift rates, and patterns of uplift. *Tectonics* **2**, 601–631.
- Pearce J. A. and Peate D. W. (1995) Tectonic Implications of the Composition of Volcanic Arc Magmas. *Annu. Rev. Earth Planet Sci.* **23**, 251-85.
- Pell J. (1994) Carbonatites, nepheline syenites, kimberlites, and related rocks in British Columbia. *BC EMPR Bulletin* **88**.
- Perkins G. B., Sharp Z. D. and Selverstone J. (2006) Oxygen isotope evidence for subduction and rift-related mantle metasomatism beneath the Colorado Plateau-Rio Grande rift transition. *Contrib. Mineral. Petrol.* **151**, 633-650.

- Peslier A. H., Reisberg L., Ludden J. and Francis D. (2000a) Re–Os constraints on harzburgite and lherzolite formation in the lithospheric mantle: A study of Northern Canadian Cordillera xenoliths. *Geochimica et Cosmochimica Acta* **166**, 85-101.
- Peslier A. H., Reisberg L., Ludden J. and Francis D. (2000b) Os isotopic systematics in mantle xenoliths; age constraints on the Canadian Cordillera lithosphere. *Chemical Geology* **166**, 85-101.
- Peslier A. H., Francis D. and Ludden J. (2002) The lithospheric mantle beneath continental margins: Melting and melt-rock reaction in Canadian Cordillera xenoliths. *Journal of Petrology* **43**, 11, 2013-2047.
- Petcovic H. L. and Dufek J. D. (2005) Modeling magma flow and cooling in dikes: implications for emplacement of Columbia River flood basalts. *J. Geophys. Res.* **110**, B10201, doi: 10.1029/2004JB003432.
- Peterson N. D., Russell J. K., and Mahoney J. B. (2006) Mantle-Derived Peridotite Xenoliths from the Western Intermontane Belt, Whitesail Lake map area (NTS 093E), Western British Columbia. In Geological Fieldwork 2005, British Columbia Ministry of Energy, Mines and Petroleum Resources, Paper 2006-1, pp. 153-162.
- Pouchou J. L. and Pichoir F. (1985) PAP $\phi(\rho Z)$ procedure for improved quantitative microanalysis. *Microbeam Analysis* **1985**, 104-106.
- Powell W. and O'Reilly S. (2007) Metasomatism and sulfide mobility in lithospheric mantle beneath eastern Australia: Implications for mantle Re-Os chronology. *Lithos* **94**, 132-147.
- Prescott J.W. (1983) Petrogenesis of ultramafic xenoliths from the Canadian Cordillera and Alaska (unpublished). M. Sc. thesis, McGill University.
- Raudsepp M. and Pani E. (2003) Application of Rietveld analysis to environmental mineralogy. In *Mineralogical Association of Canada, Short Course Series 31* (eds. J. L. Jambor, D. W. Blowes and A. I. M. Ritchie), 165-180.
- Renne P. R., Swisher, III C. C., Deino A. L., Karner D. B., Owens T. and DePaolo D. J. (1998) Intercalibration of standards, absolute ages and uncertainties in $^{40}\text{Ar}/^{39}\text{Ar}$ dating. *Chemical Geology* **145**, 117-152.
- Resnick J., Anderson R. G., Russell J. K., Edwards B. R. and Grainger N. C. (1999) Neogene basaltic flow rocks, xenoliths, and related diabase, northern Nechako River map area, central British Columbia. In Current Research 1999-A, Geological Survey of Canada, pp. 157–167.
- Rietveld H. M. (1967) Line profiles of neutron powder-diffraction peaks for structure refinement. *Acta. Cryst.* **22**, 151-152.
- Rietveld H. M. (1969) A Profile Refinement Method for Nuclear and Magnetic Structures. *Acta. Cryst.* **2**, 65-71.

- Ross J. V. (1983) The nature and rheology of the Cordilleran upper mantle of British Columbia: inferences from peridotite xenoliths. *Tectonophysics* **100**, 321–357.
- Rudnick R. L., McDonough W. F. and Chappell B. W. (1993) Carbonatite metasomatism in the northern Tanzanian mantle: petrographic and geochemical characteristics. *Earth Planet. Sci. Lett.* **114**, 463-475.
- Russell J. K. and Kopylova M. K. (1999) A steady-state conductive geotherm for the north central Slave, Canada: inversion of petrological data from the Jericho kimberlite pipe. *J. Geophys. Res.* **104**, 7089–7101.
- Russell J. K., Dipple G. M. and Kopylova M. G. (2001) Heat flow and heat production in mantle lithosphere from the Slave Craton. *Physics of Earth and Planetary Interiors* **123**, 27–44.
- Shaw C. S. J. and Dingwell D. B. (2008) Experimental peridotite–melt reaction at one atmosphere: a textural and chemical study. *Contrib. Mineral. Petrol.* **155**, 199-214.
- Shaw C. S. J., Thibault Y., Edgar A. D. and Lloyd F. E. (1998) Mechanisms of orthopyroxene dissolution in silica-undersaturated melts at 1 atmosphere and implications for the origin of silica-rich glass in mantle xenoliths. *Contrib. Mineral. Petrol.* **132**, 354-370.
- Shaw C. S. J., Heidelbach F. and Dingwell D. B. (2006) The origin of reaction textures in mantle peridotite xenoliths from Sal Island, Cape Verde: the case for “metasomatism” by the host lava. *Contrib. Mineral. Petrol.* **151**, 681-697.
- Shi L., Francis D., Ludden J., Frederiksen A. and Bostock M. (1998) Xenolith evidence for lithospheric melting above anomalously hot mantle under the northern Canadian Cordillera. *Contrib. Mineral. Petrol.* **131**, 39-53.
- Souther J.G. (1986) The western Anahim Belt: Root zone of a peralkaline magma system. *Can. J. Earth Sci.* **23**, 895-908.
- Souther J. G. (1991) Volcanic Regimes. In *Geology of the Cordilleran Orogen in Canada* (eds. H. Gabrielse and C.J. Yorath). Geological Survey of Canada, Geology of Canada, no. 4 (also Geological Society of America, The Geology of North America, v.G-2), pp. 457-490.
- Spera F. J. (1984) Carbon dioxide in petrogenesis III: role of volatiles in the ascent of alkaline magma with special reference to xenolith-bearing mafic lavas. *Contrib. Mineral. Petrol.* **88**, 217–232.
- Sun S. -s. and McDonough W. F. (1989) Chemical and isotopic systematics of oceanic basalts: implications for mantle composition and processes. *Magmatism in the Ocean Basins* (eds. A. D. Saunders and M. J. Norry). Geological Society Special Publication No. 42, pp. 313-345.
- Takazawa E., Frey F. A., Shimizu N., Obata M. and Bodinier J. L. (1992) Geochemical evidence for melt migration and reaction in the upper mantle. *Nature* **359**, 55-58.

- Taylor W. R. (1998) An experimental test of some geothermometer and geobarometer formulations for upper mantle peridotites with application to the thermobarometry of fertile lherzolite and garnet websterite. *N. Jb. Miner. Abh.* **172**, 381-408.
- Taylor Jr. H. P., Frechen J., and Degens E. T. (1967) Oxygen and carbon isotope studies of carbonatites from the Laacher See district, West Germany, and the Alnö district, Sweden. *Geochimica et Cosmochimica Acta* **31**, 407-430.
- Tuffen H., Dingwell D. B. and Pinkerton H. (2003) Repeated fracture and healing of silicic magma generate flow banding and earthquakes? *Geology* **31**, 1089-1092.
- Van Achterbergh E., Griffin W. L., Ryan C. G., O'Reilly S. Y., Pearson N. J., Kivi K. and Doyle B. J. (2002) Subduction signature for quenched carbonatites from the deep lithosphere. *Geology* **30**, 8, 743-746.
- Van der Heyden P. (1992) A middle Jurassic to early Tertiary Andean-Sierran arc model for the Coast Belt of British Columbia. *Tectonics* **11**, 1, 82-97.
- Weis D., Kieffer B., Macrschalk C., Barling J., de Jong J., Williams G. A., Hanano D., Pretorius W., Mattielli N., Scoates J. S., Goolaerts A., Friedman R. M. and Mahoney J. B. (2006) High-precision isotopic characterization of USGS reference materials by TIMS and MC-ICP-MS. *Geochemistry Geophysics Geosystems* **7**, 8, 1-30.
- Welford J. K., Clowes R. M., Ellis R. M., Spence G. D., Asudeh I. and Hajnal Z. (2001) Lithospheric structure across the craton-Cordilleran transition of northeastern British Columbia. *Can. J. Earth Sci.* **38**, 1169-1189.
- Wells P. R. A. (1977) Pyroxene Thermometry in Simple and Complex Systems. *Contr. Mineral. Petrol.* **62**, 129-139.
- Wheeler J. O. and McFeely P. (1991) Tectonic assemblage map of the Canadian Cordillera and adjacent parts of the United States of America; Geological Survey of Canada, Map 1712A, scale 1:2 000 000.
- Wheeler J. O., Brookfield A. J., Gabrielse H., Monger J. W. H., Tipper H. W. and Woodsworth G. J. (1991) Terrane Map of the Canadian Cordillera: Geological Survey of Canada Map 1713A, scale 1:2,000,000.
- Wilkinson J. F. G. (1986) Classification and average chemical compositions of common basalts and andesites. *Journal of Petrology* **27**, 31-62.
- Wilkinson J. F. G. and Le Maitre R. W. (1987) Upper mantle amphiboles and micas and TiO₂, K₂O, and P₂O₅ abundances and 100 Mg/(Mg + Fe²⁺) ratios of common basalts and andesites: Implications for modal mantle metasomatism and undepleted mantle compositions. *J. Pet.* **28**, 37-73.
- Wilson M. R., Kjarsgaard B. A. and Taylor B. (2007) Stable isotope composition of magmatic and deuteric carbonate phases in hypabyssal kimberlite, Lac de Gras field, Northwest Territories, Canada. *Chemical Geology* **242**, 435-454.

- Wood B. J. and Banno S. (1973) Garnet-orthopyroxene and orthopyroxene-clinopyroxene relationships in simple and complex systems. *Contr. Mineral. and Petrol.* **42**, 109-124.
- Yaxley G. M. and Green D. H. (1994) Experimental demonstration of refractory carbonate-bearing eclogite and siliceous melt in the subduction regime. *Earth Planet. Sci. Lett.* **128**, 313-325.
- Yaxley G. M., Crawford A. J. and Green D. H. (1991) Evidence for carbonatite metasomatism in spinel peridotite xenoliths from western Victoria, Australia. *Earth Planet. Sci. Lett.* **107**, 305-317.

APPENDIX A – SAMPLE SUITE

See attached data disc. Also available online temporarily at:

ftp://ftp.eos.ubc.ca/pub/krussell/npeterson/thesis_data_disc

APPENDIX B – GEOCHEMISTRY

Whole rock samples of the dike, country rock, and xenoliths were prepared for bulk geochemical analysis. For the dike and country rock, samples were fed through a jaw crusher to create 1-2 cm chips, which were hand-picked and powdered in a tungsten carbide ring mill, then sieved to ensure a grain size of < 0.42 mm (mesh size 40). Xenoliths were trimmed with a diamond saw before crushing to exclude weathered surfaces and veinlets of basanite. Replicate samples for the dike and for one xenolith were separated at the chip stage and then processed.

Analysis of powders for major, trace, and rare earth elements, ferrous iron, H_2O , and CO_2 was carried out at the Geochemical Laboratories, McGill University, Montreal, Quebec. Major elements were analyzed by X-ray fluorescence (XRF) on fused beads from ignited samples; trace elements were analyzed for using pressed powder pellets. XRF analysis was done on a Philips[™] PW2440 spectrometer. Rare earth element analyses were done using a PerkinElmer[™] ELAN DRCplus ICP-MS with fusion decomposition of the sample. Total iron was determined by XRF, and FeO content was determined by volumetric analysis (ammonium metavanadate titration). Samples were analyzed for CO_2 on an ELTRA[™] CS-800 carbon/sulfur infrared (IR) analyzer. H_2O^+ (structurally bonded water) was determined by difference using loss on ignition (LOI), CO_2 , SO_3 , halogens, and FeO analyses.

Tables B.1 and B.2 display major, trace, and rare earth element abundances for the Cretaceous-aged dike near the xenolith-bearing dike of interest, wall rocks to the basanite dike, and a gabbro xenolith sampled from the dike.

Table B.1 Whole rock major element compositions (wt.%) of samples of Hazelton Group wall rocks, a metamorphosed dike, and a gabbro crustal xenolith from the basanite dike.

Sample	NP-MP05-2	NP-MP05-4	NP-MP05-5	NP-MP05-7G ¹	NP-MP05-26
Rock Type	Metabasalt	Volcaniclastic	Volcaniclastic	Volcaniclastic	Gabbro
SiO ₂	47.12	61.45	71.16	65.17	51.69
TiO ₂	0.764	0.702	0.358	0.670	0.950
Al ₂ O ₃	17.11	14.12	11.63	15.14	18.59
Fe ₂ O ₃	2.94	5.46	1.32	5.50	2.82
FeO	5.38	1.22	1.09	1.67	5.58
MnO	0.949	0.170	0.139	0.165	0.148
MgO	7.16	2.06	1.15	2.32	5.73
CaO	4.02	3.83	2.70	0.92	8.49
Na ₂ O	3.80	6.49	5.00	3.50	3.85
K ₂ O	2.20	0.80	0.82	2.66	0.41
P ₂ O ₅	0.135	0.158	0.091	0.133	0.293
H ₂ O ⁺	4.42	1.29	1.02	0.81	0.95
H ₂ O ⁻	0.24	0.07	0.04	1.23	0.40
CO ₂	2.6	2.0	2.0	<d/l	0.11
Total	98.59	99.74	98.48	98.66	99.61
FeO _{Total}	8.03	6.13	2.28	6.62	8.12
LOI	7.46	3.23	4.28	2.10	0.84

¹ Partly fused sample from area near margin of dike.

Table B.2 Whole rock trace and rare earth element concentrations (ppm) of samples of Hazelton Group wall rocks, a metamorphosed dike, and a gabbro crustal xenolith from the basanite dike.

Sample	NP-MP05-2	NP-MP05-4	NP-MP05-5	NP-MP05-7G ¹	NP-MP05-26
Rock Type	Metabasalt	Volcaniclastic	Volcaniclastic	Volcaniclastic	Gabbro
Rb	45.7	15.7	13.6	56.1	13.5
Sr	216.8	63.2	85.3	94.6	959.0
Ba ²	553	112	383	612	1123
V ²	279	117	47	111	200
Cr ²	138	42	18	29	85
Co ²	46	10	10	15	36
Ni ²	62	10	8	16	38
Zn ²	1396	11	19	198	83.4
Cu ²	75	7	51	9	14
Ga	14.5	8.8	11.5	15.2	21.4
Y	15.1	15.4	21.8	22.0	9.45
Zr	32.2	94.7	76.2	96.0	46.9
Nb	0.8	1.8	2.1	2.0	1.8
Th	2.4	3.6	3.0	2.7	3.7
U	1.3	1.1	<d/l	1.7	3.0
Pb	10.1	1.5	23.1	10.8	<d/l
La	6.36	4.53	9.35	9.50	6.71
Ce	14.28	7.58	18.58	18.61	14.3
Pr	2.05	0.94	2.51	2.58	2.11
Nd	9.93	4.25	11.54	11.58	10.1
Sm	2.80	1.41	3.32	3.04	2.40
Eu	1.106	0.565	1.079	1.044	1.04
Gd	2.44	1.39	2.92	2.62	2.52
Tb	0.546	0.322	0.660	0.576	0.33
Dy	3.38	2.22	4.22	3.80	1.94
Ho	0.669	0.483	0.892	0.791	0.37
Er	1.993	1.493	2.673	2.471	1.00
Tm	0.304	0.253	0.434	0.404	0.14
Yb	1.99	1.80	2.87	2.76	0.87
Lu	0.268	0.263	0.413	0.406	0.14

¹ Partly fused sample from area near margin of dike.

² By x-ray fluorescence.

APPENDIX C – AR-AR DATING

Whole rock samples of the basanite dike and an older metamorphosed dike within the Hazelton were dated by $^{40}\text{Ar}/^{39}\text{Ar}$ techniques. Samples were fed through a jaw crusher and hand-picked for clean pieces; these were crushed in a tungsten carbide ring mill, and hand-picked for clean 1-2 mm diameter chips. The selected chips were washed in acetone, dried, and wrapped in aluminum foil. They were then stacked in an irradiation capsule with similar-aged samples and neutron flux monitors (Fish Canyon Tuff sanidine, 28.02 Ma; Renne et al., 1998).

The samples were irradiated at the McMaster Nuclear Reactor in Hamilton, Ontario, for 90 MWh, with a neutron flux of approximately 4×10^{13} neutrons/cm²/s. Analyses (n=57) of 19 neutron flux monitor positions produced errors of <0.5 % in the J value.

The samples were analyzed at the Noble Gas Laboratory of the Pacific Centre for Isotopic and Geochemical Research (PCIGR), University of British Columbia. The mineral separates were step-heated with a 10 W CO₂ laser (New Wave Research™ MIR10) until fused. The gas from each step was analyzed by a VG5400 mass spectrometer equipped with an ion-counting electron multiplier. All measurements were corrected for total system blank, mass spectrometer sensitivity, mass discrimination, radioactive decay during and subsequent to irradiation, as well as interfering Ar from atmospheric contamination and the irradiation of Ca, Cl, and K (isotope production ratios: $(^{40}\text{Ar}/^{39}\text{Ar})_{\text{K}} = 0.0302 \pm 0.00006$, $(^{37}\text{Ar}/^{39}\text{Ar})_{\text{Ca}} = 1416.4 \pm 0.5$, $(^{36}\text{Ar}/^{39}\text{Ar})_{\text{Ca}} = 0.3952 \pm 0.0004$, $\text{Ca/K} = 1.83 \pm 0.01$ ($^{37}\text{Ar}_{\text{Ca}}/^{39}\text{Ar}_{\text{K}}$)).

Plateau and correlation ages were calculated using Isoplot v. 3.09 (Ludwig, 2003). Errors are propagated from all sources except mass spectrometer sensitivity and flux monitor age. Plateau age error includes 0.5 % J error. The best statistically-justified plateau and plateau age were picked based on the following criteria:

- Three or more contiguous steps comprising more than 50 % of the ^{39}Ar ;

- Probability of fit of the weighted mean age greater than 5 %;
- Slope of the error-weighted line through the plateau ages equals zero at 5 % confidence;
- Ages of the two outermost steps on a plateau are not significantly different from the weighted-mean plateau age (at 1.8σ six or more steps only);
- Outermost two steps on either side of a plateau must not have nonzero slopes with the same sign (at 1.8σ nine or more steps only).

Specific data for the analyses used in the text are displayed in Table C.1.

Table C.1 Statistics for $^{40}\text{Ar}/^{39}\text{Ar}$ dating. Error on age is 2σ , including 0.5 % J-error.

Sample	Age (Ma)	^{39}Ar in plateau (%)	Plateau steps included	MSWD	Probability	Initial $^{40}\text{Ar}/^{36}\text{Ar}$
NP-MP05-2	87.74 ± 0.71	60.3	6 to 11	1.8	0.11	300 ± 48
NP-MP05-3	18.72 ± 0.26	96.2	4 to 14	0.31	0.98	297.8 ± 8.6

APPENDIX D – RADIOGENIC ISOTOPES

D.1 Sr-Nd-Pb Isotopes

Isotopic signatures of alkaline volcanics can be used as a measure of crustal contamination and to evaluate characteristics of mantle source regions (e.g. Cousens and Bevier, 1995; Abraham et al., 2001). Strontium, neodymium, and lead isotopes measured on whole rock samples are widely used for this purpose. Strontium isotopes were also determined on acid-leached carbonate from the dike and from mantle xenoliths, in order to assess the compositions and sources of these carbonate occurrences.

All samples were analyzed at the Pacific Centre for Isotopic and Geochemical Research (PCIGR), University of British Columbia. Isotopic compositions were measured on a Thermo Finnigan TIMS (Sr and Nd) or a Nu Instruments Plasma Nu-021 MC-ICP-MS (Pb and Nd). Methods of preparation and analysis are fully described by Weis et al. (2006). For carbonate strontium analyses, which occurred on leachate, samples were bathed with 0.5 N hydrochloric acid twice in an ultrasonic bath for 10 minutes. The leachate was then dried and analyzed as above.

D.2 Re-Os Isotopes

Rhenium-osmium isotopes are useful for evaluating ages and depletion histories for mantle rocks. Samples were trimmed with a diamond rock saw. To crush samples, a hydraulic tungsten carbide plate crusher was used. Samples were crushed to < 5 mm chips by pressing ~ 6-10 times between the plates. About 400 g of each sample was crushed. 70 g aliquots were then taken from each sample for powdering. To avoid metal contamination during powdering, a Fritsch™

Pulverisette 6 planetary mill was used with agate jars. Samples were powdered at 380 rpm for 20 to 25 minutes (3 to 4 reversals). 60 g of Ottawa sand was used between sample runs for cleaning the jars. Samples were analyzed at the Radiogenic Isotope Facility at the University of Alberta, Department of Earth and Atmospheric Sciences. Analysis techniques follow Morelli et al. (2005); approximately 0.5 g of sample powder was used per sample.

APPENDIX E – STABLE ISOTOPES

E.1 Oxygen Isotopes (Silicates)

Oxygen isotopic compositions of the silicate fraction of the basanite dike were determined by removing carbonate from the whole rock powders. Whole rock powders were immersed in 10 % hydrochloric acid, agitated in an ultrasonic bath for 10 minutes, then separated from the leachate via centrifuge, rinsed with distilled water, and dried. A test sample was analyzed before and after preparation by X-ray diffraction; the process effectively removed carbonate. Sample analysis was performed at the Facility for Isotope Research at Queen's University, Kingston, Ontario. Analysis followed the BrF_5 method of Clinton and Mayeda (1963), on a FinneganTM MAT 252 mass spectrometer.

E.2 Oxygen and Carbon Isotopes (Carbonate)

Oxygen and carbon isotopic analyses were conducted to evaluate carbonate sources within the dike, country rock, and mantle xenoliths. Isotopic analyses were performed on leachates of whole rock powders, and in the case of dike and country rock, also on carbonate recovered by microdrilling of carbonate-rich patches. For microdrilling, pieces of rock were crushed in a jaw crusher to 1-2 cm in size, cleaned, and fresh surfaces were identified. A DremelTM rotary tool with separate tungsten carbide drill bits for each rock type was then used to target distinct carbonate morphologies within each sample. Previous studies of carbonates in mantle xenoliths (e.g. Ionov et al., 1993) have used leaching of whole rocks to analyze carbonate compositions, based on the assumption that no other phases dissolve. The xenoliths in this study

are similar in composition and mineralogy to those of previous studies employing leaching, and thus should be comparable.

All powdered samples were analyzed at the PCIGR, University of British Columbia, in a Finnigan Delta XL Plus mass spectrometer, using a gas bench with A200 S autosampler as follows: between 200 and 500 mg of each sample or rock standard is weighed into a glass Exetainer vial and sealed with a cap with a pierceable septum. The gas bench is loaded with samples interspersed with standards, and set at a constant temperature of 32 °C. The autosampler flushes the closed vials with helium for 5 minutes to displace headspace air. Each vial is then acidified with 100 % phosphoric acid to liberate CO₂ gas, and allowed to equilibrate for an hour before analysis.

During analyses, 10 aliquots of the sample CO₂ are bracketed by 6 aliquots of a reference CO₂ gas for internal calibration. External calibration is monitored using the carbonate standard NBS 18 and NBS 19. A fractionation correction is applied to the sample results using these two standards.

Results are reported using the δ notation measured in ‰ relative to the VSMOW (Vienna Standard Mean Ocean Water) standard for oxygen, VPDB (Vienna Peedee Belemnite) for carbon. After correction for fractionation, repeat analyses of NBS 18 (-5.000, 7.200) give an average $\delta^{13}\text{C}$ value of -5.155 ± 0.059 ‰ and an average $\delta^{18}\text{O}$ value of 7.152 ± 0.078 ‰. Analyses of NBS 19 (1.950, 28.650) give an average $\delta^{13}\text{C}$ value of 1.840 ± 0.058 ‰ and an average $\delta^{18}\text{O}$ value of 28.887 ± 0.058 ‰.

APPENDIX F – RIETVELD METHOD

The Rietveld technique is a tool for calculating the relative abundance of individual phases in a powdered crystalline sample by analyzing X-ray diffraction (XRD) data (Rietveld, 1967; 1969). Simulated diffraction patterns, calculated from standards for individual mineral phases, are applied and scaled to the diffraction pattern for a rock sample with one or more minerals. The scaling factor for each mineral pattern is used to calculate its relative abundance in the sample. Mineral phases in the sample must be known in order to load their individual standard patterns; however, standard patterns can be added or changed in the event of unexpected phases in the sample (indicated by unfitted peaks in the sample pattern). Peridotites are ideal for the application of this technique, as they have a simple mineralogy and phases which are not problematic to analyze (e.g. preferred orientation effects in micas).

Samples were fed through a jaw crusher to create 1-2 cm chips, which were hand-picked and powdered in a tungsten carbide ring mill, then sieved to ensure a grain size of < 0.42 mm (mesh size 40). XRD sample preparation follows Raudsepp and Pani (2003). Briefly, powdered samples were further reduced to 1-10 μm particle size in a corundum mill, then loaded and pressed into an aluminum sample holder. Samples were not 'textured' with razor blades, as preferred orientation effects were not significant.

For XRD analysis, step-scan data were collected over a range of $3\text{-}80^\circ 2\theta$ (0.04° per step) for 28.8 minutes (0.8 s per step, 2093 steps). Analyses used $\text{CoK}\alpha$ radiation on a standard Siemens (Bruker) D5000 Bragg-Brentano diffractometer equipped with an Fe monochromator foil, 0.6 mm (0.3°) divergence slit, incident- and diffracted-beam Soller slits, and a Vantec-1 strip detector. The long fine-focus Co X-ray tube was operated at 35 kV and 40 mA, using a take-off angle of 6° . Data were refined with the Bruker AXS Rietveld program, TOPAS 3.0.

Figure F.1 compares modal mineralogy estimates for 15 xenoliths with 4 major phases, by the Rietveld method and by a least square calculation which reproduces bulk chemical data using mineral compositions from EMP analysis. Figure F.2 compares the deviation of modal estimates by the two methods, versus modal abundance.

The Rietveld method compares favourably with calculated abundances. Relative deviations are never above 25 % for the three major phases (OPX, CPX, olivine); in the case of CPX and olivine, they are rarely over 10 % for CPX, and never over 10 % for olivine. Due to the low modal abundance of spinel, relative deviations are higher. The accuracy of either method cannot be evaluated with these data; however, calculated abundances are often used in literature (e.g. Kopylova and Russell, 2000), and the Rietveld-derived modes are very similar. In addition, the Rietveld method has several technical advantages: speed (approximately 30 minutes preparation time and 30 minutes analysis time per sample), cost (inexpensive XRD time), and the ability to identify and include phases that had been overlooked (e.g. calcite).

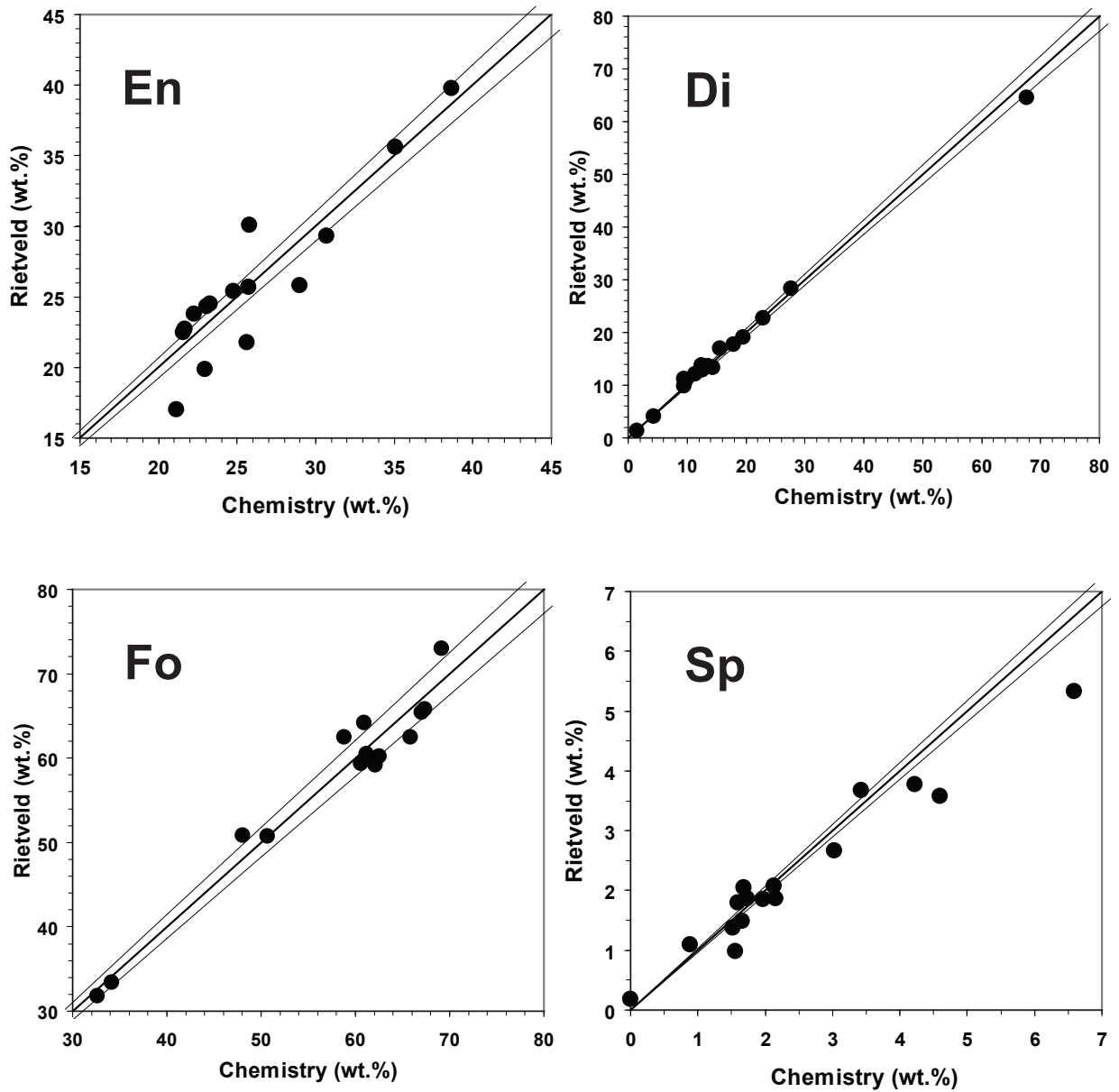


Figure F.1 Comparison of modal mineralogy estimates by the Rietveld method and by calculations using bulk chemical and mineral composition data. Lines bracketing the 1:1 line denote 5 % relative deviation. En = enstatite, Di = diopside, Fo = forsterite, Sp = spinel.

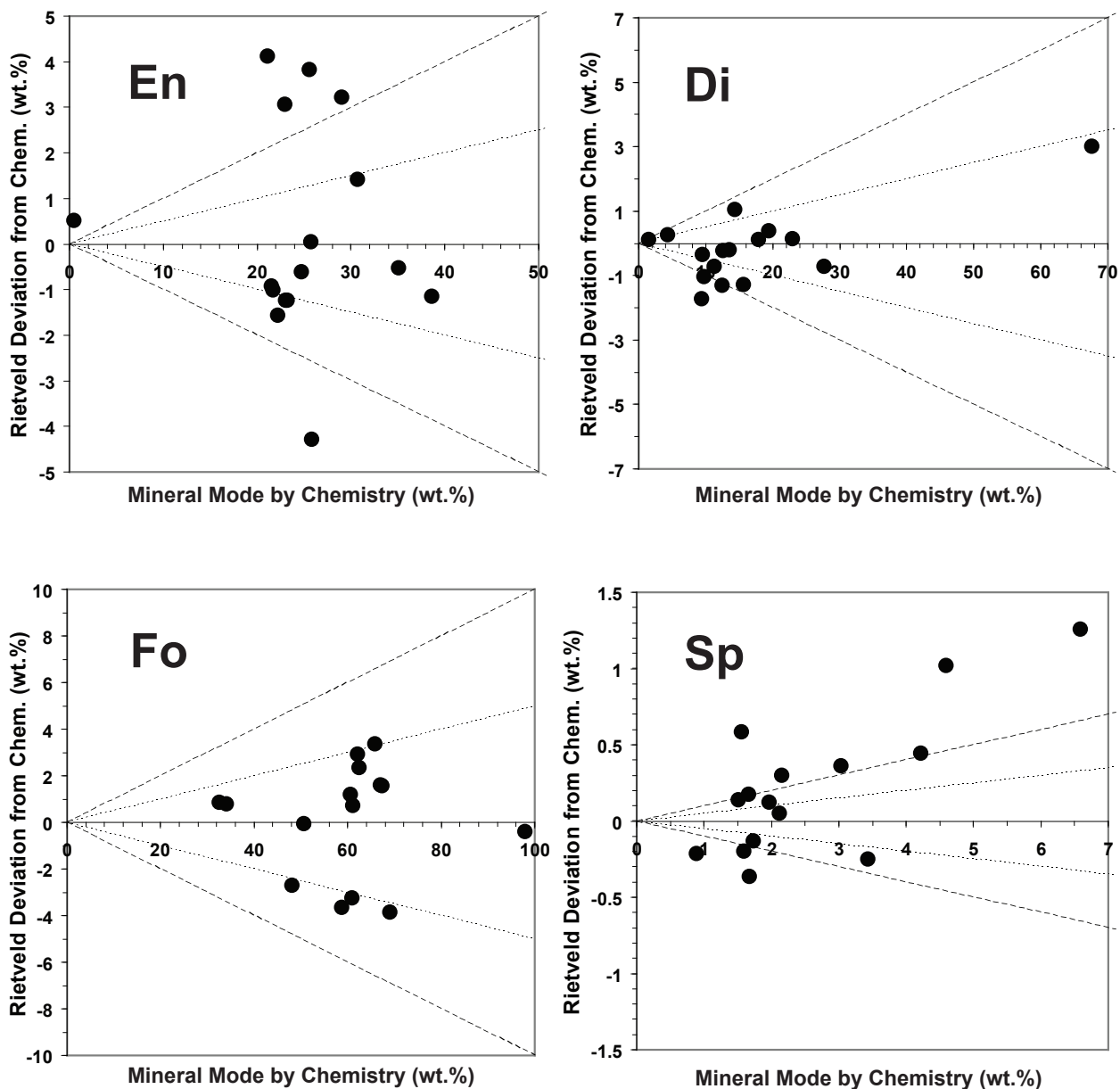


Figure F.2 Relative deviations of mineral modes determined by the Rietveld method from modes calculated by mineral chemistry. Inner set of lines marks 5 % relative deviation; outer set marks 10 %.

APPENDIX G – ELECTRON MICROPROBE ANALYSES

Compositions of minerals were measured on a fully automated CAMECA SX-50 electron microprobe (EMP) at the University of British Columbia, Department of Earth and Ocean Sciences. Operating conditions in wavelength-dispersion mode included: excitation voltage of 15 kV, beam current of 20 nA, 20 s peak count time, 10 s background count time, and a beam diameter of 5 μm . For carbonate a beam current of 10 nA and a spot diameter of 10 μm was used. Data reduction was completed using the 'PAP' $\phi(\rho Z)$ method (Pouchou and Pichoir, 1985). See Table G.1 for standards used in analyses.

Criteria for exclusion of analysis points included low or high totals (<98 or >102 %) or poor totals of oxygen relative to the cation sums. The cations sum was set to 4 for pyroxenes, 3 for olivine and spinel. Analyses were excluded if the oxygen sum was <5.95 or >6 for pyroxenes, <3.95 or >4 for olivine and spinel.

Table G.1 Standards used in electron microprobe analyses.

Element ¹	Olivine		Pyroxene		Oxides		Carbonate		Feldspar	
	Standard	Crystal	Standard	Crystal	Standard	Crystal	Standard	Crystal	Standard	Crystal
Na	Albite	TAP	Albite	TAP					Albite	TAP
Al	Kyanite	TAP	Kyanite	TAP	Spinel ²	TAP			Anorthite	TAP
Mg	Olivine	TAP	Diopside	TAP	Mg-chromite ²	TAP	Dolomite	TAP	Diopside	TAP
Si	Olivine	TAP	Diopside	TAP	Diopside	TAP			Anorthite	TAP
K	Orthoclase	PET	Orthoclase	PET					Orthoclase	PET
Ca	Diopside	PET	Diopside	PET	Diopside	PET	Calcite	PET	Anorthite	PET
Ti	Rutile	PET	Rutile	PET	Rutile	PET				
V					V Element	PET				
Cr	Mg-chromite ²	LIF	Mg-chromite ²	LIF	Mg-chromite ²	LIF				
Mn	Rhodonite ²	LIF	Rhodonite ²	LIF	Rhodonite ²	LIF	Rhodochrosite	LIF		
Fe	Fayalite ²	LIF	Fayalite ²	LIF	Fayalite ²	LIF	Siderite	LIF	Fayalite ²	LIF
Ni	Ni ₂ SiO ₄ ²	LIF	Ni ₂ SiO ₄ ²	LIF	Ni ₂ SiO ₄ ²	LIF				

¹ All x-ray lines are $K\alpha$. $VK\alpha$ is corrected for $TiK\beta$.

² Synthetic.

Table G.2 Mineral compositions for major phases in mantle xenoliths. Includes cores and rims. Minimum 10 analyses for each pyroxene, 5 for olivine, and 3 for spinel per xenolith.

Sample	OPX Mg#			CPX Mg#			Olivine Mg#			Spinel Cr#		
	Min	Mean	Max	Min	Mean	Max	Min	Mean	Max	Min	Mean	Max
A1	90.0	90.3	90.6	90.1	90.9	91.6	89.3	89.6	89.8	10.7	10.8	10.8
A2	90.4	90.7	90.8	92.0	92.6	93.0	90.0	90.1	90.2	13.4	13.6	13.7
A4	90.1	90.3	90.5	90.4	91.0	91.7	89.7	89.8	90.0	10.8	11.0	11.2
31	90.1	90.4	90.7	91.5	92.0	92.6	89.7	90.0	90.1	12.0	12.0	12.1
32	90.6	91.5	92.8	90.4	91.8	93.0	86.7	88.9	89.5	9.7	10.1	10.3
33	90.1	90.4	90.6	91.1	91.8	92.3	89.9	90.1	90.2	12.0	12.1	12.3
34A	89.3	89.7	90.2	90.0	90.4	90.8	88.9	89.1	89.4	8.1	8.9	9.6
34B	90.2	90.5	90.9	91.3	91.7	92.5	90.1	90.2	90.4	13.5	13.7	13.9
35	90.9	91.1	91.5	92.5	92.8	93.2	90.2	90.5	90.7	19.6	19.7	19.9
44	90.8	91.1	91.5	91.8	92.7	93.0	90.4	90.5	90.6	16.9	17.1	17.3
45	90.4	90.7	90.9	91.1	91.8	92.3	89.9	90.1	90.2	15.2	16.0	16.5
50	90.4	91.8	93.0	90.6	91.5	92.8	90.0	90.2	90.4	15.7	16.1	16.4
56A	88.9	89.2	89.5	89.8	90.2	90.6	88.3	88.5	88.7	7.4	7.5	7.5
69	86.6	87.1	87.5	88.5	89.3	89.8	-	-	-	2.5	3.0	4.0
70A	90.4	90.6	90.8	91.6	92.4	92.8	90.1	90.2	90.4	12.7	12.9	13.3
72	90.0	90.4	90.7	90.6	91.4	91.9	89.8	89.9	90.0	10.6	10.8	11.0
74	89.9	90.3	90.5	90.8	91.3	91.6	89.7	89.8	89.8	9.2	9.2	9.4
78	89.2	89.5	89.7	90.1	90.3	90.5	88.8	88.9	88.9	7.0	7.1	7.2
79A	86.6	89.2	89.6	89.6	90.4	91.0	88.7	88.8	89.0	6.5	6.9	7.1
81A	89.0	89.3	89.5	90.0	90.4	91.0	88.9	89.1	89.2	6.9	7.9	9.1
85	90.3	90.5	90.7	91.0	91.4	91.7	90.1	90.2	90.5	13.2	13.4	13.6
89	89.7	90.2	90.4	90.5	91.1	91.4	89.6	89.7	89.8	9.7	9.7	9.8
90	89.4	89.9	90.3	90.7	91.3	91.8	89.3	89.4	89.5	6.1	6.6	7.0
95	89.9	90.2	90.4	90.3	91.1	91.8	89.6	89.7	89.8	8.1	8.4	9.0
96	88.0	88.4	88.7	89.4	90.0	90.3	-	-	-	3.0	3.1	3.3
101	91.0	91.4	91.7	92.5	92.8	93.2	90.8	90.9	91.1	24.7	24.9	25.5
110	89.0	89.3	89.6	90.0	90.5	91.1	88.6	88.7	88.8	6.4	6.5	6.6
113	90.1	90.3	90.5	90.9	91.2	91.6	89.7	89.8	90.0	10.5	10.8	11.0
118	89.5	89.8	90.1	90.3	90.7	90.9	89.2	89.4	89.5	8.2	8.3	8.4
121A	89.0	89.6	89.8	90.1	90.6	91.3	89.0	89.0	89.1	10.5	10.7	10.9
121B	90.7	91.0	91.3	91.8	92.5	92.8	90.3	90.5	90.6	19.0	19.3	19.7
139	89.2	89.4	89.7	90.0	90.3	90.6	88.7	88.8	89.0	6.4	6.6	6.7
149	90.6	90.9	91.1	92.1	92.5	92.9	90.1	90.4	90.6	16.6	16.7	16.8
150	-	-	-	93.0	93.2	93.4	90.5	90.8	90.9	28.2	32.7	34.1

All sample numbers prefixed by "NP-MP05-"

Table G.2 (cont'd)

Sample	OPX Mg#			CPX Mg#			Olivine Mg#			Spinel Cr#		
	Min	Mean	Max	Min	Mean	Max	Min	Mean	Max	Min	Mean	Max
156A	89.8	90.0	90.4	90.3	90.8	91.2	89.3	89.5	89.7	9.6	9.8	10.0
157A	90.0	90.4	90.7	90.8	91.1	91.6	89.7	89.9	90.0	16.0	16.1	16.2
157B	90.8	91.0	91.3	92.4	92.7	93.1	90.1	90.4	90.5	31.6	32.2	32.8
159A	90.0	90.3	90.6	90.5	91.0	91.5	89.4	89.6	89.7	12.9	13.3	13.9
160A	89.1	89.4	89.6	89.3	89.5	90.0	88.6	88.7	88.8	8.5	8.8	9.0
160B	86.5	87.0	87.6	83.7	85.1	85.8	85.8	87.0	87.6	19.9	21.7	28.6
161A	90.3	90.5	90.8	90.6	91.0	91.5	89.9	90.0	90.1	10.3	10.4	10.6
161B	89.7	90.0	90.3	89.9	90.9	91.4	89.4	89.7	90.0	9.8	10.2	10.6
161D	90.6	91.0	91.3	92.3	92.7	93.3	90.2	90.4	90.5	29.5	29.9	30.3
162A	89.1	89.2	89.4	89.7	90.3	90.5	88.6	88.7	88.8	5.2	5.3	5.3
163A	87.8	88.4	89.0	89.1	89.7	90.2	87.8	88.0	88.1	3.4	4.2	4.5
163C	89.7	90.0	90.2	90.3	90.9	91.2	89.3	89.6	89.7	8.7	9.2	9.5
164A	90.1	90.5	90.6	90.5	91.1	91.5	90.0	90.0	90.2	10.3	10.6	10.7
164B	90.1	90.4	90.7	91.5	92.0	92.2	89.8	90.1	90.3	11.4	11.7	12.0
164C	90.3	90.5	90.9	91.7	92.1	92.8	89.9	90.0	90.1	16.4	16.8	17.1
165A	90.1	90.2	90.3	90.2	90.6	91.2	89.4	89.6	89.7	7.6	7.9	8.1
166	88.9	89.2	89.4	89.6	90.3	90.6	88.4	88.4	88.5	7.6	7.7	7.7

All sample numbers prefixed by "NP-MP05-"

APPENDIX H – GEOTHERMOMETRY

Geothermometers based on calcium exchange between coexisting orthopyroxene and clinopyroxene provide accurate estimations of equilibration temperatures of rocks (e.g. Wood and Banno, 1973; Wells, 1977; Brey and Köhler, 1990; Taylor, 1998). The Brey and Köhler (1990) (T_{BK90}) and Taylor (1998) (T_{TA97}) thermometers were specifically formulated for application to mantle-derived rocks. Brey et al. (1990) performed reversed experiments on lherzolitic compositions from 10-60 kbar at 900-1400 °C in order to calibrate their two pyroxene T_{BK90} thermometer (Brey and Köhler, 1990). Taylor (1998) performed reversed experiments on Na_2O - TiO_2 - and pyroxene-rich peridotite compositions from 10-35 kbar at 1050-1260 °C to calibrate his T_{TA97} thermometer, which is a modified version of T_{BK90} . For this study the T_{TA97} thermometer is preferred, because: i) it is based on reversed experiments on natural materials, ii) it was based on experiments with improved techniques over previous experiments, and iii) it is much more accurate for pyroxene-rich compositions, while also reproducing temperatures from the dataset of Brey et al. (1990) (i.e. lherzolitic compositions). Where applied to the datasets of Taylor (1998) the T_{BK90} thermometer yields a mean ΔT (i.e. $T_{calc} - T_{expt}$) of +81 °C \pm 36 (1σ), whereas the T_{TA97} mean ΔT is +6 \pm 31 (Taylor, 1998). For the dataset of Brey et al. (1990) the inherent uncertainty (1σ) of the T_{BK90} thermometer is \pm 15 °C (Brey and Köhler, 1990); the T_{TA97} thermometer predicts these data to \pm 19 °C (Taylor, 1998). When using all datasets the inherent uncertainty (1σ) of T_{TA97} is \pm 27 °C. The T_{TA97} thermometer has wider compositional applicability, and is the preferred thermometer for this study; however, the T_{BK90} thermometer was also included for this study because it is widely used in the literature, including previous studies in the Canadian Cordillera (e.g. Harder, 2004).

To calculate temperature, both thermometers require an assumed pressure. For this suite, 12 kbar was used; this pressure is a model ‘average’ value for the Cordilleran mantle lithosphere

and it allows direct comparison to another recent study (Harder, 2004). Over the entire temperature range of the suite the pressure difference is estimated at 10 kbar; changing the pressure used in the calculation to a 'corrected' value results in temperature differences of ≤ 15 °C for both thermometers.

Figure H.1 shows calculated temperatures using both thermometers. Relative to the T_{TA97} thermometer, T_{BK90} overestimates temperatures with increasing differences at higher temperatures. The exception is the plagioclase-spinel-websterite (NP-MP05-69), which has a higher equilibration temperature when using T_{TA97} .

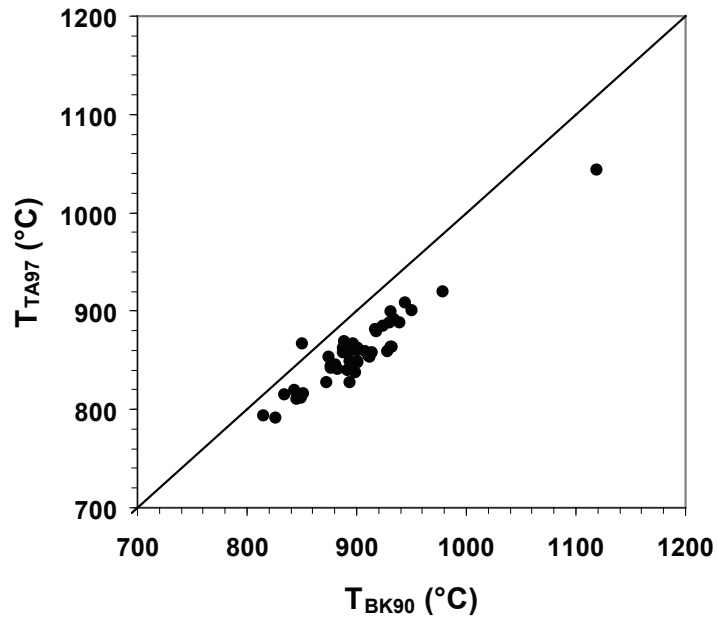
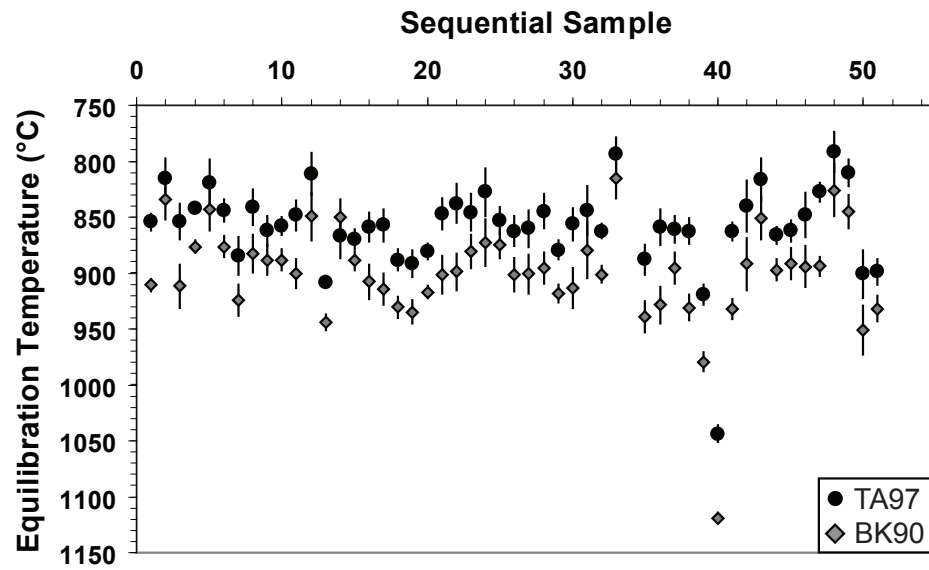


Figure H.1 Comparison of the geothermometers of Taylor (1998) (TA97), and Brey and Köhler (1990) (BK90). The BK90 thermometer produces higher temperature estimates in all xenoliths except one websterite (NP-MP05-69).

Table H.1 Geothermometry results for OPX-CPX mineral pairs in mantle xenoliths. Temperatures in °C. BK90 = Brey and Köhler (1990); TA97 = Taylor (1998).

Sample	BK90				TA97			
	T _{min}	T _{mean}	T _{max}	1 σ	T _{min}	T _{mean}	T _{max}	1 σ
A1	903	911	917	5	846	854	865	8
A2	805	834	855	17	785	815	833	18
A4	891	912	943	19	839	854	879	16
31	870	876	883	5	835	842	847	4
32	809	843	862	18	785	819	842	21
33	865	876	888	10	834	844	854	10
34A	912	924	942	14	868	885	903	17
34B	862	883	903	17	822	841	861	16
35	877	888	907	13	848	862	879	13
44	873	888	898	9	851	858	870	8
45	886	901	917	13	833	849	864	13
50	809	849	869	21	785	811	842	19
56A	936	944	952	7	904	909	917	5
69	823	850	870	17	838	867	888	20
70A	878	889	902	9	854	869	880	9
72	890	908	928	15	845	859	872	13
74	891	914	929	14	834	857	872	15
78	917	931	941	10	875	888	897	9
79A	925	935	954	10	878	891	908	12
81A	911	917	925	6	876	881	892	7
85	887	901	924	17	828	847	863	14
89	877	899	918	17	812	838	855	17
90	859	881	905	15	823	846	870	17
95	849	873	899	21	801	827	855	21
96	851	874	884	12	833	853	865	12
101	878	901	922	15	841	862	879	14
110	881	901	925	17	843	860	884	16
113	877	896	913	14	822	845	862	15
118	906	918	930	8	867	879	890	8
121A	887	913	926	18	835	856	868	15
121B	850	880	908	25	819	844	872	22
139	895	901	913	7	856	862	872	6
149	792	815	831	18	775	794	811	16

All sample numbers prefixed by "NP-MP05-"

Table H.1 (cont'd)

Sample	BK90				TA97			
	T _{min}	T _{mean}	T _{max}	1 σ	T _{min}	T _{mean}	T _{max}	1 σ
156A	914	940	955	14	866	888	905	13
157A	913	929	952	16	842	859	880	16
157B	878	896	909	14	845	860	873	12
159A	917	931	950	11	849	863	881	11
160A	962	979	987	9	902	919	929	9
160B	1112	1119	1126	5	1035	1044	1055	7
161A	917	932	942	9	850	863	870	8
161B	858	892	912	24	806	840	859	23
161D	821	851	879	19	789	816	846	19
162A	887	897	908	9	858	866	874	7
163A	870	892	909	14	847	862	876	9
163C	872	894	915	18	826	848	874	20
164A	886	894	903	8	820	828	835	8
164B	807	826	869	23	776	792	823	18
164C	828	845	868	15	796	810	827	12
165A	922	951	978	22	871	901	927	22
166	915	932	948	11	884	899	914	12

All sample numbers prefixed by "NP-MP05-"

APPENDIX I – HELIUM PYCNOMETRY

To measure the density of individual xenoliths, an automated helium pycnometer was used. A pycnometer produces sample volume estimates by measuring the pressure of displaced gas. Briefly, gas (helium) is pumped into a chamber of known volume that contains the sample of interest; the gas pressure is measured. A valve is opened to a second empty chamber of known volume, and the gas pressure equalizes between the two chambers; the gas pressure is measured again. The pressure difference is used to calculate the displaced volume (i.e. the sample volume). The sample mass and volume are then used to calculate sample density (i.e. skeletal density). The peridotites are assumed to have no isolated pore space.

Samples were split into <200 g pieces. A 200 g balance was used to measure mass, as it measures to hundredths of grams. The balance was calibrated for accuracy (200.00 g from a standard 200 g mass) before measurement of each sample. Samples masses were obtained before volume measurements to avoid sample loss problems during transfer from the pycnometer cell to the balance. Pycnometry measurements were conducted on a custom-built automated pycnometer, Volcanology and Petrology Laboratory, University of British Columbia. A full description of the device and its operation can be found in Michol (2006). Pycnometer calibration was conducted before each day's measurements. For calibration and for each sample, five cycles of measurement were conducted. During many sample measurements, the first of five runs resulted in aberrant volumes. This is a systematic anomaly, and is likely related to the design of the pycnometer. For these calibrations and samples, the first calculated volume was omitted and four measurements were used.

Depending on sample shape, steel sleeves may be used to increase the ratio of sample volume to empty space within the pycnometer's sample cell. However, due to variation in sample size, shape, and friability of the xenolith suite, the ratio of sample volume to empty space

also varies for each sample's volumetric measurements. To test the effect of empty space in the sample chamber on the accuracy of volumetric determinations, a single competent, relatively homogeneous peridotite xenolith (NP-MP05-35) was chosen. This xenolith was divided into three ~150 g pieces which were measured for volume independently, all together, and in all combinations of two, in a sample cell with no inserts. Results are shown in Figure I.1. Sample cell volume was calculated as 204.5 cm³ during calibration; the pieces consumed 22 to 71 % of the sample cell's volume. The slope of a line fit to the data (constraint of zero intercept) is a density of ~3.29 g/cm³. No density measurement differed more than 0.015 g/cm³ from this value.

Densities of mantle xenoliths are shown in Figure I.2. There appears to be a weak positive correlation between xenolith equilibration temperature and density, although the removal of the highest temperature xenolith would make this correlation much less evocative. There also appears to be a weak positive correlation with olivine content (Fig. I.3), though this is not true if the single high temperature xenolith is omitted.

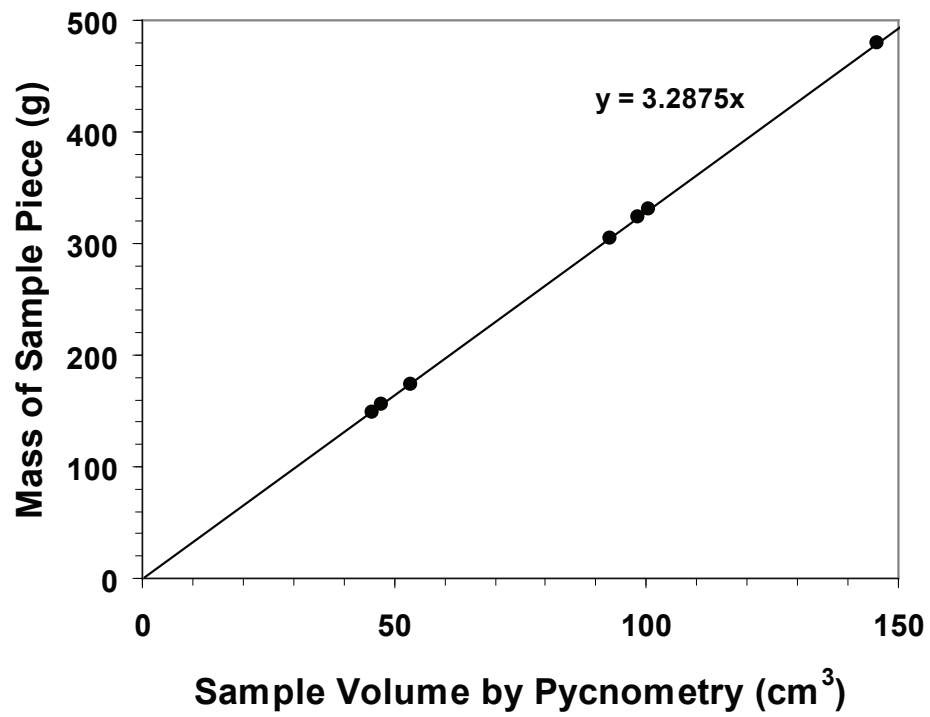


Figure I.1 Results of sample volume to cell volume ratio test. Slope of data-fitting line with zero intercept is the density of the sample (NP-MP05-35).

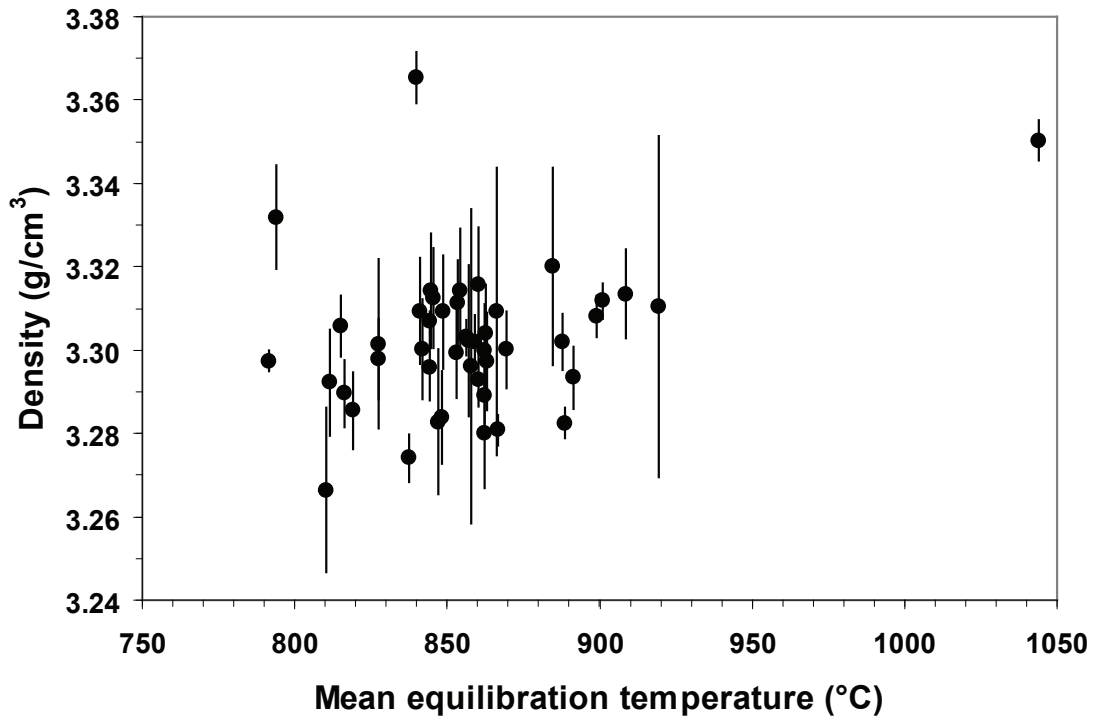


Figure I.2 Density of mantle xenoliths by helium pycnometry versus relative mantle position (equilibrium temperature) for all xenoliths measured. Errors are 1σ .

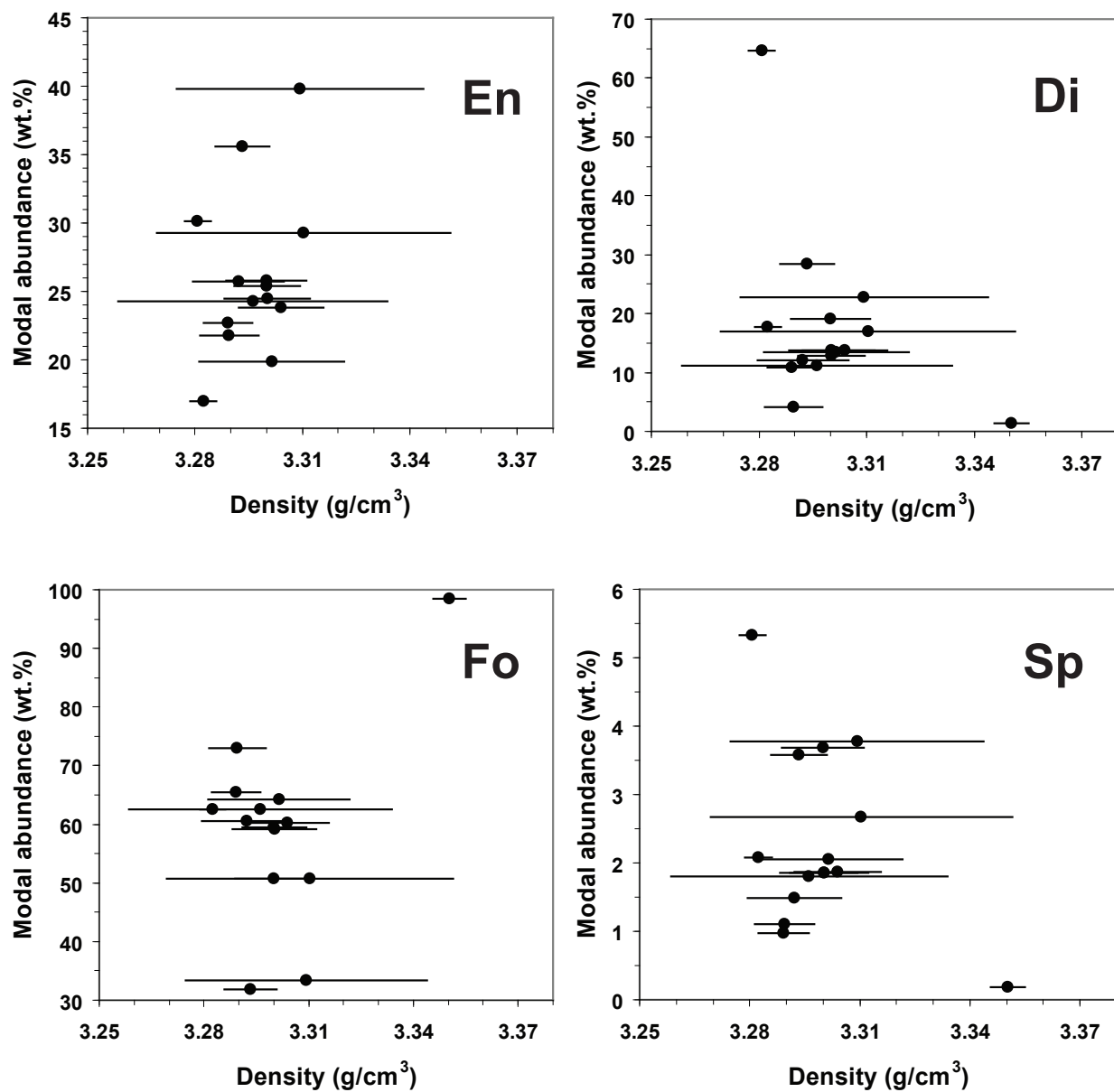


Figure I.3 Modal abundance of xenoliths' constituent phases versus density of the bulk xenoliths. Modal abundances by Rietveld XRD analysis. Errors are 1σ .